

Liquid Crystalline Polymers as Tunable Composite Resins for Composites Applications

Marchetti, M.

DOI

[10.4233/uuid:5e1093cb-5f7f-485d-9bb5-cd505a772820](https://doi.org/10.4233/uuid:5e1093cb-5f7f-485d-9bb5-cd505a772820)

Publication date

2021

Document Version

Final published version

Citation (APA)

Marchetti, M. (2021). *Liquid Crystalline Polymers as Tunable Composite Resins for Composites Applications*. [Dissertation (TU Delft), Delft University of Technology].
<https://doi.org/10.4233/uuid:5e1093cb-5f7f-485d-9bb5-cd505a772820>

Important note

To cite this publication, please use the final published version (if applicable).
Please check the document version above.

Copyright

Other than for strictly personal use, it is not permitted to download, forward or distribute the text or part of it, without the consent of the author(s) and/or copyright holder(s), unless the work is under an open content license such as Creative Commons.

Takedown policy

Please contact us and provide details if you believe this document breaches copyrights.
We will remove access to the work immediately and investigate your claim.

Liquid Crystalline Polymers as Tunable Composite Resins for Composites Applications

Dissertation

for the purpose of obtaining the degree of doctor
at Delft University of Technology
by the authority of the Rector Magnificus prof.dr.ir. T.H.J.J. van der Hagen
chair of the Board for Doctorates to be defended publicly on
Wednesday 27th of October 2021 at 15:00

By

Martino MARCHETTI
Master of Science in Polymer Chemistry
at Università degli Studi di Roma *La Sapienza*, Italy
Born in Rome, Italy

This dissertation has been approved by the promotor.

Composition of the doctoral committee:

Rector Magnificus,	Chairman
Prof. dr. T. J. Dingemans	Delft University of Technology, promotor
Prof. dr. ir. S. van der Zwaag	Delft University of Technology, promotor

Independent members:

Prof. dr. S.J. Picken	Delft University of Technology
Prof. dr. ir. J. Ivens	Katholieke Universiteit Leuven
Prof. dr. ir. R. Akkerman	University of Twente
Prof. dr. C.E. C. Koning	University of Groningen
Prof. C.A. Dransfeld	Delft University of Technology

This research was carried out under project number M42.4.11451 in the framework of the Research Program of the Materials innovation institute (M2i) supported by the Dutch government.

Printed by: Ipskamp Drukkers
Cover by: Brian UL Baldassarre
Copyright © 2021 by Martino Marchetti
ISBN: 978-94-6421-511-3

Table of contents

Chapter 1.....	1
1.1 High-performance polymers.....	1
1.2 Liquid crystalline polymers	3
1.3 Liquid crystalline thermosets	5
1.4 Fiber reinforced composites	8
1.5 Scope and outline of the thesis	9
1.6 References	12
Chapter 2	17
2.1 Introduction	18
2.2 Experimental section	21
2.2.1 Materials	21
2.2.2 Characterization	22
2.2.3 Synthesis	23
2.3 Results and discussions	27
2.3.1 Thermal properties of reactive end-groups	27
2.3.2 TGA analysis	28
2.3.3 DSC analysis	29
2.3.4 Optical microscopy	31
2.3.5 Rheology	32
2.3.6 Dynamic Mechanical Thermal Analysis	33
2.3.7 Mechanical properties	36
2.4 Conclusions	39
2.5 References	41
Chapter 3	43
3.1 Introduction.....	44
3.2 Experimental section	46
3.2.1 Materials	46
3.2.2 Characterization	46
3.2.3 Synthesis	47

3.3	Results and discussions	50
3.3.1	End-groups thermal properties	51
3.3.2	Thermal properties of oligomers	52
3.3.3	Polarized optical microscopy	55
3.3.4	Rheology	56
3.3.5	X-ray diffraction analysis	58
3.3.6	Dynamic Mechanical Thermal Analysis	59
3.3.7	Mechanical properties	60
3.4	Conclusions	63
3.5	References	64
Chapter 4		65
4.1	Introduction	66
4.2	Experimental	68
4.2.1	Materials	68
4.2.2	Characterization	69
4.3	Results and discussion	69
4.3.1	TGA analysis	70
4.3.2	DSC analysis	73
4.3.3	Rheology	74
4.3.4	Dynamic Mechanical Thermal Analysis	76
4.3.5	Thin film tensile testing	80
4.4	Conclusions	83
4.5	References	84
Chapter 5		87
5.1	Introduction	88
5.2	Materials	92
5.3	Composite manufacturing	93
5.3.1	Laminate stacking	93
5.3.2	Laminate thermopressing	94
5.3.3	Mechanical analysis	97

5.3.4	Microstructural analysis	98
5.4	Results and discussion	99
5.4.1	Microstructural observations.	99
5.4.2	Flexural properties	107
5.5	Discussion	110
5.6	Conclusions	112
5.7	References	113
	Chapter 6	117
	Summary	121
	List of publications and selected presentations	125
	Curriculum Vitae	126
	Acknowledgments	127

CHAPTER 1

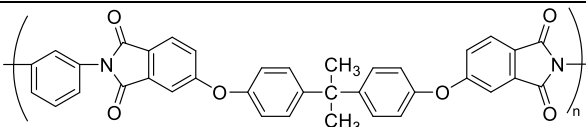
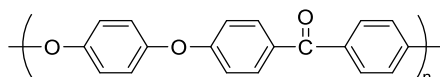
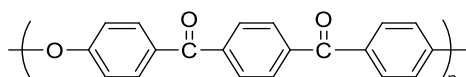
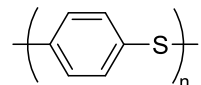
Introduction

1.1 High-performance polymers

A univocal and lasting definition of high-performance polymer has yet to be agreed upon. In polymer literature, polymers which offer a combination of high temperature stability and outstanding (thermo)mechanical properties in the presence of an aggressive chemical environment (e.g. oil, fuel, lubricants) are often referred to as high-performance polymers.^{1,2} Nowadays they find use in several demanding applications, such as resins for Fiber reinforced composites, adhesives, coatings, electronics, and advanced sports equipment.³⁻⁹ One of the strongest driver for the development of high-performance polymer technology has been the aeronautics and space industry. The design of new launch vehicles (Mercury, Gemini and Apollo program) created a need for lightweight (composite) structures that could replace metals and by doing so reduce the launch weight. Outside the aerospace environment, however, polymers were not considered as prime candidates for high-performance applications; in fact other materials would outperform them in terms of fluid stability, higher temperature stability and (thermo)mechanical performance albeit at the cost of additional weight. The situation changed with the introduction of the first generation thermoplastic all-aromatic high-performance polymers, such as polyetherimide (PEI), polyetheretherketone (PEEK), polyetherketoneketone (PEKK) and polyphenylene sulfide (PPS). Their chemical structures and some of their thermal/mechanical properties are summarized in Table 1.1, and what they have in common is a high level of aromatic units in the backbone,

which leads to a (semi)rigid polymer backbone with thermal/mechanical properties that are superior to polyolefins, aliphatic polyesters, *etc.*

Table 1.1 Examples of commercially available high-performance thermoplastic polymers.

Chemical Structure	Name	T _g [°C]	T _m [°C]
	PEI	215	–
	PEEK	143	334
	PEKK	156	338
	PPS	85	280

Despite the high level of aromaticity of the polymer backbone, most thermoplastic aromatic polymers exhibit a relatively low glass transition temperature ($T_g = 85\text{--}215\text{ }^\circ\text{C}$, Table 1), which limits the final use temperature of these polymers. Moreover, the high melting temperatures and associated high processing temperatures of high-performance polymers are close to their decomposition temperature and this leads to processing challenges. High processing temperature can cause undesired side reactions such as outgassing of small molecules and thermal crosslinking, which in turn may result in brittleness. Preparing thick neat resin or composite parts, without internal stresses, is challenging as well because the temperature gradient throughout a part upon cooling results in different degrees of crystallinity.¹⁰

One approach to deal with the complexity of processing high-performance polymers is

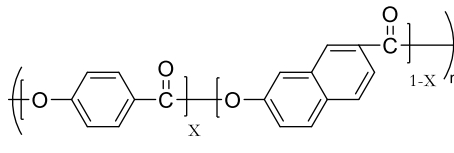
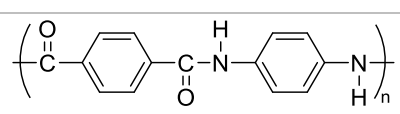
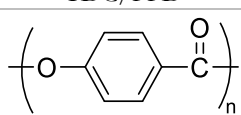
to reduce the molecular weight of the polymers to the range of 5,000 to 10,000 g·mol⁻¹, the so-called oligomer range. By reducing the molecular weight, the polymer melting point and melt viscosity decreases and this results in a more processable polymer. The tradeoff is that a lower molecular weight polymer, an oligomer, will result in lower (thermo)mechanical properties. This can be remedied by terminating the chain with reactive functionalities, which in turn can be activated in a successive thermal treatment step to form a high-molecular weight polymer network structure. The reactive functionality is present as a chain-terminating end-group in the polymer backbone and it is initially latent during polymerization and melt processing. Heating the reactive oligomer to elevated temperatures (typically > the melt processing temperature) triggers the chain-extension/crosslinking process, resulting in the formation of a network structure. This method is also called the *reactive oligomer approach*, one of the best known examples of this method was reported in the '90s by researchers at NASA Langley Research Center, where this concept was used to produce melt processable reactive polyetherimide oligomers (phenylethynyl-terminated imides or PETI's) that could be used to process carbon fiber reinforced composites for NASA's high-speed civil transport plane.¹¹

1.2 Liquid crystalline polymers

Liquid crystalline polymers (LCP) are a separate class of polymers in the domain of high-performance polymers.¹²⁻²¹ A liquid crystal (LC) material can be described as a material possessing the characteristics of both the liquid (l) and the solid (s) state, in fact a certain degree of orientational and/or positional order is maintained by the molecules while they randomly diffuse through the melt (thermotropic liquid crystals) or solution (lyotropic liquid crystals).²² The phenomenon of liquid crystallinity manifests itself with the development of domains of aligned molecules. One of the prerequisites for a polymer to display a liquid crystalline phase is molecular rigidity, given by the incorporation of rigid units in its main-chain. In the work described in this thesis the focus has been on liquid crystalline polymers with rigid units in their main-chain, the so-called *main-chain liquid crystalline polymers*. Table 1.2 shows some examples of main-chain liquid crystalline

polymers.

Table 1.2 Examples of commercially available main chain LCPs

LCP	Chemical Structure	Applications
Vectra™	 <p>HBA/HNA</p>	High-precision electronics, barrier films, chemical storage tanks
Twaron™/Kevlar™	 <p>TDC/PPD</p>	Fibers for heavy duty ropes & as reinforcement in fabrics for protective gear, space suits etc.
Ekonol™	 <p>PHBA</p>	Piston rings, heat resistant plugs & sockets, blending copolymer

As mentioned above, liquid crystals can be classified as thermotropic and lyotropic. Thermotropic liquid crystals exhibit mesophase formation in the melt within a particular temperature range, between the melting temperature $T_{K \rightarrow LC}$ and the clearing temperature $T_{LC \rightarrow i}$, see Figure 1.1. An example of such a thermotropic liquid crystal polymer is Vectra™, a random copolyester prepared from 4-hydroxybenzoic acid and 2-hydroxy-6-naphthoic acid (Table 1.2). In lyotropic liquid crystals the LC phase is observed when molecules are dissolved in suitable, typically low molecular weight, solvent. Here LC phase formation is a function of concentration and temperature.²³⁻³⁰ An example of a lyotropic polymer is Twaron™, an alternating polyamide prepared from terephthaloyl chloride and 1,4-phenylene diamine (Table 1.2). Most main-chain liquid crystal polymers tend to form nematic phases, where molecules exhibit long range order but no positional order. Another characteristic for high molecular weight liquid crystal polymers is that the LC-to-isotropic transition is often absent because either the LC-I temperature is $\gg T_{decomposition}$ (in case of thermotropic systems) or the boiling point of solvents limits

access to the isotropic state (in case of lyotropic systems).

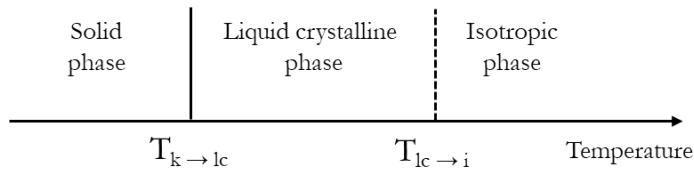


Figure 1.1 Phase transitions of thermotropic LCPs. The crystalline solid (k) melts into a fluid liquid crystal phase (LC) and upon additional heating the LC phase becomes isotropic (i)

The liquid crystalline polymers explored in this research work are all Thermotropic. They show liquid crystallinity (nematic) in the melt with their LC phase temperature dependent.

The rigid nature of the polymer backbone and the dense molecular packing typical of LCPs result in a material with outstanding properties, such as a high strength and stiffness and a low coefficient of thermal expansion, excellent solvent resistance, a low water absorption and a low gas permeability. These properties make LCPs ideal materials for lightweight structural applications, such as resins for fiber reinforced composites, high-performance fibers, or barrier films, high-precision moldings in electronics and high-performance moldings in sports goods, electro-optical displays and surgical devices.³¹

The rigidity of the backbone, which is typical of all-aromatic liquid crystalline polymers, results in rather challenging processing difficulties. Melting points and the associated melt viscosities are typically high, which significantly limits the processability of such materials. One of the approaches to overcome this issue is to co-polymerize different types of (non-linear) monomers, resulting in a polymer with a broader LC temperature range and a lower melting temperature. Successful results have been obtained by introducing crankshaft, non-linear co-monomers, monomers with bulky substituent or flexible spacers into the polymer backbone.³²⁻⁴⁵

1.3 Liquid crystalline thermosets

A second limiting factor for the use of thermotropic LCPs, in addition to their poor

processability, is that the performance at elevated temperature has been found to be rather disappointing, with relatively low glass transition temperature values, which are typically on the order of 100-130 °C and their storage modulus drops below 1 GPa when $T > 150$ °C. In order then to overcome this limitation, a new concept of liquid crystalline polymers has been investigated for the past 25 years: liquid crystalline thermosets (LCTs). The first liquid crystal thermosetting resins were introduced by Ortiz et al.⁴⁶ and Jahromi et al.,⁴⁷ with their studies on liquid crystalline epoxy resins. The work on reactive thermotropic low molecular weight liquid crystals was initiated by Hoyt et al.,⁴⁸ who end-capped amides and esters with maleimide, nadimide and methylnadimide reactive end-groups. Gavrin et al.⁴⁹ synthesized biphenol-phenylethynyl nematogens that retained their nematic order after crosslinking. Unfortunately, the crosslink density was so high that the final material was extremely brittle. In order to solve the issues caused by a low-molecular weight monomers approach, the reactive oligomer route has been applied to liquid crystalline polymers: synthesizing LCPs with a molecular weight in the order of 1,000–9,000 g/mol and end-capping the resulting oligomers with reactive end-groups. The idea behind the research when using thermotropic liquid crystalline oligomers is to bridge the gap between thermoplastics and thermosets, taking advantage of the processability of the thermotropic oligomer in the liquid crystalline phase and the excellent properties at high temperature of a crosslinked polymer. Moreover, by using thermally activated reactive functionalities in the polymer chains, the liquid crystalline state can be fixated, so that the liquid crystalline order is retained independently of the temperature.

It is clear that the choice of the reactive end-group functionality is of critical importance: the end-group must remain latent during the processing step and then be thermally activated and form a crosslinked network when the polymer is in its liquid crystalline phase, in the final stages of the polymer processing. Over the years, several reactive end-groups have been studied, Table 1.3 shows some of the most common ones.

Table 1.3 Selection of reactive end-groups that can be used for curing high temperature oligomers⁵⁰

Chemical structure	Name	Approx. T_{cure} [°C]	Comments
	Cyanate	200	Poor thermal stability
	Benzocyclobutene	220	Poor thermal stability
	Maleimide	230	Poor thermal stability
	Trifluorovinylether	250	Small processing window, cost, unknown thermal stability
	Ethynyl	250	Small processing window, cost, low toughness
	Phenylethynyl	350	High cure temperature, cost, excellent thermal stability
	Phenylmaleimide	370	High cure temperature, unknown thermal stability
	Nadimide	350	Cyclopentadiene evolution, low toughness
	Biphenylene	350	High cure temperature, low toughness

Over the past 15 years, Dingemans and co-workers^{35, 37, 39, 57} have developed several thermotropic liquid crystalline thermosets, primarily based on 4-hydroxybenzoic acid (HBA), terephthalic acid (TA), isophthalic acid (IA), hydroquinone (HQ), resorcinol (RS), 4,4'-bisphenol (BP) and 3-hydroxybenzoic acid (3-HBA) as possible co-monomers. Amongst the several reactive end-groups studied, phenylethynyl end-groups are the ones that delivered the most optimal results thanks to the fact that their curing temperature

window coincides with the oligomers processing window. Phenylethynyl-terminated oligomers exhibit excellent stability under harsh synthesis conditions and the oligomers have an infinite shelf-life at room temperature. Figure 1.2 shows the molecular structure of such a liquid crystalline reactive oligomer based on HBA, TA and BP and end-capped with phenylethynyl reactive end-groups. It serves as the starting point for the new polymers to be described in this thesis, with further modifications of the backbone and a more critical analysis of the role of the number of end-groups per oligomer.

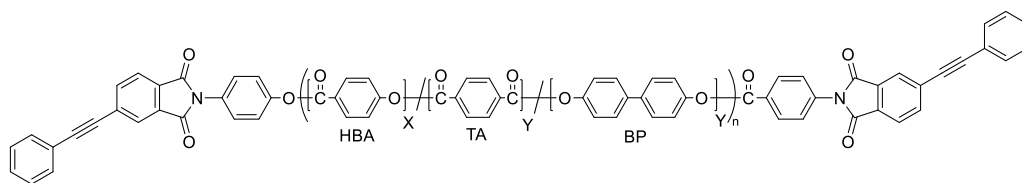


Figure 1.2 Example of a liquid crystalline reactive oligomer end-capped with phenylethynyl end-groups.

1.4 Fiber reinforced composites

A composite is defined as a combination of two or more materials with a distinguishable interface. The composite material shows properties typically not found in the single components. The individual phases, however, remain identifiable and are not chemically altered (apart from the interface between the phases).⁵¹ Depending on the nature of the matrix (polymer, metal, ceramic), composites can be classified in different categories, however in this work the discussion will exclusively focus on glass or carbon fiber reinforced polymer matrix composites. Either thermoplastic or thermoset resins can be used as the matrix in this class of composite materials, but thermoset resins cover the majority of applications. This is due to their availability and low cost. Moreover, thermoset resins are available in oligomeric form, with low viscosity at processing temperature, resulting in good flow properties, which facilitates resin impregnation of the fibers and fiber wet-out. However, thermoplastic resins have gained considerable attention since the 80s, in fact a very important class of high-performance fiber

reinforced composites is based on thermoplastic resins such as PPS, PEEK and PEI. These all-aromatic semi-crystalline polymers offer excellent properties, such as low manufacturing costs, long shelf-life and are resistant towards a variety of aggressive solvents, including hydraulic fluids and fuels.

Thermotropic liquid crystalline thermosets are considered interesting alternative matrix resins for fiber-reinforced composites because of their (thermoplastic) processing characteristics and their after cure (thermo)mechanical properties. Iqbal *et al.* presented the first examples of LCT-CF composites using a resin powder infusion process. The composite panels could be fabricated using a modified PEEK processing cycle and the after-cure thermomechanical properties of the panels were deemed to be promising enough to continue this line of research. It has been the aim of the research described in this thesis to take their approach a step further and to develop a new all-aromatic thermotropic LCT suitable for fiber composite applications.

1.5 Scope and outline of the thesis

The research work presented in this thesis describes the design, synthesis, characterization of reactive liquid crystal oligomers and their use as composite resins. The new chemistries make use of non-linear co-monomers, which allows us to tune the processing and after-cure characteristics. The chemistry, the cure characteristics and the processing behavior of the new LCTs are described in detail together with the results of first-phase composite manufacturing trials.

In **Chapter 2** we report on new modifications of a rigid LCP based on 4-hydroxybenzoic acid (HBA), terephthalic acid (TA) and 4,4'-biphenol (BP) and the aim of the work is to improve its processing characteristics by lowering the $T_{K \rightarrow LC}$ and the melt viscosity without compromising the (thermo)mechanical properties. Monomers such as 6-hydroxy-2-naphthoic acid (HNA) and 2,6-naphthalenedicarboxylic acid (NDA) introduce crank-shaft structures and 4,4'-diaminodiphenyl sulfone (DDS) and isophthalic acid (IA) introduce kinks (exocyclic bond angle of $\sim 120^\circ$) in the polymer backbone. We have

studied how said modifications affect the processing and (thermo)mechanical properties of the LC oligomers and their cured polymers.

In **Chapter 3** we describe the synthesis and properties of three liquid crystal oligomers, end-capped with either reactive (R) phenylethynyl and non-reactive (NR) phthalimide end-groups. The aim of this work is to better understand how the reactive end-groups contribute to the after cure thermo-mechanical properties of the final thermosets. This aspect has not been addressed in previous studies on LC thermoset polymers developed in the Dingemans group. The oligomer end-capped with reactive end-groups at both chain ends is predicted to have a higher concentration of crosslinks after curing compared to the oligomer end-capped with one reactive end-group due to the higher concentration of phenylethynyl functionalities. When no reactive end-groups are present the system is predicted to remain oligomeric and to show typical oligomeric behavior after cure. The three oligomers are fully characterized using TGA, DSC, rheology, DMTA and tensile testing.

In **Chapter 4** we perform backbone modifications of an LCT based on 4-hydroxybenzoic acid (HBA), terephthalic acid (TA) and 4,4'-biphenol (BP). During the synthesis we will insert a fourth co-monomer, 2,6-naphthalene dicarboxylic acid (NDA) at the expenses of TA. The inclusion of a fourth monomer to improve properties and processing is again a new step in the Delft research line. NDA appears to be promising in that it improves the processability of the oligomer. To gain a better understanding of how the presence of NDA affects the thermal and thermo-mechanical properties after curing, we have synthesized a series of reactive oligomers with varying amounts of NDA in the backbone.

In **Chapter 5** the fabrication of LCT-resin carbon and glass fiber reinforced composites is reported, together with their microstructural and mechanical characterization. The composites were produced using glass or carbon fiber woven fabrics. The carbon fiber-LCT and glass fiber-LCT reinforced composites were analyzed macroscopically using the

C-scan method and on a micro-level using optical microscopy and X-ray tomography. The mechanical behaviour of the composite panels was investigated by testing their flexural, compression and in-plane shear properties, and the results are contrasted with similar composite panels prepared using commercially available polyphenylene sulphide (PPS)

In **Chapter 6** the main findings of this thesis and recommendations for future work are presented.

1.6 References

- [1] Hergenrother, P.M. *High Performance Polymers*, **2003**, 15, 3-45, Pethrick, R.A. *Polymer Science and Technology*
- [2] Whittles Publishing: Dunbeath, 2010, Dingemans, T.J., 'High-Temperature Thermosets', in *Polymer Science: A Comprehensive Reference, Vol. 5*, 2012
- [3] Mark, J., Ngai, K., Graessley, W., Mandelkern, L., Samulski, E., Koenig, J., Wignall, G., *Physical Properties of Polymers*, Cambridge University Press, Cambridge, 2004, pp: 362-366
- [4] Donald, A.M., Windle, A.H., *Liquid Crystalline Polymers*, Cambridge University Press, Cambridge, 1992
- [5] Deporter, J., Baird, D.G., *Polymer composites*, 1993, 14, 201
- [6] Kim, Y.K., Ye, L., *Composites Part A: Appl. Sci. and Manuf.*, 2004, 35, 477
- [7] Denault, J., Dumouchel, M., *Advanced Performance Materials*, 1998, 5, 83
- [8] Economy, J., Goranov, K., *Prog. Polym. Sci.*, 1994, 117, 221
- [9] Meyer, G.W., Pak, S.J., Lee, Y.J., McGrath, J.E., *Polymer*, 1995, 36, 2303
- [10] Parlevliet, P.P.; van der Werf, W.A.W.; Bersee, H.E.N.; Beukers, A. *Compos. Sci. Technol.*, 2008, 68, 896
- [11] Connell, J.W., Smith, J.G., Hergenrother, P.M., *J.M.S.-Rev. Macromol. Chem. Phys.*, 2000, C40, 207
- [12] Jin, J.I., Antoun, S., Ober, C.K., Lenz, R.W., *Br. Polym. J.*, 1980, 12, 132
- [13] Lenz, R.W., Jin, J.I., *Macromolecules*, 1981, 14, 1405
- [14] Ober, C.K., Jin, J.I., Lenz, R.W., *Adv. Polym. Sci.*, 1984, 59, 102
- [15] Ebert, M., Schonherr, O.H., Wendorf, J.H., Tschirner, P., *Makromol. Chem. Rapid Commun.*, 1988, 9, 445
- [16] Schmucki, M., Jenkins, A.D., *Makromol. Chem.*, 1989, 190, 1303
- [17] Heitz, W., *Makromol. Chem. Macromol. Symp.*, 1989, 26, 1

- [18] Rehahn, M., Schuler, A.D., Wegner, G., Feast, W., *Makromol. Chem. Macromol. Symp.*, 1991, 47, 111
- [19] Jin, J.I., Kang, C.S., Lee, I.H., *Polym. Preprints*, 1992, 33, 233 Jin, J.I., *Mol. Cryst Liq. Cryst.*, 1994, 254, 197
- [20] Jin, J.I., Kang, C.S., Lee, I.H., Yun, Y.K., *Macromolecules*, 1994, 27, 2664
- [21] Vogit-Martin, I.G., Simon, P., Bauer, S., Ringsdorf, H., *Macromolecules*, 1995, 28, 236
- [22] Donald, A.M.; Windle, A.H., Hanna, S. *Liquid Crystalline Polymers*, 2nd ed. Cambridge University Press: Cambridge, 2006
- [23] Kelker, H., Hatz, R., *Handbook of Liquid Crystals*, Verlag Chemie, Weinheim, 1980, 593-602
- [24] Keller, A., Ungar, G., Percec, V., *Liquid Crystalline Polymers*, American Chemical Society, Washington, 1990, 314.
- [25] Khoo, I.C., *Liquid Crystals: Physical Properties and Nonlinear Optical Phenomena*, John Wiley & Sons, New York, 1995, 67-70
- [26] Klein, P.G., Evans, B.W., Ward, I.M., *Liquid-Crystalline Polymer Systems: Technology Advances*, ACS Symposium Series, 632, American Chemical Society, Washington, DC, 1996, 249
- [27] Marrucci G., *Rheology and Processing of Liquid Crystal Polymers*, Polymer Liquid Crystals Series, 2, Chapman & Hall, London, 1996, 30-48
- [28] Mulligan D.R., Imrie, C.T., Larcey P., *Journal of Materials Science*, 1996, 31, 1985
- [29] Noel C., *Liquid Crystal Polymers: From Structures to Applications*, Polymer Liquid Crystals Series, 1, Elsevier Applied Science, London and New York, 1992 31-102
- [30] Patnaiks. S., Plimpton S., Pacher R., Adams W.W., *Liquid Crystals*, 1995, 19, 213
- [31] Fink, J.K. *High Performance Polymers*. William Andrew: Norwich, 2008
- [32] Lenz RW, Jin JI., *Macromolecules*, 1981, 14, 1405
- [33] Ober CK, Jung-II J., Qifeng Z., Lenz, R.W., *Liquid Crystal Polymers* (Advances in Polymer Science, 59) 1984,103

- [34] Zhou QF, Lenz R.W., *Journal of Polymer Science: Polymer Chemistry Edition*. 1983, 21, 3313
- [35] Knijnenberg, A.; Weiser, E.; St.Clair, T.L.; Mendes, E.; Dingemans, T.J. *Macromolecules*, 2006, 39, 6936
- [36] Valery S., *Liquid Crystalline Polymers*. In: Saleem Hashmi editor. Oxford: Elsevier; 2016. pp. 1–46
- [37] Iqbal, M. (2010). *All-aromatic Liquid Crystal Thermosets and Composites Thereof*. Ph.D. Thesis. Delft University of Technology: The Netherlands
- [38] Guerriero, G.; Alderliesten, R.; Dingemans, T.J.; Benedictus, R. *Progress in Organic Coatings*, 2011, 70, 245
- [39] Dingemans, T., Knijnenberg, A., Iqbal, M., Weiser, E., Stclair, T. *Liquid Crystals Today*, 2006, 15, 4, 19
- [40] Cai, R.; Samulski, E. T.; *Macromolecules*, 1994, 27, 135 S.
- [41] Chang; C. D., Han, H., *Macromolecules*, 1996, 29, 2103
- [42] P. K. Bhowmik; H. Han, *Macromolecules*, 1993, 26, 5287
- [43] Jackson, W.J., *Macromolecules*, 1983, 16, 1027
- [44] Krigbaum, W.R, Hakemi, H., Kotek, R., *Macromolecules*, 1985, 18, 965
- [45] Antoun, S., Lenz, R.W., Jin, J.I., *Polym. Sci. Part A: Polym Chem*, 1981, 19, 1901
- [46] Ortiz, C.; Kim, R.; Rodighiero, E.; Ober, C.L.; Kramer, E.J. *Macromolecules*, 1998, 31, 4074
- [47] Jahromi, S. *Macromolecules*, 1994, 27, 2804
- [48] Hoyt, A.E., Benicewicz, B.C. *J. Polym. Sci. Part A: Polym. Chem.*, 1990, 28, 3403
- [49] Gavrin, A.J.; Curts, C.L.; Douglas, E.P. *J. Polymer. Science. Part A: Polym. Chem.*, 1999, 37, 4184
- [50] Hergenrother, P.M., Smith, J.G., Connell, J.W., *Polymer*, 2000, 41, 5073

- [51] Ratna, D. , *Handbook of Thermoset Resins*, iSmuthers ed., 2009, pp 281-290
- [52] Offringa, A.R., *Composites Part A: Applied Science and Manufacturing*, 1996, 27-4, 329
- [53] Denault, J., Dumouchel, M., *Advanced Performance Materials*, 1998, 5, 83-96, 33
- [54] Kim, Y.K., Ye, L., *Composites Part A: Appl. Sci. and Manuf.*, 2004, 35, 477-487
- [55] Deporter, J., Baird, D.G., *Polymer Composites*, 1993, 14, 201
- [56] Hou, T.H., Bryant, R.G., *High Performance Polymers*, 1997, 9, 43
- [57] Iqbal, M., Dingemans, T.J., *Composites Science and Technology*, 2011, 71, 863

CHAPTER 2

Non-linear modifications of a main-chain liquid crystal thermoset

Abstract

One of the challenges associated with using liquid crystalline polymers (LCP) comprised of all-aromatic rigid backbones is that the melting temperature (T_{k-lc}) is typically close to or above the decomposition temperature making processing very challenging. In this Chapter we will report on modifications of a rigid LCP based on 4-hydroxybenzoic acid (HBA), terephthalic acid (TA) and 4,4'-biphenol (BP) and the aim of this work is to improve its processing characteristics by lowering the T_{K-LC} and the melt viscosity without compromising the (thermo)mechanical properties. In order to achieve these goals, two synthetic approaches have been used: control the molecular weight by using reactive end-groups (target M_n of 10,000 g/mol) and by introducing non-linear monomers. Monomers such as 6-hydroxy-2-naphthoic acid (HNA) and 2,6-naphthalenedicarboxylic acid (NDA) introduce crank-shaft structures and 4,4'-diaminodiphenyl sulfone (DDS) and isophthalic acid (IA) introduce kinks (exocyclic bond angle of 120°) in the polymer backbone. We have studied how said modifications affect the processing and (thermo)mechanical properties of the LC oligomers and their cured polymers. Using both approaches we were able to substantially lower the T_{K-LC} of the oligomers from 325 to 280 °C, and lower the minimum complex melt viscosity from 10^5 Pa·s to 30 Pa·s, hence improving the processability considerably. At the same time, glass transition temperature values of the cured polymers were kept above 200 °C. Cured films exhibit a tensile strength of 85 MPa and 4% elongation at break, respectively, and Young's modulus values above 2 GPa.

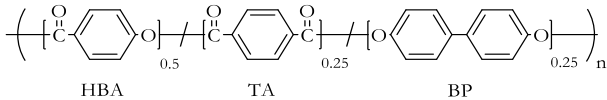
2.1 Introduction

Liquid crystalline thermosets (LCTs), are a sub-set of the thermotropic liquid crystalline polymers (LCPs) family, and are characterized by their high molecular rigidity. The latter is an important prerequisite for the formation of a stable liquid crystal phase, but at the same time it is the biggest obstacle in making liquid crystal polymers tractable, i.e. melt processable. In this *Chapter*, two synthetic strategies have been combined with the aim to develop melt processable reactive liquid crystal precursors with extremely rigid (high T_g) backbone formulations. The reactive oligomer approach, where reactive functionalities are introduced as end-groups to reduce the molecular weight of the polymer backbone,¹⁻³ has been paired with the introduction of non-linear co-monomers.^{2, 4-9} When considering backbone modifications to reduce the polymer chain rigidity, there must always be a balance between processing and the polymer's final thermo-mechanical properties. For instance, backbone modifications that decrease T_m will often decrease the after cure T_g .⁸⁻¹⁰

The scope of this chapter is to explore the designing of a new LCT that combines excellent after-cure (thermo)mechanical properties with the ability to process the precursor into fiber reinforced composites. In order to achieve this goal, a reference LCT system has been selected and several backbone modifications were synthesized, which allows us to study the structure-property relationships. When considering a resin for fiber composites, several parameters have to be considered. It is crucial to achieve a melting temperature and melt viscosity low enough that can ensure a wide processing window and an easy resin infiltration. Moreover, in this work the aim is to find a resin system that provides thermo(mechanical) properties that exceed what is currently available for commercially available state-of-the art high-performance polymers^{6, 11-14} such as polyether-ketone-ketone (PEKK) or polyphenylene sulfide (PPS): glass transition temperature after cure above 150 °C, storage modulus maintained above 1 GPa at 150 °C, strength at break and stiffness at 25 °C not less than 60-70 MPa and 2 GPa respectively. The reference polymer used for our work is based on one of the most rigid LCT formulation known to date, and is prepared from 4-hydroxybenzoic acid (HBA), terephthalic acid (TA) and 4,4'-biphenol (BP), commercially known as *Xydar*TM^{15,16},

shown in Table 2.1.

Table 2.1 Backbone composition of the thermoplastic LCP Xydar™ and its thermal properties.¹⁷

	
T_m [°C]	350
HDT [°C]	270

Over the years several attempts have been made to improve the melt processability of Xydar™ by reducing the T_m and melt viscosity. In 2012, Marchetti et al.¹⁸ continued the work of Iqbal et al.¹⁹ by incorporating reactive phenylethynyl end-groups in the backbone of Xydar™ with the aim to reduce the molecular weight and at the same they explored different monomer ratios that could lead to a more processable polymer. The combination of these two approaches resulted in a reactive oligomer with the following monomer ratio HBA(60%)/BP(20%)/TA(20%), which showed a significant improvement in melt processability. This reactive oligomer (Figure 2.1) has been labelled 20T (20 mol% TA), and this will be the reference system used in this *Chapter*.

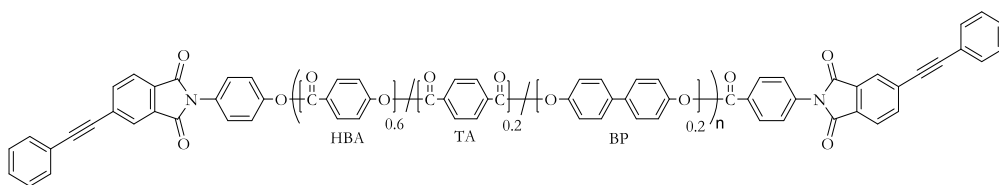


Figure 2.1 HBA/BP/TA(20) oligomer backbone (target $M_n = 10,000$ g/mol), end-capped with phenylethynyl reactive end-groups.

In this *Chapter* we will present 5 liquid crystal (LC) oligomer precursors with approximately the same M_n (10,000 g/mol, 10K) with different backbone structures. In order not to disrupt the unique molecular packing preferences that result in mesophase

behavior, only small backbone modifications of 5 mol% were considered.

The monomers 6-hydroxy-2-naphthoic acid (HNA) and 2,6-naphthalenedicarboxylic acid (NDA) were added at the expenses of respectively HBA and TA in order to introduce a so-called crank-shaft geometry (off-set the main-chain) in the polymer backbone. While 4,4'-diaminodiphenyl sulfone (DDS) and isophthalic acid (IA) introduce a 120 ° angle in the backbone, added at the expenses of respectively BP and TA. The chemical structure of the monomers used to modify the backbone are shown in Figure 2.2.

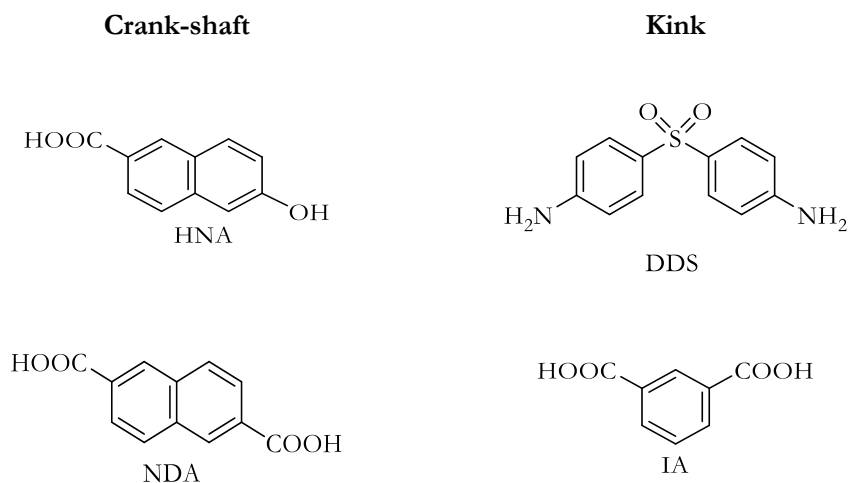


Figure 2.2 Chemical structure of the 4 monomers used to introduce different degrees of main chain disruption: 6-hydroxy-2-naphthoic acid (HNA), 2,6-naphthalenedicarboxylic acid (NDA), 4,4'-diaminodiphenyl sulfone (DDS) and isophthalic acid (IA) .

Table 2.2 Oligomer formulations with corresponding names, based on backbone modification by inserting a non-linear co-monomer. The reference polymer backbone is based on HBA(60%)/BP(20%)/TA(20%)

Oligomer formulation	Oligomer name
Reference HBA(60%)/BP(20%)/ TA(20%)-10K	20TA
HBA(55%)- HNA(5%) /BP(20%)/TA(20%)-10K	5H
HBA(60%)/BP(15%)- DDS(5%) /TA(20%)-10K	5D
HBA(60%)/BP(20%)/TA(15%)- IA(5%) -10K	5I
HBA(60%)/BP(20%)/TA(15%)- NDA(5%) -10K	5N

In this chapter we will discuss how the backbone modifications affect the melting temperature (T_{k-c}), the melt viscosity of the oligomers, the thermal stability, and the thermo-mechanical properties of the final cured polymers (LCTs).

2.2 Experimental section

2.2.1 Materials

All the chemicals used for synthesis of end-groups and the oligomers were obtained from the indicated sources and used as received. For the synthesis of the reactive end-groups, 4-phenylethynylphthalic anhydride (PEPA) was purchased from Hangzhou Chempro Tech Co; acetic acid, 4-aminobenzoic acid, acetic anhydride were received from Aldrich, and 4-aminophenol from Acros Organics. For the synthesis of the reactive oligomers, 4,4'-biphenol (BP) and 2,6-naphthalenedicarboxylic acid were purchased from TCI, and 4-hydroxybenzoic acid (HBA), terephthalic acid (TA), isophthalic acid (IA), 6-hydroxy-2-naphthoic acid (NDA), 4,4'-diaminodiphenyl sulfone (DDS), acetic anhydride and potassium acetate were obtained from Sigma Aldrich.

2.2.2 Characterization

The thermal stability of the cured polymers was analyzed by dynamic thermogravimetric analysis (TGA) using a Perkin-Elmer Pyris Diamond TG/DTA. Samples were investigated using a heating rate of 10 °C/min under a nitrogen atmosphere. Thermal properties of the reactive oligomers and cured polymers were investigated using a Perkin-Elmer Sapphire DSC, all measurements conducted under a nitrogen atmosphere with a heating rate of 20 °C/min. Dynamic mechanical thermal analysis was performed on a Perkin-Elmer Diamond DMTA, using cured thin films (20 mm x 5 mm x 0.25 mm) under a nitrogen atmosphere with a heating rate of 2 °C/min and frequency of 1 Hz, static tension force of 2000 mN, minimum tension force of 200 mN, tension gain of 1.5 and length amplitude of 5 μm .

^1H NMR and ^{13}C NMR spectra were recorded in DMSO-*d*₆ using a 400 MHz Bruker WM-400 operated at 400 MHz (^1H) and 75 MHz (^{13}C), respectively. The recorded spectra were referenced to the solvent residual peak (DMSO-*d*₆: ^1H , 2.50 ppm and ^{13}C 39.51 ppm) relative to TMS. MS analyses were performed on a Shimadzu QP2010S with a direct injection port and using electron impact to generate the spectrum. Mass range was set to 45-900. Infrared spectra were recorded on a Perkin Elmer Spectrum 100, equipped with an ATR unit.

The mesophase behavior of the oligomers was investigated with a Leica DMLM optical microscope equipped with a Linkham hot-stage. Samples were placed between glass slides and heated up to 370 °C using a heating rate of 50 °C/min.

The melt and cure behavior of the oligomers were studied with Thermoscientific Mars III parallel-plate rheometer equipped with a force-rebalanced transducer. Tests were performed at a frequency of 5 rad/sec and heating rate of 5 °C/min under a nitrogen atmosphere. Sample disks of 8 mm diameter and 0.5 mm thickness were prepared by compression molding.

Tensile tests on hot pressed fully cured thin film (18 mm x 5 mm x 0.25 mm) were performed at 25 °C with a strain rate of 0.25 mm/min, using an Instron Model 3365

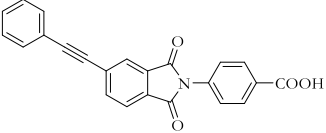
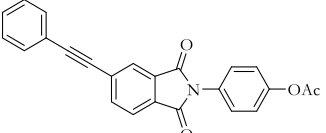
universal testing systems equipped with 1 kN load cell.

2.2.3 Synthesis

2.2.3.1 End-groups synthesis

A standard, acid-catalyzed imidization technique was used for the synthesis of the reactive end-groups N-(4-carboxyphenyl)-4-phenylethynylphthalimide (PE-COOH), N-(4-acetoxyphenyl)-4-phenylethynylphthalimide (PE-OAc) reported by Knijnenberg et al.² The molecular structures of the end-groups, their melting points and cure range are listed in Table 2.3. The syntheses of PE-COOH and PE-OAc are described in the following paragraphs.

Table 2.3 Chemical structures, melt points and cure range of the phenylethynyl reactive end-groups.

End-group structure	Abbreviation	Melting temperature [°C]	Cure range [°C]
	PE-COOH	348	310-400
	PE-OAc	242	310-400

Synthesis PE-COOH

A 2-liter round-bottom flask equipped with a mechanical stirrer and reflux condenser was charged with 1 L glacial acetic acid and phthalic anhydride (0.25 mol, 37.03 g). During heating to 120 °C, all solids dissolved. Upon the addition of 0.25 mol (34.28 g) 4-aminobenzoic acid a thick mixture formed which was stirred at reflux temperature for 2 h. After cooling to 70 °C the precipitated crystals were collected by filtration and washed twice with acetic acid and twice with ethanol. The crystals were dried in vacuum at 150 °C

for 48 h. The final yield was 92% (65 grams, 170 mmol).

$^1\text{H-NMR}$ PE-COOH (DMSO-*d*₆): 13.14 (s, 1H), 8.1-8.0 (m, 5H), 7.65 (m, 4H), 7.48 (m, 3H); $^{13}\text{C NMR}$ PE-COOH (DMSO-*d*₆): 166.4, 165.7, 165.6, 137.0, 135.4, 131.9, 131.4, 130.5, 129.8, 129.5, 129.3, 128.6, 128.3, 126.6, 125.6, 123.6, 121.1, 93.2, 87.7; FTIR: 2214, 1782, 1702, 1686, 1609, 1380, 1278, 1088, 739; MS: 367.10 (40%, M⁺), 323.10 (15%), 278.15 (8%), 203.05 (12%), 176.10 (28%), 126.10 (100%)

Synthesis PE-OAc

The PE-OAc end-groups were prepared in a similar fashion from phthalic anhydride (0.25 mol, 37.03 g) and 4-aminophenol (0.25 mol, 27.28 g), with an additional step. After washing, the crystals were refluxed for 2 h in acetic anhydride, the reaction product was precipitated upon cooling, followed by filtration, washed twice with acetic acid and twice with ethanol and dried as mentioned above. The final yield was 90% (58 grams, 170 mmol).

$^1\text{H-NMR}$ PE-OAc (DMSO-*d*₆): 8.01 (s, 1H), 8.05 (d, J = 8.0 Hz, 1H), 8.01 (d J = 7.6 Hz, 1H), 7.65 (m), 7.49 (m), 7.31 (m), 7.29 (m), 2.31 (s, 3H); $^{13}\text{C NMR}$ PE-OAc (DMSO-*d*₆): 169.6, 166.74, 166.66, 150.3, 137.6, 132.6, 132.1, 131.2, 130.0, 129.6, 129.3, 128.89, 128.84, 126.2, 124.2, 122.8, 121.8, 93.8, 88.4, 21.3; FTIR: 2214, 1782, 1702, 1686, 1609, 1380, 1278, 1088, 739; MS: 367.10 (40%, M⁺), 323.10 (15%), 278.15 (8%), 203.05 (12%), 176.10 (28%), 126.10 (100%)

2.2.3.2 Oligomers synthesis

A series of liquid crystal reactive polyester oligomers was synthesized using standard melt condensation techniques.

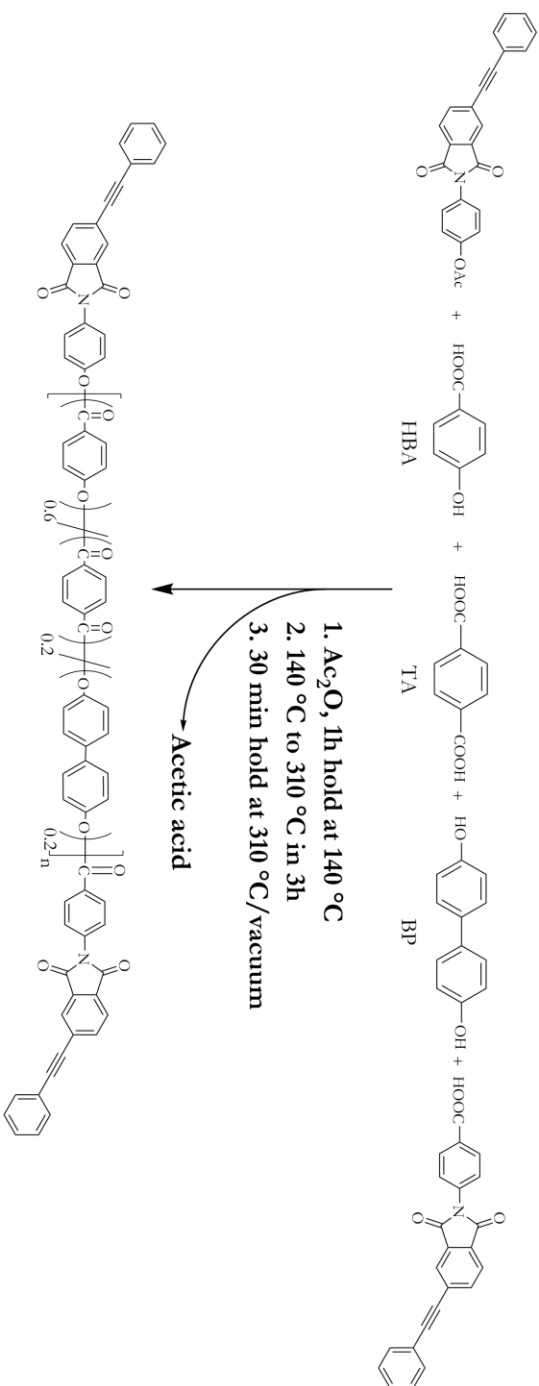
Five reactive oligomers with a target number average molecular weight M_n of 10,000 g/mol were prepared by controlling the concentration of the reactive end-groups using the Carothers equation.¹⁹

As a 4.6 example we will describe the synthesis of a 10,000 g/mol reactive oligomer (20TA-10K) with the following monomers ratio: HBA 60%, BP 20% and TA 20%, see Figure 2.3. HBA (1.2 mol, 165.7 g), BP (0.4 mol, 74.5 g), TA (0.4 mol, 66.4 g), PE-OAc (0.0157 mol, 12.0 g), PE-COOH (0.0157 mol, 11.6 g) and potassium acetate (0.0001 mol, 10 mg) were charged to a 1000 ml three-necked, round-bottom flask. The flask was initially equipped with a nitrogen gas inlet, a mechanical stirrer, and a reflux condenser and was purged with nitrogen for 0.5 h prior to the start of the reaction and a slow nitrogen flow was maintained throughout the duration of the synthesis. An excess of acetic anhydride (332 g, 3.25 mol) was added for the in-situ acetylation of the monomers. The reaction mixture was slowly stirred under a nitrogen atmosphere and heated to 140 °C to allow acetylation to take place. After a 1 h isothermal hold, the temperature of the reaction mixture was increased to 310 °C using a heating rate of 1 °C/min. During this process, acetic acid was collected as a condensation by-product. At 310 °C, the nitrogen flow was stopped and a vacuum (~20 mbar) was applied in order to remove the remaining acetic acid and other small molecular side products. The reaction flask was allowed to cool down overnight under a nitrogen flow and the final product was removed from the flask.

Next, the solidified oligomer was processed into a powder and it underwent a final post-condensation step at 265 °C for 24 hours under vacuum in order to guarantee removal of all volatile components and to ensure full polymerization. The molecular weight (M_n) of this reactive oligomer could not be confirmed as the oligomer is not soluble in known solvents, excluding GPC or dilute solution viscometry experiments.

The yield for this synthesis after product work-up was >90%.

Figure 2.3 Synthesis and backbone composition of the Reference HBA(60%)/BP(20%)/TA(20%)-10K LC oligomer end-capped with reactive phenylethyne end-groups (labeled 20T'A).

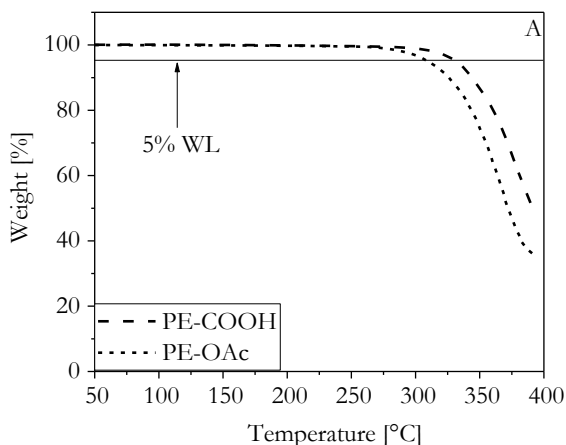


2.3 Results and discussions

Based on the inter-sample variations and instrument accuracies the reported degradation temperatures are accurate within 12.7 °C, the DSC peak temperatures are accurate up to 6.6 °C, the T_g values as determined from the 2nd derivative of the $\log E'-T$ curve are accurate up to 11.4 °C. The scatter (standard deviation) in the mechanical properties is reported explicitly.

2.3.1 Thermal properties of reactive end-groups

The thermal stability and the thermal behavior of the reactive end-groups have been analyzed by using TGA and DSC, respectively. The thermogravimetric signals of the reactive end-groups are shown in Figure 2.4-A, evidencing the stability of the two molecules even when the temperature is above 300 °C. Reactive end-group PE-OAc reaches a weight loss of 5% when the temperature is 315 °C, while PE-COOH has a weight loss of 5% at 332 °C.



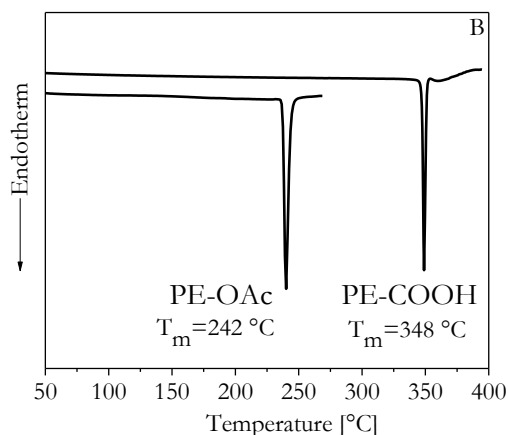


Figure 2.4 A. TGA signals for the PE-OAc and PE-COOH end-groups. The traces were recorded at a heating rate of 10 °C/min under a nitrogen atmosphere. B. DSC signals (first heat) for the PE-OAc and PE-COOH end-groups. The traces were recorded at a heating rate of 20 °C/min under a nitrogen atmosphere.

2.3.2 TGA analysis

The thermal stability of the cured LCT samples was investigated using dynamic thermogravimetric analysis (TGA). After curing the oligomers at 370 °C for 60 minutes, all the samples were analyzed from 25 °C to 595 °C with a heating rate of 10 °C/min under a nitrogen atmosphere. In order to evaluate the thermal stability of the samples, the decomposition temperature T_d was defined at the temperature where 5% of weight loss was observed. For all samples, high values of T_d and char yield at 595 °C are measured, in the range of 474-507 °C and 52-57% respectively (data shown in Table 2.4). The TGA curves for five representative oligomers are shown in Figure 2.5. The decomposition behaviour of all the oligomers are similar and the T_d values are in the same range. The backbone composition seems to play a minor role as the thermal stability of all five samples is comparable.

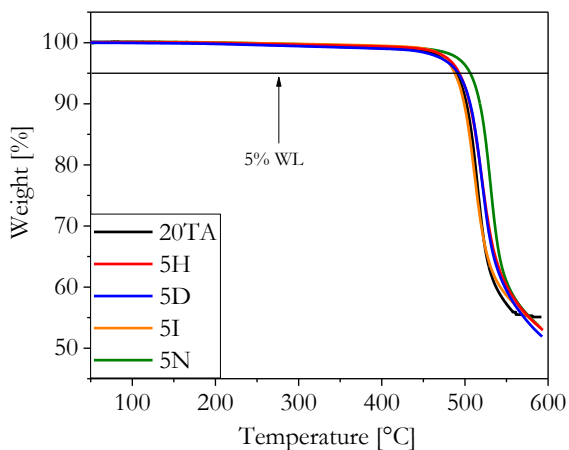


Figure 2.5 TGA signals of the fully cured oligomers 20TA (black), 5H (red), 5D (blue), 5I (orange) and 5N (green) as representative examples. Measured at a heating rate of 10 °C/min in nitrogen atmosphere.

2.3.3 DSC analysis

The thermal behavior of the oligomers was studied with differential scanning calorimetry (DSC). The first heating cycle was used to detect the glass transition temperature (T_g) and the melting temperature at which the crystalline state transforms into the nematic liquid crystalline state (T_{k-lc}) of the oligomers, and five representative thermal traces are summarized in Figure 2.6, and all the results shown in Table 2.4. For all the oligomers synthesized it was not possible to discern a clear and identifiable glass transition temperature (second order phase transition). The series of oligomers shows a wide range of T_{k-lc} transitions, caused by the backbone modification, and varies from 280 to 344 °C. When introducing 5 mol% of HNA we do observe negligible differences in the melting temperature with respect to the reference system 20TA. An even higher value of T_{k-lc} is detected for the 5D sample, 20 °C higher than the reference system. The presence of 5 mol% of IA does not affect the T_{k-lc} of the oligomer, as its melting temperature is comparable with that of the reference system. A decrease in the melting temperature, when compared with the reference system, is achieved when 5 mol% of NDA is

introduced in the polymer backbone: T_{k-lc} is lowered by 42 °C, from 324 °C for 20TA to 282 °C of the 5N.

From the DSC analysis of the oligomers it is possible to conclude that the presence of HNA, DDS or IA as co-monomer does not result in an effective reduction in T_{k-lc} of the oligomers. On the other hand, when inserting 5 mol% of NDA in the polymer backbone, the T_{k-lc} transition is reduced by 42 °C when compared with the reference system. A melting temperature of 282 °C is well below the temperature where chain-extension and crosslink chemistry becomes a factor, hence this backbone modification provides an attractive processing window for processing continuous fiber reinforced composites.

Table 2.4 Thermal properties of the liquid crystalline reactive oligomers and their cured polymers.

Sample	T_{k-lc} [°C] ^a	T_d [°C] ^b	Char Yield [wt %] ^c
20TA (ref)	324	489	57
5H	318	493	53
5D	344	484	51
5I	323	487	55
5N	285	507	54

^a T_{k-lc} data obtained by DSC experiments, performed at a heating rate of 20 °C/min, N₂ atmosphere.

^b Thermal stability evaluated by dynamic TGA on fully cured samples (the samples were cured by isothermal hold at 370 °C for 60 minutes, N₂ atmosphere), heating rate of 10 °C. T_d is defined as the temperature at which a weight loss of 5% occurs.

^c Char yield expressed as weight % at 595 °C.

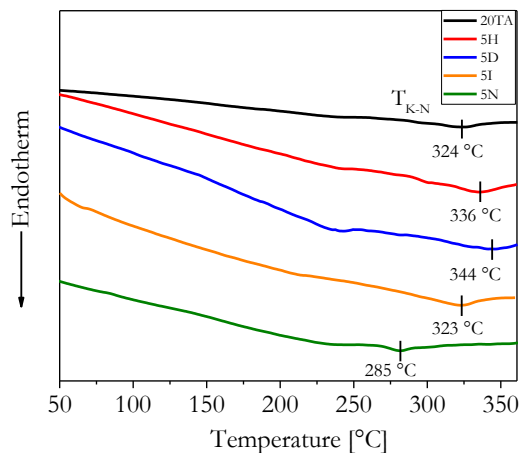


Figure 2.6 DSC traces of the reactive oligomers 20TA (black), 5H (red), 5D (blue), 5I (orange) and 5N (green) as representative examples. First heat, measured at a heating rate of 20 °C/min in nitrogen atmosphere.

2.3.4 Optical microscopy

An optical microscope equipped with cross polarizers was used to investigate the melt behavior of the oligomers: by heating the samples with a hot stage it was possible to study the melting range and the phase behavior of the reactive oligomers. Samples were heated with a heating rate of 50 °C/min up to the melting temperature, and all the oligomers of the series showed nematic textures, as can be seen in a representative example in Figure 2.7-A. The oligomers were then cured at 370 °C for 60 minutes and none of the samples showed a nematic-to-isotropic (N-I) phase transition during or after curing. Only a nematic phase could be observed, as shown in Figure 2.7-B, indicative of a nematic phase. As already observed by Iqbal et al.¹⁹ for LC oligomer end-capped with reactive phenylethynyl end-groups, after 1 hour hold at 370 °C the viscosity of the samples increased dramatically upon solidification.

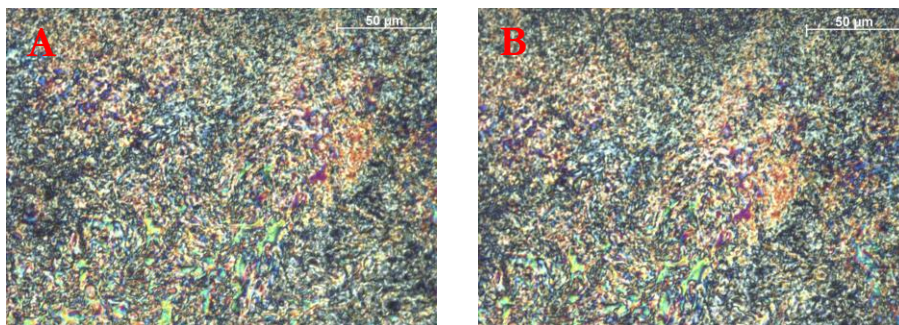


Figure 2.7 A. The nematic texture of oligomer 5N while in its initial low viscosity state at 370 °C, observed by polarized microscopy. B. Nematic texture of cured (solidified) oligomer 5N as representative example, after 60 minutes of isothermal hold at 370 °C, observed by polarized microscopy.

2.3.5 Rheology

The oligomer complex melt viscosity ($|\eta|^*$) and cure behavior was investigated by analyzing all samples using a parallel-plate rheometer and the results are summarized in Figure 2.8. For all the oligomers the complex melt viscosity starts decreasing when the melting temperature (T_{k-lc}) is reached and, after reaching a minimum, it increases due to chain-extension and crosslinking when the end-groups are activated.

Due to the different backbone modifications, it is possible to observe different viscosity behaviors. The reference sample TA20 and 5H show a similar behavior: the drop in viscosity is in the range of one order of magnitude, the viscosity minimum is reached when the samples are at a temperature of 370 °C, and then the phenylethynyl end-groups are thermally activated leading to an increase in viscosity. Due to the higher value of the T_{k-lc} for the 5D oligomer, the minimum viscosity is reached after the sample was at 370 °C. The insertion of a kinked molecule in the polymer backbone, such as IA, promotes the mobility of the polymer chain, and that is clear when one considers the IA rheology curve in Figure 2.8. Both 20TA and 5I samples show the same melting temperature, but the latter reaches a minimum in melt viscosity at a lower temperature than the reference 20TA system. Despite the higher mobility of the 5I polymer chains, the drop in viscosity for the 5I oligomer is comparable with the reference system, one order of magnitude from 10^6 Pa·s to 10^5 Pa·s. The most significant difference in viscosity

profiles has been observed when comparing the reference system with the oligomer modified with 5 mol% of NDA. Not only does the 5N oligomer have a much lower melting temperature than 20TA (Table 2.4), but as shown in Figure 2.8, the difference in viscosity profile is very clear. The viscosity of the 5N oligomer starts decreasing at the very beginning of the experiment, due to its lower melting temperature, and reaches a minimum that is almost 5 orders of magnitude lower than the starting viscosity value, from $2 \cdot 10^5$ to $2.5 \cdot 10^0$ Pa·s. Not only does the presence of NDA reduce the melting temperature (T_{k-lc}) of the oligomer, but a small amount of 5 mol% results in a major reduction in the complex melt viscosity by ~ 5 orders of magnitude over what has been observed for the reference system (20TA).

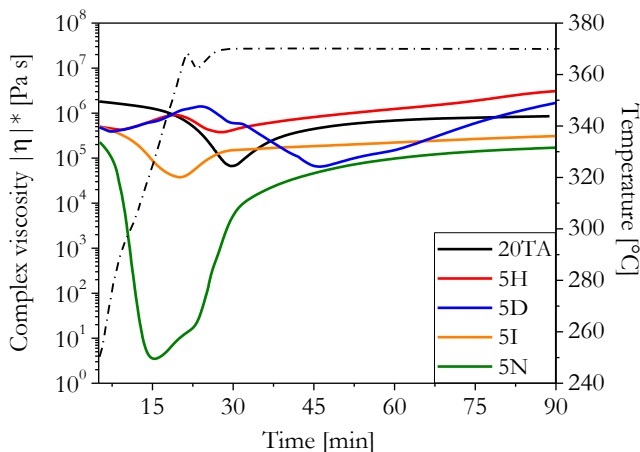


Figure 2.8 Complex melt viscosity of the oligomers 20TA (black), 5H (red), 5D (blue), 5I (orange) and 5N (green) as a function of temperature and a 60 minutes isothermal hold at 370 °C. Experiments were performed using a frequency of 5 rad/s and a heating rate of 5 °C/min and under N₂ atmosphere. The dashed black line represents the imposed temperature profile.

For all samples with backbone modification synthesized, a decrease in the melt viscosity was expected. However, it was only observed in the case of the 5N material. This is because for the all other samples the processing window, defined by the difference between the melting temperature and the crosslinking temperature, is too narrow: the lowest point of the melt viscosity is never reached due to the activation of the end-groups which increases the viscosity. Only the 5N sample has a melting temperature low enough

to allow the viscosity to reach a deeper minimum before being increased by the chain-extension and crosslinking reaction of the end-groups.

2.3.6 Dynamic Mechanical Thermal Analysis

Information regarding the glass-transition temperature (T_g) and the storage modulus (E') of the cross-linked LCT films were obtained using dynamic mechanical thermal analysis (DMTA). The measurements were performed on cured films with a thickness of ~ 0.25 mm in a temperature range of 0 to 500 °C, applying a frequency of 1 Hz. Determining T_g for complex polymers such as the ones studied in this thesis is non-trivial and the outcome is, to some degree, method dependent. One of the common methods to identify the glass transition temperature is the use of the peak of the storage modulus E'' -temperature curve. However, for the polymers of this thesis, due to their nature, the peaks in the E'' signals are weak and not easy to identify with some accuracy. Hence the decision was taken to identify the T_g values from the second derivative of the storage modulus E' vs. Temperature (T) curve. Storage modulus E' vs. T results are shown in Figure 2.99 and the extracted values at specific temperatures are listed in Table 2.5.

As expected, the reference system 20T shows a higher value for the glass transition temperature and a first small drop of E' at 275 °C and a second more pronounced drop at 380 °C. The 5H sample has the lower value of T_g , and all the specimens tested failed prematurely at ~ 350 °C. 5D and 5I show a similar E' behavior, as evident in Figure 2.99, and all film failed around 410 °C. Looking at the 5N sample, it is evident that the storage modulus drops around 250 °C. 5N it is the only sample where it is possible to observe a rubber plateau above T_g , from 290 to 375 °C. Despite the low melting temperature ($T_{K-N} = 282$ °C) and a low complex melt viscosity (30 Pa·s), the cured 5N film exhibits a high glass transition temperature of 243 °C.

All samples show high values for the room temperature storage modulus, well above 2.5 GPa, as is clear from both Figure 2.99 and Table 2.5. 20TA has the higher values of E' due to the more rigid backbone, compared to the other polymers in the series, as 5D, 5I and 5N display a storage modulus between 3 and 4 GPa and 5H at 5 GPa.

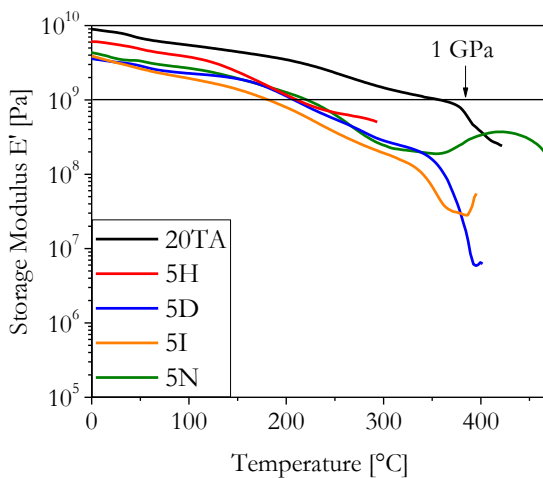


Figure 2.9 Storage moduli of the films: 20TA, 5H, 5D, 5I and 5N. All measurements were conducted at a frequency of 1 Hz, from 0 to 475 °C, heating at 2 °C/min in N₂ atmosphere.

Table 2.5 Storage Modulus (E') and T_g data of the fully cured films as determined by dynamic mechanical thermal analysis (DMTA)

Sample	E' [GPa] ^a 25 °C	E' [GPa] 100 °C	E' [GPa] 200 °C	E' [GPa] 300 °C	E' [GPa] 400 °C	T_g [°C] ^b
20TA	8.1	5.4	3.5	1.4	0.4	380
5H	3.2	2.2	1.1	0.3	/	260
5D	3.2	2.0	1.3	0.2	0.05	195
5I	3.2	2.0	1.3	0.2	0.05	165
5N	3.7	2.8	0.8	0.2	0.3	243

^a Storage modulus (E') obtained from DMTA analysis performed on fully cured films. Measurement conducted at a frequency of 1 HZ, heating rate of 2 °C/min, N₂ atmosphere. Storage moduli have a typical variation of +/- 7.5%.

^b T_g data obtained from DMTA analysis performed on fully cured films, T_g considered at E' second derivative. Measurement conducted at a frequency of 1 HZ, heating rate of 2 °C/min, N₂ atmosphere.

2.3.7 Mechanical properties

Tensile tests were performed following the ASTM D-1078-10 in order to investigate the effect of the backbone modifications on the mechanical properties of the polymers. All samples could be processed into thin films by using a hot press, films of 8 x 8 cm were then cut into dog-bone specimens by using a dog-bone shaped die.

It is appropriate to mention that apparent static stiffness was determined from slope of the force-cross-head displacement data (over the stress range 2-5 MPa) and the values are to be taken as lower boundary estimates of the real E-modulus values. The polymer films were not robust enough to use an extensometer to determine a more accurate estimate of the Young's modulus value. For future work, a recommendation is to use contactless (optical) strain measurements.

Figure 2.10 and Figure 2.11 shows respectively a representative example of the stress-strain signals and the results of the analysis as bar plots to better visualize and compare the results. The plots show apparent static stiffnesses, strength at break and elongation at break data, each value calculated as an average of three specimen for each polymer. The overall results are then summarized in Table 2.6.

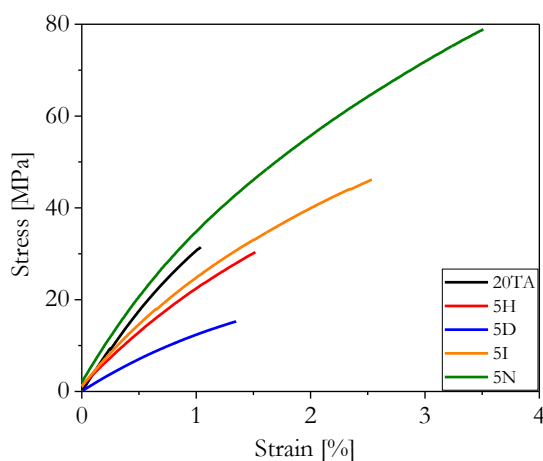
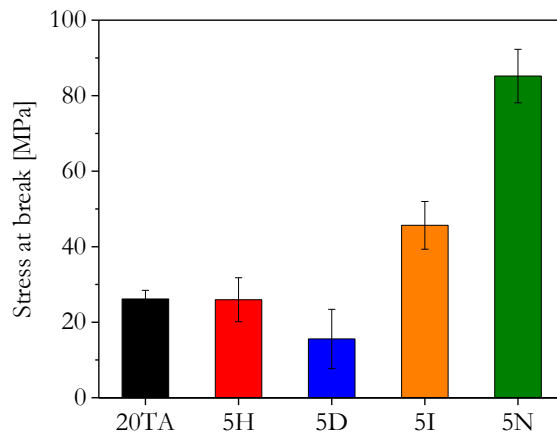
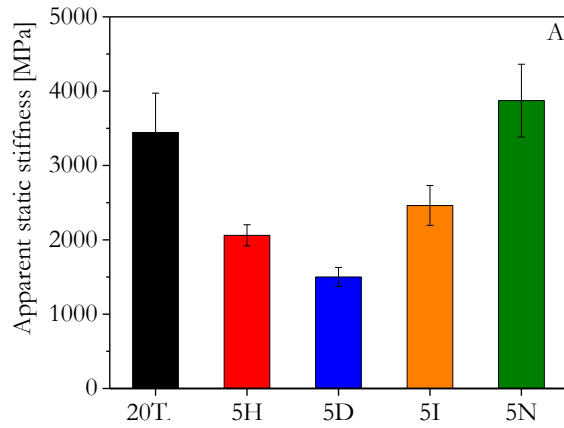


Figure 2.10 Representative stress-strain curves of cured films, samples 20TA (black), 5H (red), 5D (blue), 5I (orange) and 5N (green). Test speed was 0.25 mm min⁻¹. All

stress-strain curves were recorded at room temperature.



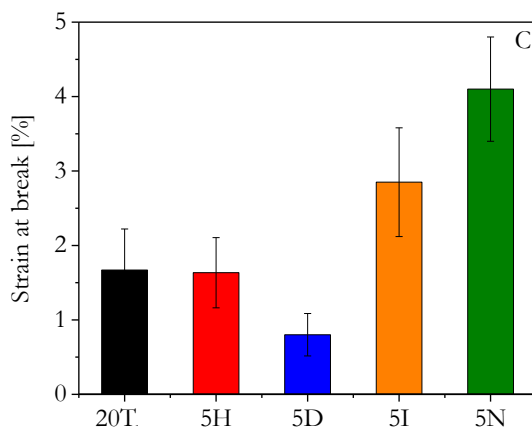


Figure 2.11 Tensile properties of the cured films (average and standard deviation values based on tests of 3 specimens). A- Apparent static stiffness. B- Stress at break. C- Strain at break.

When considering the values of the apparent static stiffness and stress at break of the samples, it was not possible to find a trend in the values that could be in line with the backbone modifications. The samples that are expected to have a less rigid backbone, hence lower values of the apparent static stiffness, are the ones which display the higher values, 5I and 5N. Not only the backbone composition plays a role in the mechanical properties of a material, but the presence of defects and the processing of the samples as well, that can result in a more *defect-free* sample. Since the presence of defects cannot directly be controlled for the thin films here analyzed, the ease of processing plays a major role in the final mechanical properties. Due to the lower T_{k-lc} and lowest value for the complex viscosity, samples 5I and 5N shows an ease of processing superior to all the other polymers here analyzed, with consequential better performances on the mechanical level. With the exception of 5I and 5N, all the other samples showed a strain at break lower than 3%, that can be considered in line with the values of cured liquid crystal aromatic polyester.^{[4] [22]} With no exception, all the samples show a brittle fracture with very little yielding.

Table 2.6 Tensile properties of the films. The data shown is an average with standard deviation based on testing 3 tensile specimens per sample.

Sample name	Apparent static stiffness [MPa] ^a	σ at break [MPa] ^a	ϵ at break [%] ^a
20TA	3445 (528)	26.0 (2.3)	1.7 (0.5)
5H	2060 (141)	25.9 (5.8)	1.6 (0.4)
5D	1501 (128)	15.6 (4.8)	0.9 (0.3)
5I	2462 (268)	45.6 (6.3)	2.8 (0.7)
5N	3872 (490)	85.2 (7.1)	4.1 (0.7)

^a Tensile tests performed with a strain rate of 0.25 mm/min on a load cell of 1 kN, 25 °C and air atmosphere.

2.4 Conclusions

In this Chapter we have reported on how co-monomer backbone modifications affect the physical properties of a series reactive liquid crystalline oligomers. The starting point for this series was a reference LCT system based on the *Xydar* formulation using the monomers HBA, BP and TA, with the following molar ratios: HBA(60%)/BP(20%)/TA(20%), named 20TA. By inserting a fourth co-monomer at 5 mol% in the polymer backbone, 4 different oligomers were synthesised and analyzed. While the above-mentioned backbone modifications did not have a significant effect on the liquid crystalline mesophase of the oligomers or thermal stability of the cure polymers, processing was mostly impacted. Particularly, using 5 mol% N (2,6-naphthalene diacid) appeared to be most effect. DSC and rheology experiments showed that the T_{k-lc} could be suppressed by 42 °C when compared to the reference oligomer 20TA. The complex melt viscosity ($|\eta|^*$) could be lowered of almost 5 orders of magnitude for the 5N sample. On the other hand, no significant changes in T_{k-lc} and $|\eta|^*$ could be observed for the other backbone modifications.

Thermo-mechanical analysis of cured thin films showed that, no matter which backbone modification was performed, the result was a LCT with lower T_g and storage modulus compared to the reference 20TA sample. Despite this fact, all samples retained high T_g values (165-380 °C).

Preliminary mechanical testing using thin films shows that the 5 mol% 2,6-naphthalene diacid (N) modification give the best stress-strain performance. Cured films show a tensile strength of 85 MPa at a strain of 4%, which are promising values and makes these resins of interest as resins for fiber reinforced composites that can be used for high temperature applications.

2.5 References

- [1] Connell, J. W., Smith, J. G., Hergenrother, P. M., *J. Macromol. Sci., Rev. Macromol. Chem. Phys.*, 2000, 40, 207
- [2] Knijnenberg, A.; Weiser, E.; St.Clair, T.L.; Mendes, E.; Dingemans, T.J., *Macromolecules*, 2006, 39, 6936
- [3] Iqbal, M., Dingemans, T. J., *Eur. Polym. J.*, 2010, 46, 2174
- [4] Iqbal, M. (2010). *All-aromatic Liquid Crystal Thermosets and Composites Thereof*. Ph.D. Thesis. Delft University of Technology: The Netherlands
- [5] Guerriero, G.; Alderliesten, R.; Dingemans, T.J.; Benedictus, R. *Progress in Organic Coatings*, 2011, 70, 245
- [6] Dingemans, T.J., Knijnenberg, A., Iqbal, M., Weiser, E., Stclair, T. *Liquid Crystals Today*, 2006, 15, 4, 19
- [7] Cai, R.; Samulski, E. T.; *Macromolecules*, 1994, 27, 135
- [8] S. Chang; C. D. Han; *Macromolecules*, 1996, 29, 2103
- [9] P. K. Bhowmik; H. Han; *Macromolecules*, 1993, 26, 5287
- [10] Dingemans, T.J., 'High-Temperature Thermosets', in *Polymer Science: A Comprehensive Reference*, Vol 5, 2025
- [11] Denault, J., Dumouchel, M., *Advanced Performance Materials*, 1998, 5, 83
- [12] Kim, Y.K., Ye, L., *Composites Part A: Appl. Sci. and Manuf.*, 2004, 35, 477
- [13] Offringa, A.R., *Composites Part A: Appl. Sci. and Manuf.*, 1996, 27, 329
- [14] Chapman, T. J., Gillespie, J. W., Pipes, R. B., Manson, J. A., Seferis, J.C., *J. Comp. Mater.*, 1990, 24, 616
- [15] Hummel, D. O., Neuhoff, U., Bretz, A., Dussel, H.-J., *Macromol. Chem.*, 1993, 194, 1545
- [16] Sueoka, K., Nagata, M., Ohtani, H., Naga, N., Tsuge, S., *J. Polym. Sci., Part A: Polym. Chem.*, 1991, 29, 1903

- [17] Ellis, B., Smith, R., *Polymers: A Property Database* (Second Edition), CRC Press, 2009, pp 652
- [18] Marchetti, M. (2012) *All aromatic high T_g liquid crystal thermosets*, MSc. Thesis. Università degli Studi di Roma “La Sapienza”, Italy
- [19] Iqbal, M.; Norder, B.; Mendes, E.; Dingemans, T. J., *Polymer Science Part A: Polymer Chemistry*, 2009, 1368
- [20] H. R. Allcock, F.W. Lampe, J. E. Mark *Contemporary Polymer Chemistry*, Pearson Education, Inc., NJ USA 2003
- [21] Lee, J., Y., Jang, J., *Polymer Bulletin*, 1997, 38, 447
- [22] Guan, Q. (2016). *Design, Synthesis and Characterization of Novel (Multiblock) Copoly(esterimide)s and their Shape-memory Properties*. Ph.D. Thesis. Delft University of Technology: The Netherlands

CHAPTER 3

Thermotropic liquid crystal thermoset: the role of the phenylethynyl reactive end-group

Abstract

In this chapter we describe the synthesis and properties of three liquid crystal oligomers, end-capped with reactive (R) phenylethynyl and non-reactive (NR) phthalimide end-groups. Our aim is to better understand how the reactive end-groups contribute to the after cure thermo-mechanical properties of the final thermosets. The oligomer end-capped with reactive end-groups at both chain ends (labelled 2R) is predicted to have a higher concentration of crosslinks after curing compared to the oligomer end-capped with one reactive end-group (labelled 1R-1NR) due to the higher concentration of phenylethynyl functionalities. When no reactive end-groups are present (oligomer 2NR) the system is predicted to remain oligomeric and a typical oligomer behavior is expected after cure, such as stable low melt viscosity and a brittle behavior from processed films. The three oligomers ($M_n = 10,000$ g/mol, 10K), 2R, 1R-1NR and 2NR, are fully characterized using TGA, DSC, rheology, DMTA and tensile testing. Despite the differences of the end-groups, all the cured thermosets exhibit high decomposition temperatures in nitrogen environment, i.e. $T_d^{5\%} (N_2) = 500$ °C at a heating rate of 10 °C/min. DMTA analyses showed that fully cured films exhibit glass-transition temperatures (T_g) in the range of 120-150 °C. In addition, the cured films exhibit high storage moduli (E') at room temperature (above 8 GPa) and stress at break values up to 90 MPa and strain at break of 5%.

3.1 Introduction

The work on the backbone modifications of reactive liquid crystal oligomer presented in *Chapter 2* furtherly confirmed that by inserting non-linear co-monomers is possible to lower the oligomers melting temperature and melt viscosity.^{1, 2} We also showed that we were able to maintain the values of glass transition temperature after cure to levels equal or above 150 °C, by keeping the amount of non-linear co-monomers below 10 mol%.

In order to gain a better understanding of how the reactive end-groups affect the final after cure properties of these LC reactive oligomers, in this chapter we synthesized 3 liquid crystal oligomer precursors with approximately the same M_n (10,000 g/mol, 10K, same molecular weight of the oligomers explored in Chapter 2), end-capped with reactive (R) and non-reactive (NR) end-groups. The backbone of the oligomers used is based on HBA, BP, TA and IA, with the following monomers ratio: HBA(60%)/BP(20%)/TA(10%)/IA(10%), labelled HBA/BP/TA(10)-IA(10). The backbone structure of the oligomer can be seen in Figure 3.1, together with both end-groups: reactive (R) phenylethynyl-based and non-reactive (NR) phthalimide-based.

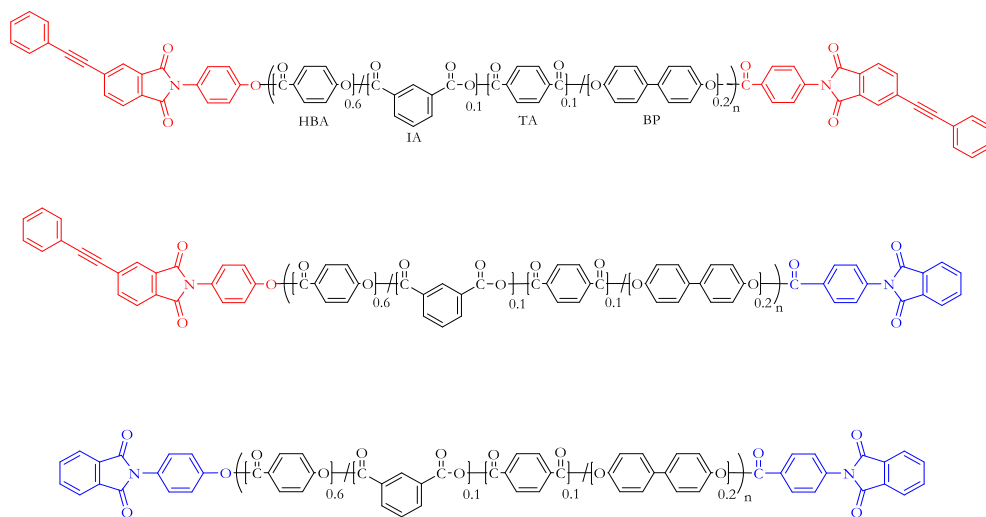


Figure 3.1 HBA/BP/TA(10)-IA(10) oligomer backbones ($M_n = 10,000$ g/mol), end-capped with reactive (red) and non-reactive (blue) end-groups. From top to bottom: 2R, 1R-1NR and 2NR.

This type of oligomer was selected at the time before the full results of *Chapter 2* were fully available. If that had not been the case, in retrospect it would've made more sense to use the 5N sample. However, the scope of the chapter is to investigate the role of the end-groups, independently of the polymer backbone. The reason for selecting the IA oligomer at the time was that it could be processed most easily into good quality films for further testing. Additional criteria to select this particular oligomer were its good thermal stability (5% weight loss at 475 °C) and a clear and identifiable pre- and post-cure glass transition temperature (from 125 to 150 °C).

By varying the reactivity of the end-group, we synthesized 3 series 10K oligomers: 2R (the series with reactive end-groups at both chain ends), 1R-1NR (one reactive and one non-reactive chain end) and 2NR (both chain ends terminated with non-reactive end-groups), as shown in Figure 3.1. The crosslinks that are formed in a thermoset during the curing process are one of the main factors determining the overall final properties (thermal, thermo-mechanical and mechanical) of the thermoset itself. The reactive phenylethynyl end-group have been used as chain-extenders and/or crosslinkers in several high-performance polymers.^{3, 4, 5} Jensen et al.⁶ studied the curing chemistry of phenylethynyl reactive end-groups with DSC, FTIR and LCMS, then Roberts et al.⁷ analyzed it with solid state NMR techniques. Roberts work shows a combination of crosslinks and chain-extensions functionalities dependent on, amongst other factors, end-group concentration when both chain ends are end-capped with reactive end-groups. The 2R system is predicted to have a higher concentration of crosslinks after curing compared to the 1R-1NR one due to the higher concentration of phenylethynyl functionalities. When the oligomers are end-capped with only one reactive end-group (1R-1NR), the system is still able to crosslink, but the crosslinks density is reduced. On the other hand, when no reactive end-groups are present (2NR) the system is predicted to remain oligomeric and a typical oligomer behavior is expected after cure, such as stable low melt viscosity and a brittle behavior for processed films.

Here we will compare the reactive versions of the oligomer and the non-reactive oligomer, and their cured networks, in terms of thermal, thermo-mechanical and mechanical properties.

3.2 Experimental section

3.2.1 Materials

All chemicals used for synthesis of end-groups and the oligomers were obtained from the indicated sources and used as received. For the synthesis of the reactive end-groups: 4-phenylethynylphthalic anhydride (PEPA) was purchased from Hangzhou Chempro Tech Co; acetic acid, 4-aminobenzoic acid, acetic anhydride, phthalic anhydride were purchased from Sigma Aldrich and 4-aminophenol from Acros Organics. For the synthesis of the oligomers: 4-hydroxybenzoic acid (HBA), terephthalic acid (TA), isophthalic acid (IA), acetic anhydride and potassium acetate were obtained from Sigma Aldrich, and 4,4'-biphenol (BP) was purchased from TCI.

3.2.2 Characterization

The thermal stability of the cured polymers was analyzed by dynamic thermogravimetric analysis (TGA) using a Perkin-Elmer Pyris Diamond TG/DTA. Samples were investigated using a heating rate of 10 °C/min under a nitrogen atmosphere. Thermal properties of the reactive oligomers and cured polymers were investigated using a Perkin-Elmer Sapphire DSC, all measurements conducted under a nitrogen atmosphere with a heating rate of 20 °C/min. Dynamic mechanical thermal analysis was performed on a Perkin-Elmer Diamond DMTA, using cured thin films (20 mm x 5 mm x 0.25 mm) under a nitrogen atmosphere with a heating rate of 2 °C/min and frequency of 1 Hz, static tension force of 2000 mN, minimum tension force of 200 mN, tension gain of 1.5 and length amplitude of 5 µm.

¹H NMR and ¹³C NMR spectra were recorded in DMSO-d₆ using a 400 MHz Bruker WM-400 operated at 400 MHz (¹H) and 75 MHz (¹³C), respectively. The recorded spectra were referenced to the solvent residual peak (DMSO-d₆: ¹H, 2.50 ppm and ¹³C 39.51 ppm) relative to TMS. MS analyses were performed on a Shimadzu QP2010S with a direct injection port and using electron impact to generate the spectrum. Mass range was set to 45-900. Infrared spectra were recorded on a Perkin Elmer Spectrum 100, equipped with an ATR unit.

The melt and cure behavior of the oligomers were studied with Thermoscientific Mars III parallel-plate rheometer equipped with a force-rebalanced transducer. Tests were performed at a frequency of 5 rad/sec and heating rate of 5 °C/min under a nitrogen atmosphere. Sample disks of 8 mm diameter and 0.5 mm thickness were prepared by compression molding.

The mesophase behavior of the oligomers was investigated with a Leica DMLM optical microscope equipped with a Linkham hot-stage. Samples were placed between glass slides and heated up to 370 °C using a heating rate of 50 °C/min.

Wide angle X-ray diffraction (WAXD) analysis was conducted on a Bruker AXS D8 Discovery diffractometer, with a Cu-K α radiation source. The distance between the sample and the detector was set to 60 mm, and the exposure time was 5 minutes, all tests were conducted at 25 °C.

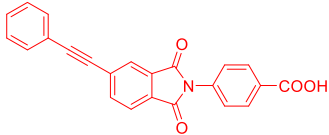
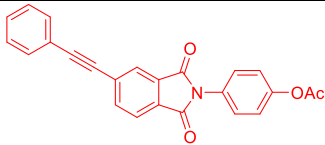
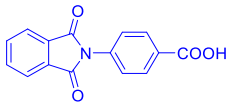
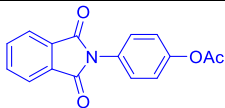
Tensile tests on hot pressed fully cured thin film (18 mm x 5 mm x 0.25 mm) were performed at 25 °C with a strain rate of 0.25 mm/min, using an Instron Model 3365 universal testing systems equipped with 1 kN load cell.

3.2.3 Synthesis

3.2.3.1 *End-groups synthesis*

A standard, acid-catalyzed imidization technique was used for the synthesis of the reactive end-groups N-(4-carboxyphenyl)-4-phenylethynylphthalimide (PE-COOH), N-(4-acetoxyphenyl)-4-phenylethynylphthalimide (PE-OAc) reported by Knijnenberg et al.⁸ For the synthesis of the non-reactive end-groups N-(4-carboxyphenyl)-4-phthalimide (NR-COOH) and N-(4-acetoxyphenyl)-4-phthalimide (NR-OAc) a procedure published by Lima et al.⁹ and described in Vogel's textbook¹⁰ was followed. The molecular structures of the end-groups, their melt point and cure range are listed in Table 3.1.

Table 3.1 Chemical structures, melting points and cure range of the reactive R (red) and non-reactive NR (blue) end-groups.

End-group structure	Abbreviation	Melting temperature [°C]	Cure range [°C]
	PE-COOH	348	310-400
	PE-OAc	242	310-400
	NR-COOH	294	/
	NR-OAc	248	/

The synthetic details regarding the synthesis of the reactive end-groups are reported in Chapter 2. The syntheses of NR-COOH and NR-OAc are described in the following paragraphs, and shown in Figure 3.2 and Figure 3.3.

Synthesis NR-COOH

A 2-liter round bottom flask equipped with a mechanical stirrer and reflux condenser was charged with glacial acetic acid (1 L) and phthalic anhydride (0.25 mol, 37.03 g) and heated to 120 °C. Upon the addition of 0.25 mol (34.28 g) 4-aminobenzoic acid a suspension formed which was stirred at reflux temperature for 2 h. After cooling to 70 °C the precipitated crystals were collected by filtration and washed twice with acetic acid and twice with ethanol. The crystals were dried in vacuum at 150 °C for 48 h, yielding 65 gram (92%, 240 mmol) of the title compound.

¹H-NMR NR-COOH: 13.11 (s, 1H), 8.08 (d, $J = 8$ Hz, 2H), 7.99 (m, 2H), 7.92 (m, 2H),

7.61 (d, $J = 8.4$ Hz, 2H); ^{13}C NMR NR-COOH: 166.6, 166.5, 135.7, 134.7, 131.4, 129.9, 129.8, 126.9, 123.5; FTIR: 1720, 1690, 1375, 1289, 767, 707; MS m/z (relative intensity): 267,05 (66%), 223,10 (32%), 178,10 (10%), 104,15 (38%), 76,05 (100%), 50,05 (33%)

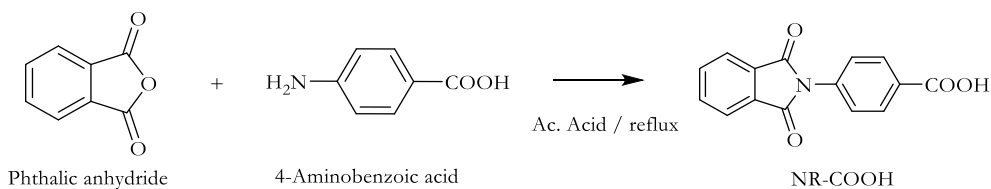


Figure 3.2 Synthesis of the NR-COOH non-reactive end group.

Synthesis NR-OAc

A 2-liter round bottom flask equipped with a mechanical stirrer and reflux condenser was charged with glacial acetic acid (1 L) and phthalic anhydride (0.25 mol, 37.03 g) and heated to 120 °C. Upon the addition of 0.25 mol (27.28 g) 4-aminophenol a suspension formed which was stirred at reflux temperature for 2 h. After cooling to 70 °C the precipitated crystals were collected by filtration and washed twice with acetic acid and twice with ethanol. The solid residue were refluxed for 2 h in acetic anhydride, cooled to 70 °C, filtered and washed twice with acetic acid and twice with ethanol. The obtained crystals were dried in vacuum at 150 °C for 48 h, yielding 58 gram (90%, 206 mmol) of the title compound.

^1H -NMR NRE OAc: 7.96 (m, 2H), 7.89 (m, 2H), 7.47 (d, $J = 8$ Hz, 2H), 7.27 (d, $J = 8.8$ Hz, 2H), 2.29 (s, 3H); ^{13}C NMR NRE OAc: 169.0, 166.8, 149.7, 134.5, 131.4, 129.2, 128.4, 123.3, 122.2, 20.7; FTIR: 1739, 1711, 1285, 1368, 1221, 1113, 842, 716; MS m/z (relative intensity): 281.20 (8%), 239.10 (100%), 195.10 (32%), 167.05 (10%), 104.10 (23%), 76.05 (46%), 50,05 (13%).

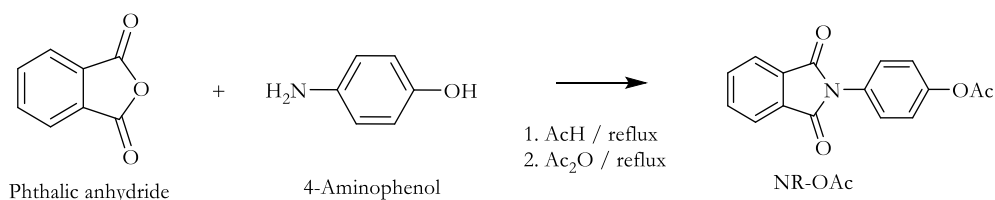


Figure 3.3 Synthesis of the NR-OAc non-reactive end group.

3.2.3.2 Oligomers synthesis

All reactive and non-reactive oligomers (shown in Figure 3.1) were synthesized in high yields using a two-step in-situ melt polymerization method. The synthetic details can be found in Chapter 2 and in reference 11. After the synthesis, the oligomers were post-condensed at 265 °C for 24 hours under vacuum. After the post-treatment, all samples showed a weight loss of less than 2% at 370 °C. Due to the all-aromatic nature of the oligomers, they are insoluble in solvents suitable for GPC analysis or inherent viscosity measurements. This means we were unable to confirm the molecular weight of our oligomers.

3.3 Results and discussions

In section 3.3.1 we will discuss the thermal properties of the reactive and non-reactive end-groups. Both the reactive and the non-reactive end-groups could be prepared in high yields using standard acid-catalyzed imidization technique, as shown in Figure 3.2 and Figure 3.3.

From section 3.3.2 on, we will discuss the thermal, rheological, thermo-mechanical and mechanical results of the oligomers and their cured counterparts. All the three oligomers, 2R, 1R-1NR and 2NR, could be prepared in high yields by using a one-pot melt polycondensation technique.

The accuracy of the reported characteristic temperatures and mechanical properties is

the same as reported in Chapter 2.

3.3.1 End-groups thermal properties

Thermal stability of both reactive and non-reactive end-groups was analyzed with thermogravimetric analysis (TGA), and the results are shown in Figure 3.4. Reactive end-groups PE-COOH and PE-OAc show a weight loss less than 5% when exposed to temperatures below 330 °C and 310 °C, respectively. On the other hand, non-reactive end-groups NR-COOH and NR-OAc show lower values of thermal stability, with 5% of weight loss at 280 °C for NR-OAc and 297 °C for NR-COOH. The consequences on the final properties of the oligomers given by the difference of the thermal stability between the R and NR end-groups will be analyzed in Section 3.3.2 and 3.3.4.

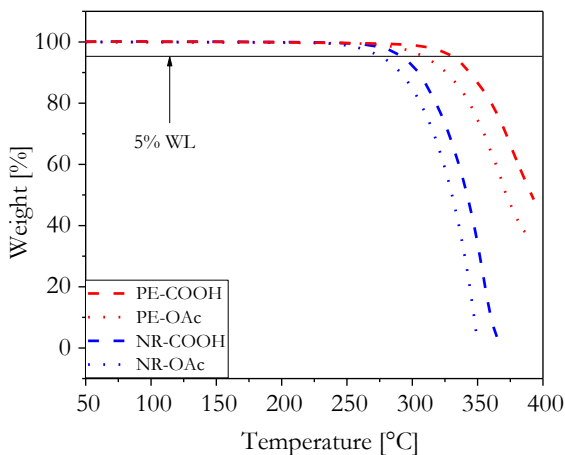


Figure 3.4 TGA signals for the PE-OAc, PE-COOH (red) and NR-OAc, NR-COOH (blue) end-groups. The traces were recorded at a heating rate of 10 °C/min in nitrogen atmosphere.

The thermal behavior of the end-groups was investigated using DSC, and the results are shown in Figure 3.5. All compounds synthesized show sharp endothermic peaks in correspondence of the melting points, 348 °C for PE-COOH, 235 °C for PE-OAc, 294 °C for NR-COOH and 248 °C for NR-OAc.

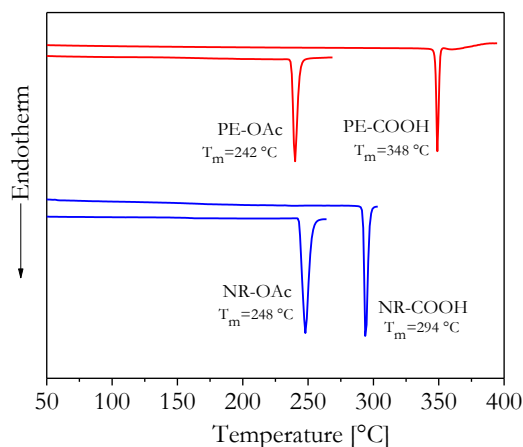


Figure 3.5 DSC signals for the PE-OAc, PE-COOH (red) and NR-OAc, NR-COOH (blue) end-groups. The traces were recorded at a heating rate of 20 °C/min in nitrogen atmosphere.

3.3.2 Thermal properties of oligomers

Table 3.2 Thermal properties of the liquid crystalline reactive and non-reactive oligomers and their cured polymers.

Sample	T_g Oligomer [°C]	T_{k-ic} ^b Oligomer [°C]	T_d N ₂ ^c Cured Oligomer [°C]	Char Yield ^d Cured oligomer [wt % at 595 °C]
2R	Not detected	284	475	55
1R-1NR	150	307	477	53
2NR	Not detected	296	467	50

^a T_g data obtained by DSC experiments, performed at a heating rate of 20 °C/min, N₂ atmosphere.

^b T_{k-ic} data obtained by DSC experiments, performed at a heating rate of 20 °C/min, N₂ atmosphere.

^c Thermal stability evaluated by dynamic TGA on fully cured samples (the samples were cured by isothermal hold at 370 °C for 60 minutes, N₂ atmosphere), heating rate of 10 °C. T_d is defined as the temperature at which a weight loss of 5% occurs.

^d Char yield expressed as weight % at 595 °C.

3.3.2.1 TGA Analysis

The thermal stability of the cured samples was investigated using dynamic thermogravimetric analysis (TGA). After curing the oligomers at 370 °C for 60 minutes, all the samples were analyzed from 50 °C to 595 °C with a heating rate of 10 °C/min under a nitrogen atmosphere. In order to evaluate the thermal stability of the samples the decomposition temperature T_d was defined at the temperature where 5% of weight loss was observed. For all samples, high values of T_d and char yield at 595 °C are measured, in the range of 467-477 °C and 50-55% respectively (data shown in Table 3.2). The TGA curves for the three oligomers are shown in Figure 3.6. The decomposition behavior of 2R and 1R-1NR are similar and the T_d values are in the same range (475 and 477 °C). Due to the negligible difference in thermal stability for this two samples, the contribution given by two or one reactive end-groups plays a minor role compared to the contribution of the polymer backbone.

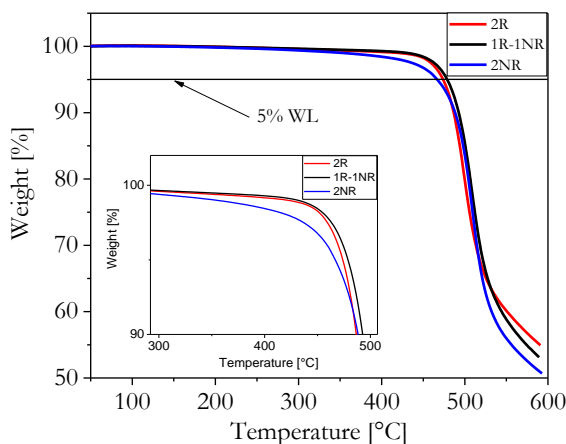


Figure 3.6 TGA signals of fully cured oligomers 2R (red), 1R-1NR (black) and 2NR (blue). Measured at a heating rate of 10 °C/min in nitrogen atmosphere.

3.3.2.2 DSC Analysis

The thermal behavior, glass transition temperature (T_g) and melting temperature (T_{k-lc}) of the oligomers, was studied with differential scanning calorimetry (DSC). The DSC traces are summarized in Figure 3.7, and the results shown in Table 3.2.

Only the 1R-1NR oligomer shows a discernible T_g of 150 °C. The other two oligomers do not exhibit a clear T_g but based on the fact that they have the same polymer backbones and a predicted M_n of 10,000 g/mol they are expected to have similar T_g 's.

The T_{k-lc} range for the three oligomers is between 284 and 307 °C, hence the T_{k-lc} transitions seem not to be drastically affected by the use of different end-groups, as is evident from Figure 3.7. When examining the melt behavior, the 2R oligomer has a ΔH_f of 8.0 J/g, 1R-1NR = 11.0 J/g and 2NR has a ΔH_f of 14 J/g. The minimal, though clear, trend in ΔH_f of the oligomers, is very likely to be caused by the suppress in crystallisation as a result of the bulky phenylethynyl end-groups in the 2R and 1R-1NR oligomers.

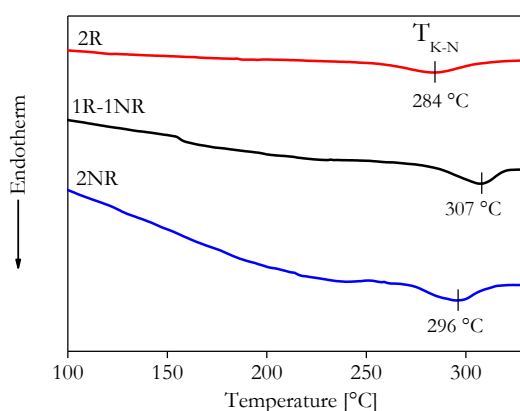


Figure 3.7 DSC traces of the oligomers 2R (red), 1R-1NR (black) and 2NR (blue). Measured at a heating rate of 20 °C/min in nitrogen atmosphere.

Besides the thermal behavior of the oligomers, cured polymers as hot pressed thin films were studied with DSC, in order to evaluate how the presence of the end-groups affects the thermal behavior. The results are shown in Figure 3.8 where for the 2NR film the presence of a clear endothermic peak at 420 °C was taken to indicate the melting of crystalline domains. In contrast, no such peaks were detected for the 2R and 1R-1NR films, but both films showed broad exothermic events above 400 °C. Given that the curing was performed at the lower temperature of 370 °C these exothermic events are attributed to chain extension and crosslinking reactions involving the remaining unreacted phenylethynyl end-groups. An explanation for this phenomenon is that the presence of reactive end-groups suppresses the crystallization, hence it's not possible to

discern an endothermic peak. Simultaneously, exothermic signal of the residual curing, if present, could also be superimposed on an endothermic melting event, preventing a clear view on the latter.

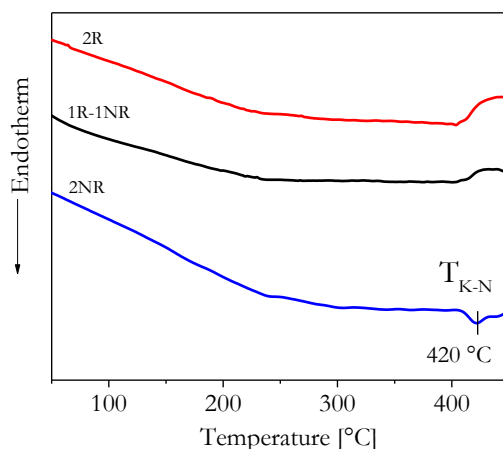


Figure 3.8 DSC traces of fully cured films of 2R (red), 1R-1NR (black) and 2NR (blue), first heat. Measured at a heating rate of 20 °C/min in nitrogen atmosphere.

3.3.3 Polarized optical microscopy

The melt behavior of the oligomers was investigated with an optical microscope equipped with cross polarizers and a hot stage and by heating the samples the melting range of the reactive oligomers and the phase behavior could be determined.

Samples were heated with a heating rate of 50 °C/min up to the melting temperature, and the 2NR oligomers showed nematic textures, as can be seen in a representative example in Figure 3.9. The oligomers were then cured at 370 °C for 60 minutes and none of the samples showed a nematic-to-isotropic (N-I) phase transition during or after curing. Only a nematic phase could be observed, as shown in Figure 3.9, indicating that the curing chemistry doesn't interfere with the mesophase stability.⁸

As already observed by Mazhar et al. for LC oligomer end-capped with reactive phenylethynyl end-groups,¹¹ after 1 hour hold at 370 °C the viscosity of the 2R sample increased dramatically upon solidification. On the other hand, after 60 minutes isothermal hold at 370 °C the mobility of the melt of the 1R-1NR and 2NR samples was

more notable when compared to the 2R one. A more exact analysis on the mobility of the melt behavior will be discussed in Section 3.3.4.

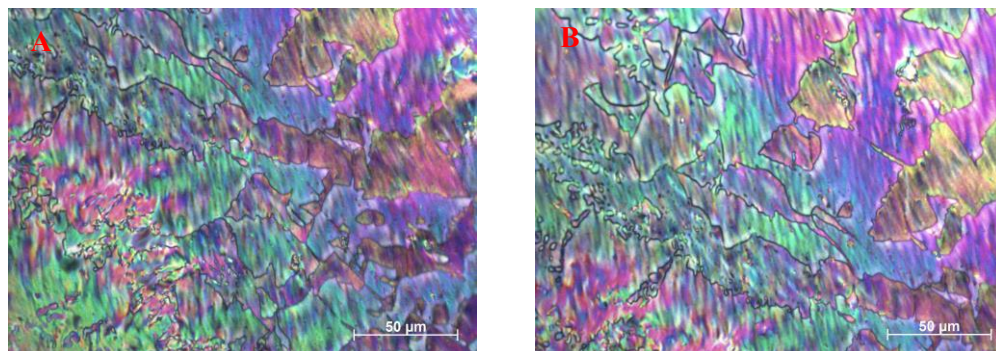


Figure 3.9 A - Nematic textures of oligomers 2R just heated to 370 °C, observed by polarized microscopy. B- Nematic textures of cured oligomers 2R after 60 minutes of isothermal hold at 370 °C, observed by polarized microscopy.

3.3.4 Rheology

Oligomer melt viscosities and curing behavior were investigated by analyzing the samples using a parallel-plate rheometer. Figure 3.10 shows cure behaviors for 2R, 1R-1NR and 2NR oligomers. For all three oligomers, the viscosity starts decreasing when the melting temperature of the oligomers is reached, and after touching a minimum it increases when the end-groups are activated, resulting in chain-extension and crosslinking. Not only the curing temperature, but also the reactive end-groups concentration plays a role in the curing mechanism.⁷ A higher concentration of end-group will result in a predominance of crosslinks, while a lower concentration will lead to a prevalence of chain-extension reactions. After a one hour hold at 370 °C, the complex melt viscosity of the 2R oligomer exceeds that of the 1R-1NR sample, caused by the higher concentration of reactive end-groups in 2R, leading to both chain extension and crosslinking, whereas in the 1R-1NR oligomer, chain-extension is expected to be the predominant polymerization mechanism. Moreover, it is evident from Figure 3.10 that the 2R oligomer shows a faster cure when compared to the 1R-1NR reactive oligomer, which is again due to the presence of a higher amount of reactive end-groups.

As can be seen in Figure 3.10, the behavior of the 2NR oligomer appears to be similar

to 1R-1NR, despite the fact that no reactive end-groups are present that can react in the 2NR sample. After reaching the minimum value, the viscosity of 2NR oligomer increases during the isothermal hold at 370 °C. A possible explanation for this behavior can be the increase of molecular weight of 2NR oligomer due to the lower thermal stability of the non-reactive end-groups. When exposed to the isothermal hold at 370 °C, the non-reactive end-groups will decompose subliming, leaving polymer chain-ends free to react with each other. An increase in molecular weight will result in an increase of viscosity that is evident in Figure 3.10. Judging from these results we conclude that the presence of reactive end-groups at both chain ends is beneficial in terms of achieving the higher after-cure viscosity and the faster cure rate. In addition, the curing of the polymer with one reactive end-groups leads to a similar behaviour compared to 2NR, due to the fact that this system is not fully non-reactive.

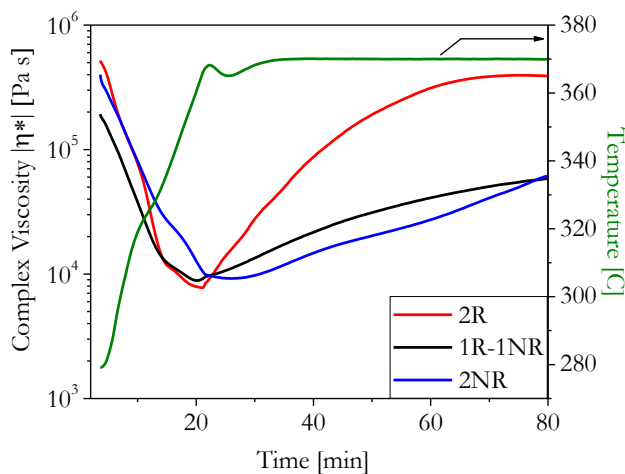


Figure 3.10 Complex melt viscosity for 2R (red), 1R-1NR (black), 2NR (blue) oligomers as a function of temperature and a 60 minutes isothermal hold at 370 °C. Experiments were performed using a frequency 5 rad/s and a heating rate of 5 °C/min and under N₂ atmosphere. The green line represents the imposed temperature profile.

3.3.5 X-ray diffraction analysis

Wide angle X-ray diffraction studies were performed on cured films in order to investigate whether the presence and amount of end-groups affect the morphology of the samples. Figure 3.11 shows the diffraction pattern at 25 °C of the cured films. In

both diffraction patterns of powders and films, a peak at 2θ angle of 19° and a low shoulder peak centered at 26.5° is observed. Both peaks are reported to be characteristic for main chain nematic liquid crystal polymers.¹² By using the Bragg equation it is possible to correlate the 2θ angle with the d-spacing, so the $2\theta = 19^\circ$ is associated with a distance of 4.5 \AA , the average intermolecular spacing between rod-like liquid crystalline mesogens.¹³ The shoulder-peak at 26.5° corresponds to a d-spacing of 3.3 \AA that is the (211) crystallographic plane of poly-HBA (pHBA), indicating the presence of pHBA crystallite in the films.¹⁴

Despite the presence of a small melting peak detected with DSC for the 2NR film, see Figure 3.8, the corresponding peak in the diffraction pattern was not observed. This peak can be obscured by the broad peak centered at 2θ angle of 19° , see Figure 3.11.

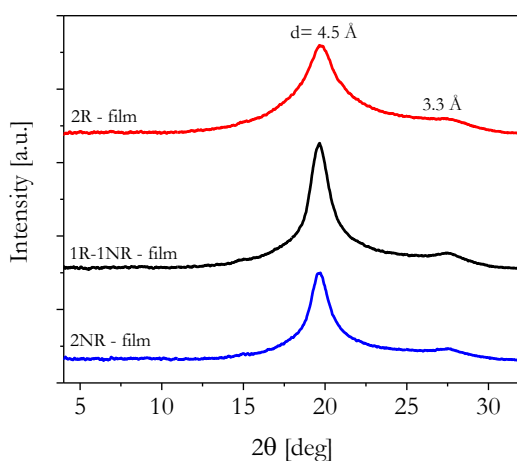


Figure 3.11 XRD intensity as function of scattering angle 2θ of cured films of 2R (red), 1R-1NR (black), 2NR (blue). Measurement performed at 25°C .

3.3.6 Dynamic Mechanical Thermal Analysis

Dynamic Mechanical Thermal Analysis (DMTA) was performed on thin films (0.25 mm) at a frequency of 1 Hz in the temperature range of 0°C to 475°C with a heating rate of $2^\circ\text{C}/\text{min}$ under a nitrogen atmosphere to study the thermo-mechanical behavior. The results are summarized in Table 3.3 and in Figure 3.12 the storage moduli as a function of temperature are shown. The T_g values are defined as the second derivative of E' .

Storage moduli are reproducible with accuracy of $\pm 6.0\%$

The 2R sample has a higher T_g than the 1R-1NR and the 2NR caused by the higher number of crosslinks reducing the mobility of the polymer. Another proof of the higher concentration of crosslinks is found in Figure 3.12 when comparing the storage moduli of 2R and 1R-1NR above T_g : with 2R a rubber plateau is present from 250 to 400 °C, while for 1R-1NR a rubber plateau can be observed over a much narrower temperature range, between 220 and 285 °C, followed by a subsequent drop at 290 °C due to melting of the crystal phase. The E' signals for both polymer films 2R and 1R-1NR, show evidence of crosslinking with the crosslink density in 2R being higher. The 2NR sample has a T_g of 125 °C, showing that the glass transition temperature is lowered when no crosslinks or chain-extension are present. The 2NR samples repeatedly failed prematurely at temperatures around 275 °C.

The storage moduli of both 2R and 1R-1NR have similar values at 25 °C, 6-6.5 GPa, whereas the 2NR display an E' of 8.5 GPa. This higher value of the storage modulus can be explained by the fact that the presence of the non-reactive end-groups does not suppress crystallization, which leads to a higher E' , compared to 2R and 1R-1NR.

Table 3.3 Storage Modulus (E') and T_g data of the fully cured films as determined by dynamic mechanical thermal analysis (DMTA).

Sample	E' [GPa] 25 °C	E' [GPa] 100 °C	E' [GPa] 200 °C	E' [GPa] 300 °C	T_g [°C]
2R - film	6.0	4.0	0.4	0.1	150
1R-1NR - film	6.5	4.7	1.0	0.2	135
2NR - film	7.7	5.4	0.8	/	125

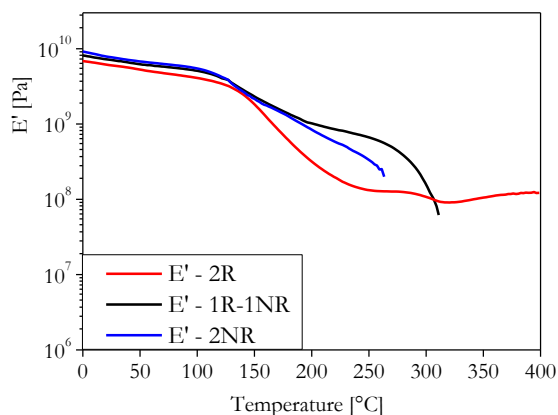


Figure 3.12 Storage moduli of the films: 2R (red), 1R-1NR (black) and 2NR (blue). All measurements were conducted at a frequency of 1 Hz, heating at 2 °C/min in N₂ atmosphere.

3.3.7 Mechanical properties

Tensile tests were performed following the ASTM D-1078-10 in order to investigate the effect of the end-groups on the mechanical properties of the polymers at 25 °C. All samples could be processed into thin films and then cut into dog-bone specimens by using a dog-bone shaped die. A representative example of stress-strain curves is provided in Figure 3.13, where the best results for each sample, 2R, 1R-1NR and 2NR, are shown.

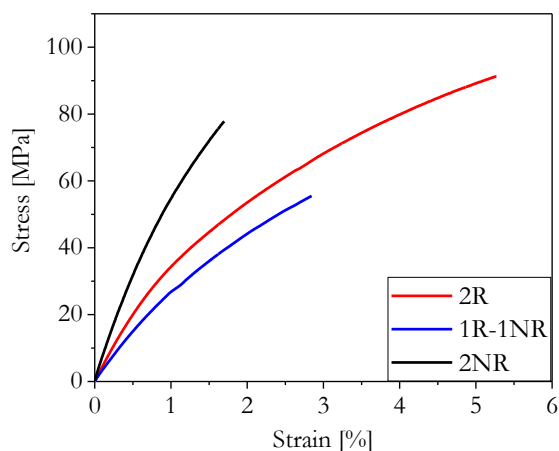


Figure 3.13 Stress-strain curves of cured films, 2R (red) and 1R-1NR (black) and 2NR (blue). The best results of each sample shown is presented as illustrative example. Test speed was 0.25 mm min⁻¹, all data were collected at room temperature.

In Table 3.4 the apparent static stiffness, the strength at break and elongation at break are listed, each value calculated as an average of five specimens. The same values are shown as bar plot in Figure 3.14 in order to better visualize and compare the results.

The apparent static stiffness values reported, being determined from force-crosshead displacement data are to be considered as lower bound estimates.

Table 3.4 Tensile properties of the films. The data shown is an average and standard deviation of 3 tensile specimens.

Films	Apparent static stiffness [MPa] ^a	σ at break [MPa] ^a	ϵ at break [%] ^a
2R - film	3700 (532)	85.5 (8.2)	4.1 (0.8)
1R-1NR - film	2900 (238)	51.1 (4.9)	2.4 (0.51)
2NR - film	5900 (490)	77.5 (7.1)	1.9 (0.2)

^a Tensile tests performed with a strain rate of 0.25 mm/min on a load cell of 1 kN, 25 °C and air atmosphere.

From the values shown in Table 3.4 it is evident that the 2R cured film exhibits higher strength at break when compared to the corresponding cured 1R-1NR and 2NR. As for the strain at break, the average value of the 2R is almost twice as the value of the 1R-1NR and more than double of the 2NR. The 2R sample shown in Figure 3.13 reaches maximum values of strain at break above 5%, exceeding the typical values of strain for thermoset polymers.^{15, 16}

The 2R-polymer films was created using oligomers with reactive end-groups at both chain ends yielded the highest strength and failure strain values. Somewhat surprising the highest apparent static stiffness values were determined for the 2NR system, but there is no obvious explanation why this is the case other than due to a measurement error. The low failure strain level is more in accordance with expectations.

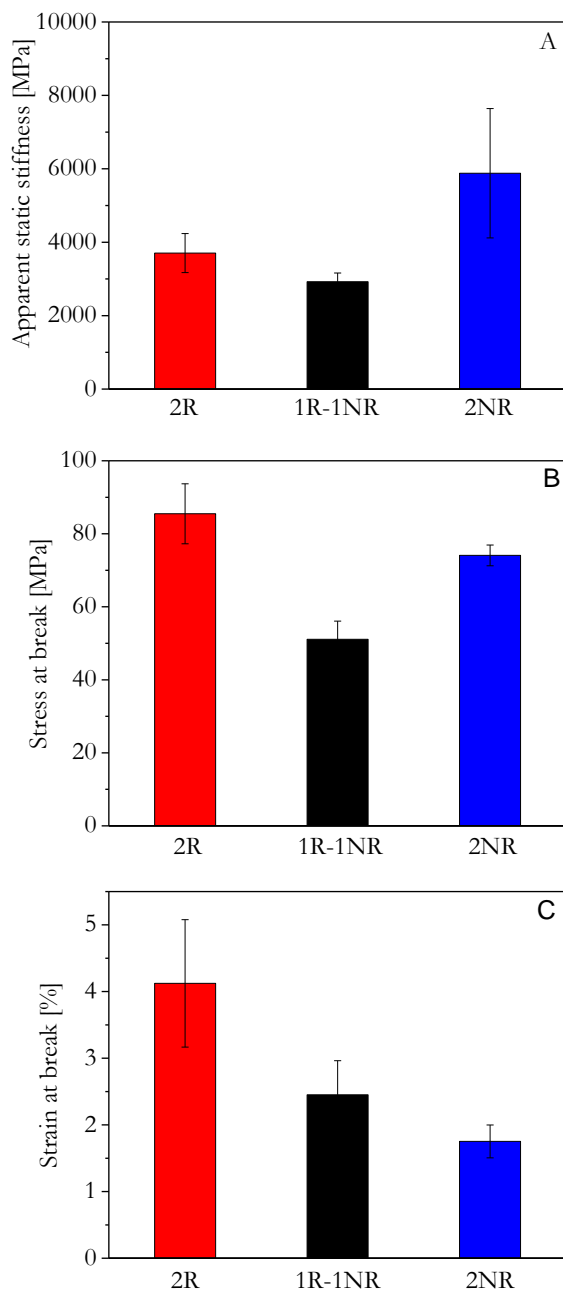


Figure 3.14 Room temperature tensile properties of the cured films (average and standard deviation values based on tests of 5 specimens). A- Apparent static stiffness. B- Stress at break. C- Strain at break.

3.4 Conclusions

We have synthesized and characterized a series of all-aromatic LC thermosetting oligomers based on HBA, BP, TA and (10%)IA. The oligomers synthesized were end-capped with reactive (R) and non-reactive (NR) end-groups. The results presented in this chapter prove that oligomers end-capped with reactive end-groups at each chain end of the liquid crystal oligomers are essential to obtain thermosets with the optimal thermo-mechanical properties, such as T_d , T_g , mechanical properties and stress and strain at break. Moreover, it has been proven that the curing rate is much faster and leads to a higher viscosity when compared to samples end-capped with one or no reactive end-groups. To the best of our knowledge, this is the first time that an analysis and comparison are performed on (thermo)mechanical properties of fully cured oligomers end-capped with phenylethynyl reactive and groups and their non-reactive counterparts, proving the importance of using reactive end-groups at both chain ends for obtaining the optimal (thermo)mechanical results.

By analysing the samples with optical microscopy and XRD we conclude that the presence of both R and/or NR end-groups does not affect the liquid crystalline mesophase of the cured polymers. From TGA analysis it has been proven that the thermal stability of the oligomers is not highly affected by the type of end-groups present. Viscosity analysis of the curing process showed faster kinetics in the 2R oligomer compared to 1R-1NR and 2NR, whereas the minimum viscosities are comparable: in this case the type of end-groups does not interfere with the melt viscosity of the oligomers. Moreover, the 2NR oligomer shows a similar curing process compared to the 1R-1NR oligomer. This unexpected behaviour can be attributed to the fact that the non-reactive end-groups sublime at the curing temperature, leaving polymer chain-ends free to react, increasing the molecular weight hence the viscosity.

While the study in this *Chapter* was not performed on the polymer with the optimal backbone which could lead to the optimal processing and (thermo)mechanical properties identified in Chapter 2, we believe that the findings of this chapter would also apply to the 5N polymer presented in Chapter 2.

3.5 References

- [1] Chang, S., Han, C. D., *Macromolecules*, 1996, 29, 2103
- [2] Bhowmik, P. K., Han, H., *Macromolecules*, 1993, 26, 5287
- [3] Dingemans, T.J., *Polymer Science: A Comprehensive Reference*, (Ed: M. Möller), Elsevier, Amsterdam 2012, 753
- [4] Dingemans, T.J., Knijnenberg, A., Iqbal, M., Weiser, E., Stclair, T., *Liquid Crystals Today*, 2006, 15, 19
- [5] Hergenrother, P. M., *High Performance Polymers*, 2003, 15, 3
- [6] Bryant, R. G., Jensen, B. J., Hergenrother, P. M., *Journal of Applied Polymer Science*, 1996, 59, 1249
- [7] Roberts, C. C., Apple, T. M., Wnek, G. E., *Journal of Polymer Science Part A: Polymer Chemistry*, 2000, 38, 3486
- [8] Knijnenberg, A., Weiser, E., StClair, T., Mendes, E., Dingemans, T.J., *Macromolecules*, 2006, 39, 6936
- [9] Lima, L. d. M. , Castro, P., Machado, A. L., Fraga, C. A. M., Lugnier, C., de Moraes, V. L. G., Barreiro, E. J., *Bioorganic & medicinal chemistry*, 2002, 10, 3067
- [10] Furniss, B.S., Hannaford, A.J.; Smith, P.W.G.; Tatchell, A.R., *Vogel's Textbook of Practical Organic Chemistry*, Longman Scientific & Technical, New York 1991
- [11] Iqbal, M., Norder, B., Mendes, E., Dingemans, T.J., *Journal of Polymer Science Part A: Polymer Chemistry*, 2009, 47, 1368
- [12] D. J. Wilson, C. Vonk, A. Windle, *Polymer*, 1993, 34, 227
- [13] D. Acierno, F. P. La Mantia, G. Polizzotti, A. Ciferri, B. Valenti, *Macromolecules*, 1982, 15, 1455
- [14] Wei, P., Cakmak, M., Chen, Y., Wang, X., Wang, Y., Wang, Y., *Journal of applied polymer science*, 2014, 131
- [15] Iqbal, M. (2010). *All-aromatic Liquid Crystal Thermosets and Composites Thereof*. Ph.D. Thesis. Delft University of Technology: The Netherlands
- [16] Guan, Q. (2016). *Design, Synthesis and Characterization of Novel (Multiblock) Copoly(esterimide)s and their Shape-memory Properties*. Ph.D. Thesis. Delft University of Technology: The Netherlands

CHAPTER 4

Exploring the role of 2,6-naphthalene dicarboxylic acid

Abstract

In this chapter we have performed backbone modifications of one of the most rigid LCT formulations known to date, which is based on 4-hydroxybenzoic acid (HBA), terephthalic acid (TA) and 4,4'-biphenol (BP). During the synthesis we have inserted a fourth co-monomer, 2,6-naphthalene dicarboxylic acid (NDA) at the expenses of TA, NDA being responsible of improving the processability of the oligomer. To gain a better understanding of how the presence of NDA affects the thermal and thermo-mechanical properties after curing, we have synthesized a series of 4 reactive oligomers, varying the amount of NDA: 0% (reference), 1, 2.5 and 5 mol%. The new LCT formulations exhibit high decomposition temperatures (T_d , temperature at which 5% weight loss occurs) independently of the amount of NDA present in the backbone, on the contrary the polymer ease of processing (T_{k-lc} and the melt viscosity) has been highly affected by the presence of NDA: the higher NDA-mol%, the lower the T_{k-lc} and the melt viscosity. The glass transition temperature (T_g) of fully cured films, on the other hand, drops from 380 to 243 °C when increasing the amount of NDA to 5 mol%. In addition, the stress and strain at break of thin films show higher values when increasing the amount of NDA into the backbone, reaching values of 85 MPa for the stress at break and 4% elongation at break for the sample with 5 mol% of NDA. All samples showed Young's modulus values above 3 GPa.

4.1 Introduction

One of the main challenges when working with thermotropic liquid crystalline polymers (LCP) is their high melt viscosity; a fact that is not surprising as most of the main-chain thermotropic LCP chemistries are characterized by a rigid aromatic backbone. Over the past 40 years there have been many researchers, both in academia and industry, who focused on improving the processability of thermotropic LCPs. The research described in *Chapter 2* of this thesis, which has expanded on the work published by Iqbal et al.,¹ describes two different approaches on how to improve the melt processability of one of the most rigid backbone LCPs known to date. One of the approaches is to lower the crystalline-to-nematic (T_{k-lc}) transition of the polymer by introducing co-monomers, which will reduce the inter molecular interactions, but at the same time maintain overall chain stiffness and linearity.²⁻⁶ This approach is referred to as the frustrated chain-chain packing method,^{7, 8} and the most commonly used co-monomers are crank-shaft type monomers such as 6-hydroxy-2-naphthoic acid (HNA), 2,6-naphthalene dicarboxylic acid (NDA) or monomers that introduce a 120° exo-cyclic bond angle in the polymer backbone, e.g. isophthalic acid and resorcinol.

In this Chapter we will report on the use of a particular crank-shaft type monomer for backbone modification and processability improvement: 2,6-naphthalene dicarboxylic acid, here called NDA. The monomer is shown in Figure 4.1.

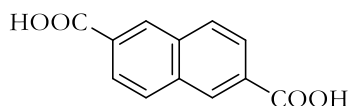


Figure 4.1 2,6-naphthalene dicarboxylic acid (NDA) monomer.

The use of NDA introduces an offset in the polymer main-chain, however maintaining at the same time the overall linearity. Over the years it has been demonstrated that NDA, together with other 2,6-naphthalene based units, is one of the monomers that has produced the best results in terms of improving processability of main-chain fully aromatic thermotropic polymers. Already at the beginning of the 80s several research

groups were working on improving LCP processing by using NDA as an additional co-monomer, Calundann et al. for Celanese,⁹ Jackson et al. for Eastman^{10, 11, 12} and Kleinshuster et al. for DuPont.^{13, 14}

The scope of this chapter is to explore the role of NDA and how its presence affects the (thermo)mechanical properties of the final after-cure liquid crystalline polymer. The reference liquid crystalline precursor used for our work is based on one of the most rigid formulation known to date, which is prepared from 4-hydroxybenzoic acid (HBA), terephthalic acid (TA) and 4,4'-biphenol (BP), based on the commercial LCP *Xydar*TM.^{15, 16} Here we present 4 liquid crystal oligomer precursors with approximately the same M_n (10,000 g/mol, labelled 10K) with different mol% of NDA. The number average molecular weight (M_n) of the oligomers has been controlled with the use of phenylethynyl reactive end-groups, for details see *Chapter 2* and *3*. In order not to disrupt the unique molecular packing preferences that result in mesophase behavior, only small backbone modifications up to 5 mol% were considered. NDA has always been inserted only at the expenses of TA. Below in Table 4.1 we listed the oligomer formulations synthesized, and Figure 4.2 shows the backbone structure of the reference oligomer 0N and the modified ones with NDA.

Table 4.1 Oligomer formulations with corresponding names, based on backbone modification by inserting 2,6-naphthalene dicarboxylic acid co-monomer. The reference polymer backbone is based on HBA(60%)/BP(20%)/TA(20%)

Backbone formulation	Oligomer name
<u>Reference</u> HBA(60%)/BP(20%)/ TA(20%)-10K	0N
HBA(60%)/BP(20%)/TA(19%)- NDA(1%) -10K	1N
HBA(60%)/BP(20%)/TA(17.5%)- NDA(2.5%) -10K	2.5N
HBA(60%)/BP(20%)/TA(15%)- NDA(5%) -10K	5N

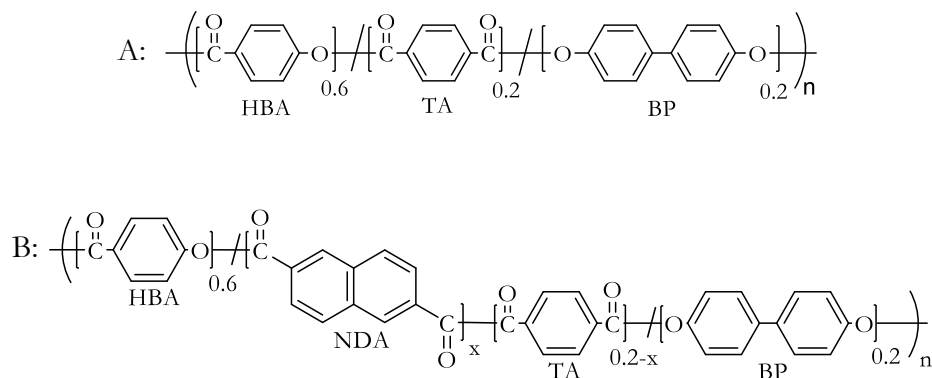


Figure 4.2 Oligomer backbone formulations. A: reference oligomer. B: Oligomer modified with NDA co-monomer.

While the main aim of this chapter is to study the effect of using NDA as a co-monomer, it is important to consider the physical properties of the N-series in perspective of using the N-series oligomers as resins in fiber reinforced composites, hence thermal stability and processability are to be considered important parameters as well.

4.2 Experimental

4.2.1 Materials

All the chemicals used for synthesis of end-groups and the oligomers were obtained from the indicated sources and used as received. For the synthesis of the reactive end-groups, 4-phenylethynylphthalic anhydride (PEPA) was purchased from Hangzhou Chempro Tech Co; acetic acid, 4-aminobenzoic acid, and acetic anhydride were received from Sigma-Aldrich, and 4-aminophenol from Acros Organics. For the synthesis of the reactive oligomers, 4,4'-biphenol (BP) and 2,6-naphthalenedicarboxylic acid were purchased from TCI, and 4-hydroxybenzoic acid (HBA), terephthalic acid (TA), 6-hydroxy-2-naphthoic acid (NDA), acetic anhydride and potassium acetate were obtained from Sigma-Aldrich.

4.2.2 Characterization

The thermal stability of the cured polymers was analyzed by dynamic thermogravimetric analysis (TGA) using a Perkin-Elmer Pyris Diamond TG/DTA. Samples were investigated using a heating rate of 10 °C/min under a nitrogen atmosphere. Thermal properties of the reactive oligomers and cured polymers were investigated using a Perkin-Elmer Sapphire DSC, all measurements conducted under a nitrogen atmosphere with a heating rate of 20 °C/min.

The melt and cure behavior of the oligomers were studied with Thermoscientific Mars III parallel-plate rheometer equipped with a force-rebalanced transducer. Tests were performed at a frequency of 5 rad/sec and heating rate of 5 °C/min under a nitrogen atmosphere. Sample disks of 8 mm diameter and 0.5 mm thickness were prepared by compression molding.

Dynamic mechanical thermal analysis was performed on a Perkin-Elmer Diamond DMTA, using cured thin films (20 mm x 5 mm x 0.25 mm) under a nitrogen atmosphere with a heating rate of 2 °C/min and frequency of 1 Hz, static tension force of 2000 mN, minimum tension force of 200 mN, tension gain of 1.5 and length amplitude of 5 µm.

Tensile tests on hot pressed fully cured thin film (18 mm x 5 mm x 0.25 mm) were performed at 25 °C with a strain rate of 0.25 mm/min, using an Instron Model 3365 universal testing systems equipped with 1 kN load cell.

4.3 Results and discussion

The reactive end-groups, and all the reactive oligomers, could be prepared in high yields, the synthetic details are discussed in Chapter 2. From Paragraph 4.3.1 to Paragraph 4.3.5 the rheology and (thermo)mechanical analyses of the reactive oligomers is described. In Table 4.2 we summarized the results of the thermal and rheological analyses. The uncertainties in the parameters determined are comparable to those defined in Chapter

2 or specified explicitly.

Table 4.2 Thermal properties of the liquid crystalline reactive and non-reactive oligomers and their cured polymers.

Sample	T _{k-le} Oligomer [°C] ^a	Melt viscosity Oligomer [Pa·s] ^b	T _d N ₂ Cured Oligomer [°C] ^c	Char Yield Cured oligomer [wt % at 595 °C] ^d
0N	324	10 ⁴	491	52
1N	320	10 ²	494	53
2.5N	295	10 ²	503	55
5N	285	10 ⁰	501	54

^a T_{k-le} data obtained by DSC experiments, performed at a heating rate of 20 °C/min, N₂ atmosphere.

^b Complex melt viscosity obtained from experiments performed using 20 mm diameter compressed pellets, using a frequency of 5 rad/s and a heating rate of 5 °C/min (N₂ atmosphere).

^c Thermal stability evaluated by dynamic TGA on fully cured samples (the samples were cured by isothermal hold at 370 °C for 60 minutes, N₂ atmosphere), heating rate of 10 °C. T_d is defined as the temperature at which a weight loss of 5% occurs.

^d Char yield expressed as weight % at 595 °C.

4.3.1 TGA analysis

Dynamic and isothermal thermogravimetric analysis has been used to study the thermal stability of the cured oligomers. For both methods, the oligomer powder sample was first cured in the TGA oven chamber at 370 °C for 60 minutes, followed by the actual TGA experiment. Paragraph 4.3.1.1 and 4.3.1.2 describe the results of the Dynamic and Isothermal TGA experiments, respectively.

4.3.1.1 Dynamic TGA

The thermal stability of the cured samples was investigated using dynamic thermogravimetric analysis. After curing the oligomers at 370 °C for 60 minutes, all the

samples were scanned from 50 °C to 595 °C using a heating rate of 10 °C/min in a nitrogen atmosphere. The decomposition temperature (T_d) can be used to evaluate the thermal stability of the samples, where T_d is the temperature at which a 5% weight loss is observed. For all samples, high values of T_d and char yield are measured, in the range of 491-503 °C and 52-55%, respectively (Table 4.2). In Figure 4.3 the T_d values of all the samples are plotted versus the NDA content. It is clear that the presence of NDA at 1, 2.5 and 5% does not really affect the thermal stability and keeps it at high levels.

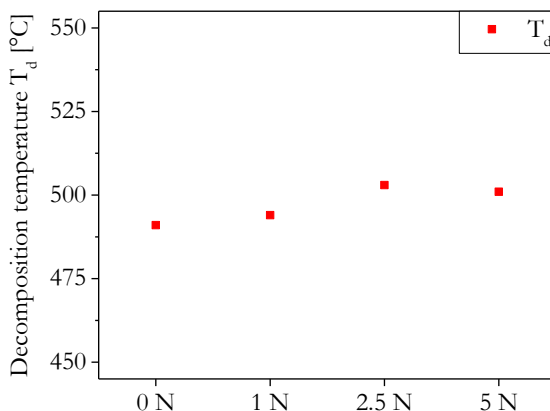


Figure 4.3 Decomposition temperatures (T_d) of the cured oligomers, obtained by TGA analysis. Measured at a heating rate of 10 °C/min in nitrogen atmosphere.

4.3.1.2 Isothermal TGA

Isothermal thermogravimetric analysis experiments were performed to evaluate how the cured oligomers behave when exposed to high temperatures for a prolonged period of time, i.e. 24 hours. After the samples were cured, they were heated to the desired temperature by using a heating rate of 50 °C/min, and then the samples were kept at that temperature for 24 hours. Isothermal hold temperatures used: 200, 250, 300 and 350 °C, the results of the experiments are summarized in Table 4.3 and Figure 4.4, where the value of the final weight, expressed as weight %, of the samples at the end of the test is reported. Not only the N series has been tested, but two commercially available high-performance polymers widely employed in fiber reinforced composites applications have been used as reference material. Our N-series results have been contrasted with

polyphenylene sulfide (PPS) and polyetherketoneketone (PEKK). When testing the samples at temperatures of 200 and 250 °C, all the cured oligomers, PPS and PEKK show a similar decomposition behavior, as in all samples are relatively stable and weight loss is minimal (~1.5%). However, when the isothermal hold temperature was increased to 300 and 350 °C, the difference between the LCT and PPS and PEKK becomes evident, see Figure 4.4 and Table 4.3. Under the most extreme testing conditions, i.e. an isothermal hold of 24 h. at 350 °C, both PPS and PEKK show a final weight loss of 6.5 and 5.5 % respectively, whereas all the samples of the N series show a maximum weight loss of 3 %.

Table 4.3 N series, PPS and PEKK values of weight% residue as a result of an isothermal hold at 200, 250, 300 and 350 °C for 24 hours.

Sample	200 °C Weight [%]	250 °C Weight [%]	300 °C Weight [%]	350 °C Weight [%]
0N	99.8	99.8	98.9	97.0
1N	99.7	99.4	98.7	97.0
2.5N	99.6	99.3	98.4	97.2
5N	99.8	99.2	98.8	97.0
PPS	98.8	98.7	94.67	93.9
PEKK	98.9	98.6	96.4	94.6

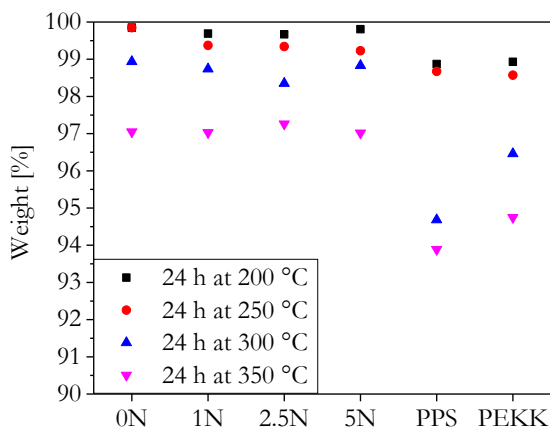


Figure 4.4 N series, PPS and PEKK weight loss values expressed in weight% as a result of isothermal hold at 200, 250, 300 and 350 °C for 24 hours.

4.3.2 DSC analysis

In order to study how the presence of NDA at different weight % affects the melting temperature (T_{k-lc}) of the oligomers, differential scanning calorimetry (DSC) experiments were performed on all the samples. The oligomers were heated from 25 to 370 °C, by using a heating rate of 20 °C/min under a nitrogen atmosphere. The results are summarized in Table 4.2 and the DSC curves are shown in Figure 4.5. The insertion of 1% of NDA in the backbone does not seem to have a major effect on the melting temperature of the oligomer, as it lowers from 324 °C (0N, the reference system) to 320 °C (1N). On the other hand, when increasing the amount of NDA at the expenses of TA, the T_{k-lc} drops by as much as 30 and 35 °C, for 2.5N and 5N respectively. The presence of NDA at different weight % did not have a deleterious effect on the thermal stability of the cured samples, however a remarkable difference can be observed with respect to the onset of melting (T_{k-lc}): by increasing the amount of NDA in the backbone, the T_{k-lc} of the oligomers decreases. As already stated in Chapter 2, there seems not to be a good explanation in the present literature why NDA has such a strong effect on the processing properties.

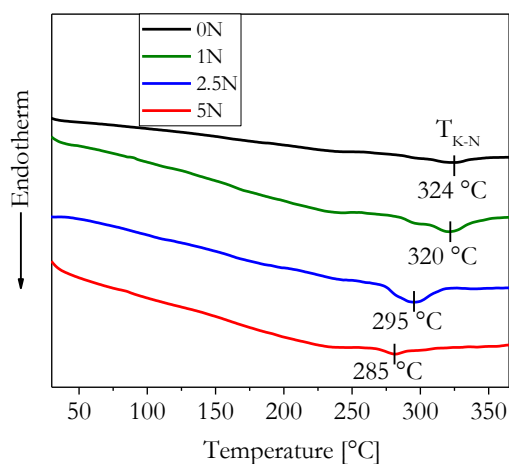


Figure 4.5 DSC signals of the reactive oligomers. First heat, measured at a heating rate of 20 °C/min in nitrogen atmosphere.

4.3.3 Rheology

The melt and cure behavior of the reactive oligomers, from a rheological point of view, were analyzed using a parallel plate rheometer. The disc samples were prepared by compression molding and then heated from 250 to 370 °C, by using a heating rate of 5 °C and a frequency of 5 rad/sec. When the optimal curing temperature¹⁷ was reached, this temperature was held for 60 minutes in order to evaluate the oligomers' behavior when curing. Representative results of the measurements are shown in Figure 4.6, where the complex melt viscosity is plotted vs. time and temperature.

The melt behavior is clearly influenced by the presence of NDA, even if at concentration as low as 1%. The 0N sample shows a viscosity drop at melting of 1.5 orders of magnitude, from 10^6 to $5 \cdot 10^4$ Pa·s, while the viscosity drops of the samples with NDA in the backbone are more dramatic. By only inserting 1% of NDA, the melt viscosity drops of more than 4 orders of magnitude, reaching a minimum of 100 Pa·s, value, which is similar to the minimum viscosity reached by the 2.5N sample as well, as can be seen in Figure 4.6. However, despite the fact that 1N and 2.5N show similar values of melt viscosity, the latter reaches its minimum at 314 °C whereas 1N reaches the lowest viscosity at 351 °C, due to their melting temperature difference, see Figure 4.5. When 5 mol%

NDA was incorporated, the viscosity drops to a 2.5 Pa·s, which is an unprecedented low viscosity for a main-chain all-aromatic liquid crystal 10,000 g/mol oligomer.

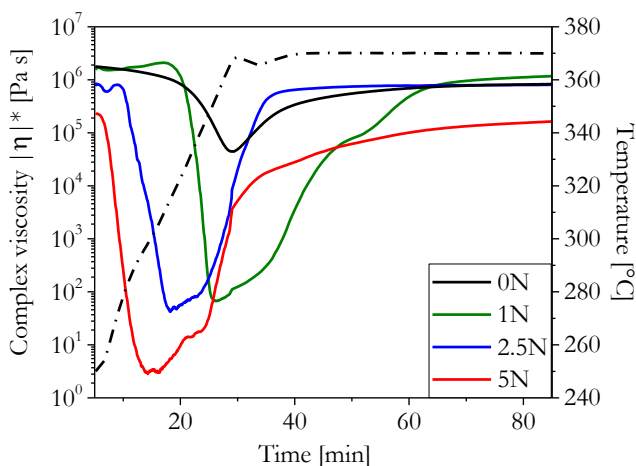


Figure 4.6 Complex melt viscosity of the oligomers ($M_n = 10K$) as function of temperature and a 60 min. isothermal hold at 370 °C. Experiments were performed using 20 mm diameter compressed pellets, a frequency of 5 rad/s and a heating rate of 5 °C/min (N_2 atmosphere). The dashed black line represents the imposed temperature profile.

As stated in this *Chapter's* introduction, together with studying the role of NDA in the polymer backbone of the LCT's, the aim of this work is to select one resin formulation that can be used in fiber reinforced composites. Not only the thermal properties are an important factor, but the processing properties as well, because they will reflect on the ease of composite processing. One of the most utilized high-performance polymers in fiber reinforced composites is polyphenylene sulfide (PPS), and its melt viscosity behavior does not greatly differ from one of the oligomers studied in this *Chapter*, the 2.5N, when considered below its curing temperature. Figure 4.7 shows the comparison of the melt viscosity of PPS and the 2.5N reactive oligomer. It should be pointed out that this low viscosity value is maintained only for a relatively short amount of time at 370 °C, while for PPS the viscosity would barely change with time. This time difference at low viscosity will have a big effect on processability of thicker and larger composite structures.

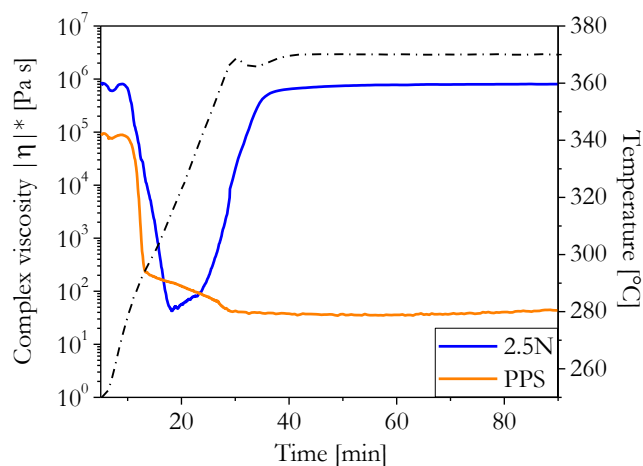


Figure 4.7 Complex melt viscosity of the oligomer 2.5N and PPS as a function of temperature and a 60 min. isothermal hold at 370 °C. Experiments were performed using 20mm diameter compressed pellets, a frequency of 5 rad/s and a heating rate of 5 °C/min (N₂ atmosphere). The dashed black line indicates the imposed temperature profile.

4.3.4 DMTA analysis

Information regarding the glass-transition temperature (T_g) and the storage modulus (E') of the cross-linked LCT films were obtained using dynamic mechanical thermal analysis (DMTA). The measurements were performed on cured films with a thickness of approximately 0.20 mm in a temperature range of 0 to 450 °C, applying a frequency of 1 Hz. Glass transition temperature values are reported as the second derivative of the storage modulus (E'). The storage modulus (E') vs. temperature T signals are shown in Figure 4.8 and summarized in Table 4.4.

Table 4.4 Storage Modulus (E') and T_g data of the fully cured films as determined by dynamic mechanical thermal analysis (DMTA)

Sample	E' [GPa] ^a 25 °C	E' [GPa] 100 °C	E' [GPa] 200 °C	E' [GPa] 300 °C	E' [GPa] 400 °C	T_g [°C] ^b
0N	8.1	5.4	3.5	1.4	0.4	380
1N	7.3	4.9	2.5	0.9	0.2	349
2.5N	6.6	4.2	2.3	1.0	0.1	323
5N	3.7	2.8	0.8	0.2	0.3	243

^a Storage modulus (E') obtained from DMTA analysis performed on fully cured films. Measurement conducted at a frequency of 1 Hz, heating rate of 2 °C/min, N₂ atmosphere.

^b T_g data obtained from DMTA analysis performed on fully cured films, T_g considered as second derivative of E' . Measurements conducted at a frequency of 1 Hz, heating rate of 2 °C/min, N₂ atmosphere.

Sample 0N shows the highest values of E' over the whole temperature range of the series, as expected due to the higher level of backbone rigidity. Moreover, 0N is the sample that retains a high storage modulus all the way up to the onset of the glass transition temperature (T_g) at 380 °C. Samples 1N and 2.5N display similar behavior, however the storage modulus of 2.5N drops at 323 °C, while the one of 1N shows a drop at 349 °C, reflecting the difference of amount of NDA introduced into the backbone. The film with the lowest storage modulus values and glass transition temperature (T_g of 243 °C) is the 5N sample.

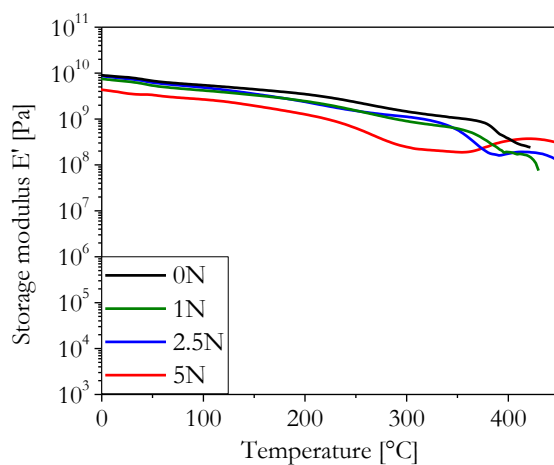


Figure 4.8 Storage moduli (E') of cured thin films (20x5x0.2 mm). All measurements were conducted at a frequency of 1 Hz, a heating rate of 2 °C/min in N_2 atmosphere.

4.3.4.1 *Dynamic Mechanical Thermal Analysis strain behavior*

From the DMTA experiments we could also extract information with respect to the strain behavior of the cured films as a function of temperature.

Figure 4.9 shows the storage moduli of the cured LCT films and the corresponding strains during the DMTA experiments. A line indicating a strain of 5% has been added for reference purposes. In order to better observe the strain behavior, the temperature range of the analysis has been chosen to be from 200 to 450 °C, considering as well the fact that below 200 °C the strain curves are uneventful. It is evident from Figure 4.9 that the strain of the samples is influenced by the glass transition temperature of the polymers, which is highly affected by the rigidity of the polymer backbone. The sample that elongates at the lowest temperature is 5N, as expected due to the lowest T_g value, followed by 2.5N, 1N and lastly 0N.

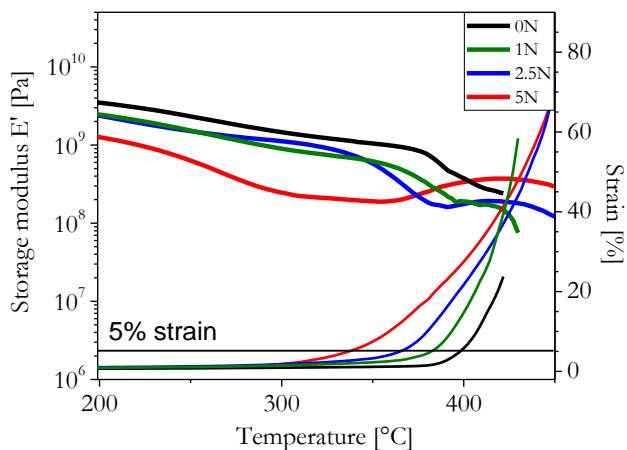


Figure 4.9 Storage moduli and (elastic + viscoelastic) strain values of cured thin films (20x5x0.2 mm). All measurements were conducted at a frequency of 1 Hz and a heating rate of 2 °C/min in N₂ atmosphere.

It is interesting to notice that the abrupt increase of the strain of the samples does not occur in correspondence of the glass transition temperature, as it could be expected, but at a higher temperature. For instance, the 5N sample has a glass transition temperature of 243 °C, however the sample shows an elongation that surpasses the value of 1% only when the temperature is above 290 °C. Different is the case when considering two widely used thermoplastic high-performance polymers, PPS and PEKK. Figure 4.10 shows the storage modulus (E') and elongation of the samples vs. temperature. It is evident that in this case the abrupt variation of the strain occurs concurrently with the glass transition temperature.

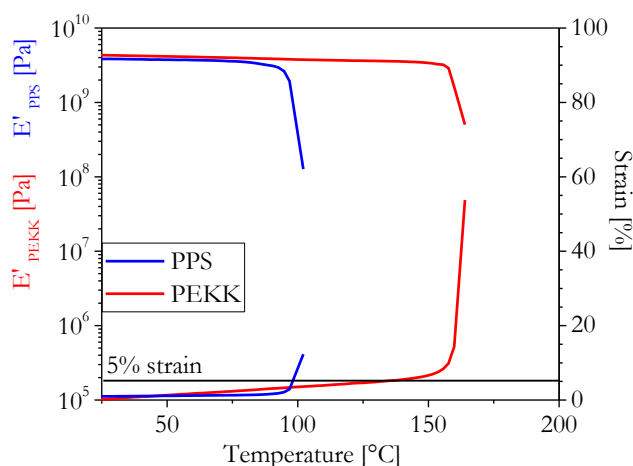


Figure 4.10 Storage moduli and strain values of PPS (blue) and PEKK (red). All measurements were conducted at a frequency of 1 Hz, heating rate of 2 °C/min in N₂ atmosphere.

They fact that the N series samples show straining at temperatures higher than the corresponding glass transition temperatures can be explained by the presence of the reactive end-groups and their ability to form crosslinks, even at relatively low concentration to form oligomers with a molecular weight of 10,000 g/mol.

4.3.5 Thin film tensile testing

Tensile tests were performed, following the ASTM D-1078-10 standard, in order to investigate the effect of the backbone modifications on the mechanical properties of the polymers. All samples could be processed into thin films by using a hot press, films of 8 x 8 cm were then cut into dog-bone specimens by using a dog-bone shaped die. The results are summarized in Table 4.5, while Figure 4.11 shows the results of the analysis as bar plots to better visualize and compare the results. The plots show the apparent static stiffness, strength at break and elongation at break data, each value calculated as an average of three specimen for each polymer. The apparent static stiffnesses were determined from the force – cross-head displacement curves.

Table 4.5 Tensile properties of fully cured thin films. The data shown is an average with standard deviation based on testing 3 tensile specimens per sample.

Sample name	Apparent static stiffness [MPa] ^a	σ at break [MPa] ^a	ϵ at break [%] ^a
0N	3445 (528)	26.0 (2.3)	1.7 (0.5)
1N	4811 (340)	49.6 (5.8)	2.1 (0.7)
2.5N	5120 (118)	81.3 (4.2)	2.5 (0.2)
5N	3872 (490)	85.2 (7.1)	4.1 (0.7)

^a Tensile tests performed on fully cured film samples, with a strain rate of 0.25 mm/min using a load cell of 1 kN, at 25 °C and air atmosphere.

The results of stress at break and strain at break of the series show a clear trend: the higher the backbone flexibility, hence increasing the mol% of NDA, the higher the mechanical performance. While this trend is not a surprise when considering the strain values of a polymer, it is not expected regarding the stress at break. However, due to the lower T_{k-lc} and minimum viscosity values, backbone compositions with a higher amount of NDA have superior ease of processing, which results to higher level of defect-free samples, hence better mechanical properties. With the exception of the 5N specimen, all the other samples showed a strain at break lower than 3%, which can be considered in line with the values of cured liquid crystal aromatic polyesters.^{1, 18}

Without exception, all samples show brittle fracture with very little yielding.

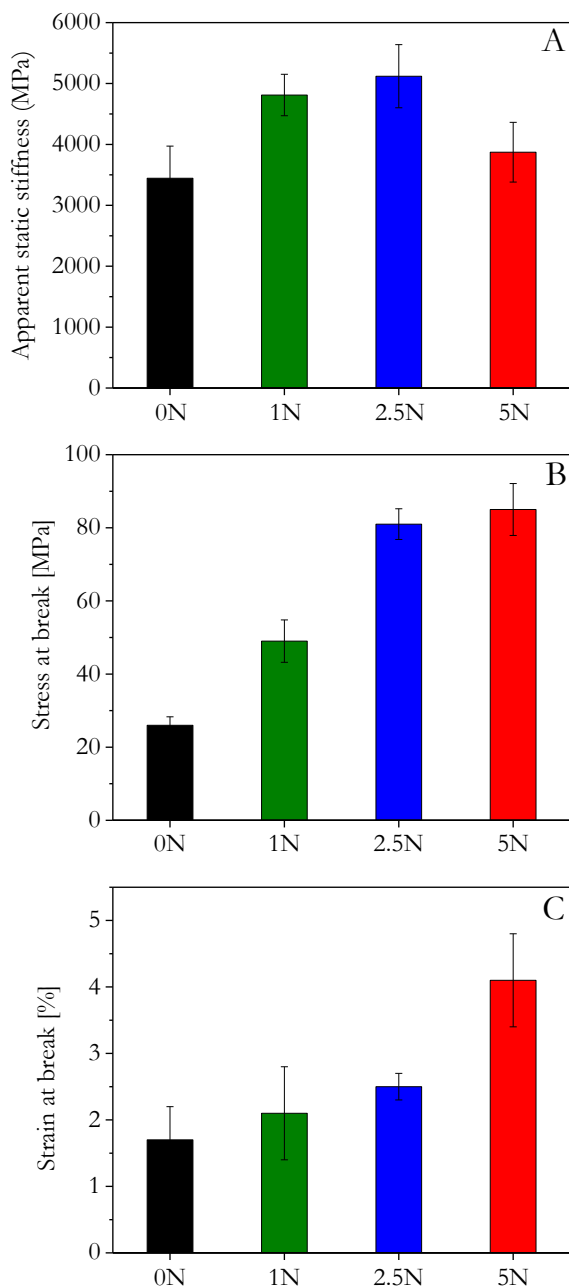


Figure 4.11 Tensile properties of the cured thin films (average and standard deviation values based on tests of 3 specimen). A- Apparent static stiffness. B- Stress at break. C- Strain at break.

4.4 Conclusions

In this Chapter we have explored the influence of 2,6-naphthalene dicarboxylic acid (NDA) when inserted in the backbone of a liquid crystalline oligomer as fourth co-monomer. The starting point for this series was a reference LCT system based on the *Xydar*TM formulation using the monomers 4-hydroxybenzoic acid (HBA), terephthalic acid (TA) and 4,4'-biphenol (BP), with the following molar ratios: HBA(60%)/BP(20%)/TA(20%), named 0N. By inserting NDA as a co-monomer at 1, 2.5 and 5 mol% in the oligomer backbone, 4 different oligomers were synthesised and analyzed.

The presence of NDA at different mol% did not affect the thermal stability of the samples, on the contrary the T_{k-lc} and the complex melt viscosity $|\eta|^*$ of the oligomers appeared to be highly dependent by the amount of NDA present in the backbone. Going from 0N to 5N we observed a decrease in the T_{k-lc} of 40 °C, and a decrease in melt viscosity of 4 orders of magnitude, from 10^4 to 10^0 Pa·s. All cured samples retained high T_g values (from 380 °C for 0N to 243 °C for 5N), however it was clear that the higher the NDA concentration, the lower the thermo-mechanical performance of the final thermoset. Mechanical tests on cured films show that 2.5N and 5N samples give the optimal values in terms of stress and strain at break. Sample 2.5N was then selected to be the resin of choice for our composite work, which will be discussed in Chapter 5. The selection criteria were based on the low melt viscosity of the reactive oligomer and the thermo-mechanical properties of cured thin films.

4.5 References

- [1] Iqbal, M. (2010). *All-aromatic Liquid Crystal Thermosets and Composites Thereof*. Ph.D. Thesis. Delft University of Technology: The Netherlands
- [2] Knijnenberg, A.; Weiser, E.; St.Clair, T.L.; Mendes, E.; Dingemans, T.J. *Macromolecules*, 2006, 39, 6936-6943
- [3] Guerriero, G.; Alderliesten, R.; Dingemans, T.; Benedictus, R. *Progress in Organic Coatings*, 2011, 70, 245-251
- [4] Dingemans, T., Knijnenberg, A., Iqbal, M., Weiser, E., Stclair, T. *Liquid Crystals Today*, 2006, 15(4), 19-24
- [5] Cai, R.; Samulski, E. T.; *Macromolecules*, 1994, 27, 135] [S. Chang; C. D. Han; *Macromolecules*, 1996, 29, 2103
- [6] P. K. Bhowmik; H. Han; *Macromolecules*, 1993, 26, 5287
- [7] Collyer, A.A. (Editor), *Liquid Crystal Polymers: From Structures to Applications*, 1992, pp: 408-412
- [8] Acierno, D., Collyer, A.A. (Editors), *Rheology and Processing of Liquid Crystal Polymers*, 1996, pp: 11-15
- [9] Calundann G.W., Jaffe, M., *Proceedings of the Robert A. Welch Foundation Conference on Chemical Research, XXVI Synthetic Polymers*, 1982, 247-291
- [10] Jackson, W.J., Morris, J.C., Ger Offen Patent 2.834.535, 1979
- [11] Jackson, W.J., Morris, J.C., Ger Offen Patent 2.834.536, 1979
- [12] Jackson, W.J., Morris, J.C., Ger Offen Patent 2.834.536, 1979
- [13] Kleinshuster, J.J., Pletcher, T.C., Shaefgen, J.R., Luise, R.R., Ger Offen Patent 2.520.819, 1985
- [14] Kleinshuster, J.J., Pletcher, T.C., Shaefgen, J.R., Luise, R.R., Ger Offen Patent 2.520.820, 1985
- [15] Hummel, D. O., Neuhoff, U., Bretz, A., Dussel, H.-J., *Macromol. Chem.*, 1993, 194, 1545
- [16] Sueoka, K., Nagata, M., Ohtani, H., Naga, N., Tsuge, S., *J. Polym. Sci., Part A: Polym. Chem.*, 1991, 29, 1903
- [17] Iqbal, M., Norder, B., Mendes, E., Dingemans, T. J., *J. Polym. Sci., Part A: Polym. Chem.*, 2009, 47, 5, 1368–1380

[18] Guan, Q. (2016). *Design, Synthesis and Characterization of Novel (Multiblock) Copoly(esterimide)s and their Shape-memory Properties*. Ph.D. Thesis. Delft University of Technology: The Netherlands

CHAPTER 5

Thermotropic liquid crystal thermosetting resins and their use in carbon- and glass-fiber reinforced composites

Abstract

In this chapter the preparation of LCT carbon- and glass- fiber reinforced composites, and their microstructural and mechanical characterization is reported. The LC oligomer precursor, labelled 2.5N and described in detail in Chapter 4, was used because of its superior processing and thermomechanical properties relative to PPS or PEEK. The composite panels were analyzed macroscopically using the C-scan method and on a micro-level using optical microscopy and X-ray tomography. The mechanical behaviour of the composites was investigated by testing their flexural, compression and in-plane shear properties, and the results are contrasted with polyphenylene sulphide (PPS) carbon- and glass- fiber reinforced composite panels. The results show that PPS composites outperformed our novel early-stage-of-development 2.5N-based composites due to a high volume fraction of pores of relatively large dimensions. The porosity patterns in the thin glass fiber panels was found to differ from that of the thicker carbon fiber panels. While no conclusions can be drawn regarding the true potential of the new polymer as the matrix polymer for carbon- or glass- fiber composites, it is clear that defect-free processing of the polymer in the production of composites is more complex than envisaged and that we have not found the optimal processing conditions yet.

5.1 Introduction

A *composite* can be defined as a combination of two or more materials with a distinguishable interface. The composite material shows properties typically not found in each of the single components and the individual phases, however, remain identifiable and are not chemically altered (apart from the interface between the phases).^{1, 2} Depending on the nature of the matrix and the reinforcement, composites can be classified in different categories, however in this Chapter we will exclusively discuss (glass or carbon) fiber reinforced polymer matrix composites.

From the mid-1970s the demand for lightweight composite structures in the aerospace industry has continuously increased. One of the main reasons for the use of composites was, and still is, the reduction in mass that can be achieved when using a fiber reinforced polymer composite instead of (monolytic) metallic alloys having an intrinsically higher density.³ Fiber reinforced composites based on thermosetting polymer matrices have dominated the first decade of fiber reinforced composites industry in the aerospace sector because of their ease of fabrication and seemingly better long-term behaviour. However, the use of high-performance thermoplastic composites has been increasing since their market introduction, in the mid-1980s.⁴

Particularly important for the aerospace industry is a class of high-performance fiber reinforced composites which is based on high- T_g thermoplastic resins such as PPS and PEEK. These all-aromatic semi-crystalline polymers offer excellent properties, such as very long shelf life, excellent short-term and long-term mechanical properties and their resistance towards a variety of aggressive solvents, including hydraulic fluids and fuels.⁵ ⁶ Moreover, the use of thermoplastic composites is advantageous compared to thermosetting ones when considering speed of production and the fact that thermoplastic polymers are generally tougher, more damage resistant, more ductile, can be reshaped and scrap can be reused.^{7, 8}

An important factor to be taken into account when using semi-crystalline polymers for the production of composites is the effect of processing conditions and thermal history

on the overall morphology and crystallinity of the thermoplastic matrix and hence mechanical properties.^{7, 9} Lustiger et al.¹⁰ and later Deporter et al.⁷ investigated the relationship between processing/thermal history and mechanical properties in two of the most common high-performance thermoplastic composite matrices: PEEK and PPS. Both research teams showed that ultimate composite properties are strongly dependent on the processing conditions used such as heating rate, cooling rate and hold time at temperature. Small variations in said processing conditions may result in large variations in the degree of polymer crystallinity and hence final composite (thermo)mechanical properties.

Another important, but often overlooked factor highly influencing the mechanical properties of composites is the presence of voids and delaminations in the polymer matrix.^{11, 12} As the properties of the composites to be presented were found to be highly affected by the presence of large volume fractions of pores, in this Introduction it is appropriate to reflect on the effect of pores on properties in some greater detail. The number of defects in the composite structure depends strongly on the processing parameters, hence determine the optimal processing conditions for a fiber reinforced polymer composite is an important step, not only for thermoplastic composites but also for the thermosetting ones. It is almost unavoidable to obtain composites which are completely defect-free but optimizing the processing parameters and conditions such as temperature profile, pressure, curing time (for thermosetting matrices), vacuum and resin degassing is crucial to obtain composites with stable and reproducible overall mechanical properties.¹³ However, such optimization work can take years. It has been shown that the presence of voids negatively influences the mechanical properties of not only woven fiber composites, but also unidirectional and multidirectional ones. Laminates properties such as tensile,¹⁴ flexural,¹⁵ compressive¹⁶ have been shown to be affected by the presence of voids, which influence the crack growth mechanism in the matrix.¹⁷ Flexural strength in woven composites, for instance, is highly affected by the void content even up to the point that a laminate with 6% of voids can decrease its flexural strength by 40%.¹⁸ The flexural modulus is generally less affected by the void content, meaning that the loss of

modulus due to porosity is (percentage wise) less than the loss of flexural strength.¹⁹ The same applies to properties, such as compression, tensile and interlaminar shear strength. The effect of voids on the laminate mechanical properties have been related primarily to their volume fraction while some studies report a critical void content limit, where below this value the voids have a negligible effect on the laminate mechanical properties.^{20, 21, 22, 23} However, in several studies it is reported that the volume fraction of the voids itself is not sufficient to predict the resulting mechanical behavior of the laminate.^{24, 25, 26, 27} Other parameters to be considered are void size, void shape and their spatial distribution in 3 dimensions.

Several techniques have been developed over the years to intentionally introduce voids into a composite to study the effect on the laminate properties. The first one involves deliberately deviating from the optimal processing parameters such as incorrect pressures^{28, 29}, temperatures and temperature profiles,^{30, 31} and insufficient degassing.^{32, 33, 34} For instance, Hernandez et al.³⁵ found evidence that when processing composites in a hot press, one of the main factors influencing the void content is the optimization of the temperature cycle, particularly the heating rate when using polymers that undergo a curing step. The second approach consists of introducing external objects into the laminate, such as moisture or foaming agents,^{36, 37, 38} which will produce additional intra and interlaminar voids. For instance, Cinquin et al.³⁹ selected different external compounds to be added to the laminate to create porosity during processing: foaming agent DY5054 and azobisisobutyronitrile which produce nitrogen when it degrades, both to produce inter and intralaminar pores, and spherical material (Expancel) to produce inter laminar porosity.

The origin of the matrix pores in polymer- fiber composites in relation to the processing conditions for different composite making processes such as liquid composite molding (LCM) to out of autoclave (OoA) processing such as hot pressing, have been studied in recent years.

In 2019, Studer, Dransfeld et al.⁴⁰ have studied compression resin transfer molding (CRTM) in low viscosity thermoplastics, observing that viscous flow is an important parameter: the first impregnation step is the one filling the empty spaces at the inter tow level, while at a second stage the intra tow ones are filled. The porosity of the laminates reflects such impregnation stages.

Furthermore, in out of autoclave hot pressing composite processing, used both for thermoplastics and thermosets with viscosity generally higher than 100 Pa·s, Hernandez et al.^{41, 42} and Akkerman et al.⁴³ also concluded that the final void content depends on the evolution of the dynamic viscosity of the polymer matrix and how fiber impregnation takes place. Fiber impregnation normally occurs on two length scales, interbundle and intrabundle and void formation can occur at both scales. Akkerman and Groupe have analyzed the processing of thermoplastic PPS carbon reinforced composites, with the matrix having a viscosity in the order of 10² Pa·s. The impregnation at the interbundle scale is the first one to be completed and only when the matrix fully surrounds the bundles, the second impregnation stage, the intrabundle one, can be finalized as well. It should be pointed out that in the publications cited above no polymer reactions take place leading to the formation of volatiles, and all pores are due to moisture insufficiently removed or allowed to escape during consolidation.

Given the many parameters involved in the processing of thermoplastic composites, it can take a long time to reach optimal process condition settings and obtain optimal final mechanical properties even without changing the materials (matrix polymer and reinforcing fabric) involved. In the 90s, i.e 30 years ago, the flexural strength of PPS/Carbon woven composites reached values below 700 MPa,⁴⁴ while nowadays such values are above 850 MPa, touching the 1000 MPa, meaning an improvement of up to 30%. The improvement in properties is due to improved material properties and fine tuning of the numerous processing conditions (which themselves are invariably considered as company secrets and hence are not disclosed to the outside world).

In this Chapter we present the first results of our new LC thermoset fiber reinforced composite using both commercial plain weave glass fiber and carbon fabrics and describe the manufacturing process, the microstructural and mechanical character and compare the properties with those of identical composites but using PPS or PEEK as the matrix material.

5.2 Materials

In this Chapter, two types of aerospace-grade plain-woven fabrics were used for the construction of the experimental composites:

- TenCate carbon fiber fabric T300JB 3000 40B, 5 harness satin, 277 g/m², 0.37 mm fabric thickness.
- HexForce glass fiber fabric, 7781, 8 harness satin, 299 g/m², 0.22 mm fabric thickness

Due to confidentiality issues it was not possible for Tencate (now Toray) to disclose information regarding the sizing of both carbon and glass fibers used for making the fabrics. However, the TenCate carbon fiber fabric used (T300JB 3000 40B) is the same type as used in previous work on LCT composites. Iqbal et al.⁴⁵ successfully produced six-ply laminates which exhibit (thermo)mechanical properties that outperformed PPS and PEI-based composites. It is to be expected that the sizing on the fibers is in principle appropriate for the polymer and the processing conditions used here

The matrix material used is the 10,000 g/mol LCT precursor HBA/BP/TA17.5-NDA2.5, in this chapter labelled as the 2.5N oligomer. Details regarding the before- and after-cure properties of this reactive oligomer can be found in Chapter 4 of this thesis.

A schematic representation of the backbone is shown in Figure 5.1.

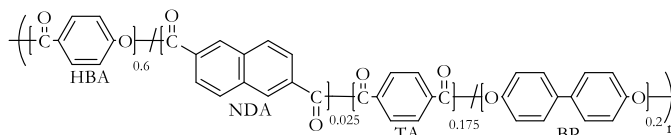


Figure 5.1 Backbone structure of the 2.5N reactive liquid crystalline oligomer

To benchmark the properties of the composites manufactured with the new polymer, similar composites, but using commercial PPS as the matrix polymer, were produced as well. Such reference composites were produced at Ten Cate under undisclosed specific processing conditions.

5.3 Composite manufacturing

5.3.1 Laminate stacking

The composites panels that were produced and analyzed in this Chapter, both carbon and fiber reinforced, were made by film stacking the fabric and distributing the LCT precursor powder homogenously on the fabric surface. Carbon and glass fabric were cut to 400x400 mm dimensions using a Gerber cutting machine. The final overall fiber/resin volume ratio was calculated to be on the order of 60/40. The nominal fiber to resin volume should have been 60/40% excluding effects due to porosity and matrix polymer outflow.

For company confidential reasons the carbon fiber composites had a different thickness than the glass fiber composites. For the glass fiber composites we stacked **4 plies** $[0, 90]_{2s}$ while for the carbon fiber composites we used stacks of **8 plies** $[0, 90]_{4s}$. These differences in stacking also applied to the reference PPS composites.

5.3.2 Laminate thermopressing

Subsequent to the stacking procedure, each sample was vacuum bagged by using Tack sealant tape and Kapton foil, and the packed sample was placed between two 2 mm thick flat steel plates used as moulds for the thermopressing. All experimental composites were processed using the Joos press at the Faculty of Aerospace Engineering.

Curing cycle

The temperature and cure state viscosity were studied using the protocol developed by Knijnenburg⁴⁶ and Iqbal.⁴⁷ The aim of the protocol was to obtain both a low viscosity at the start of the curing cycle to facilitate complete fabric impregnation and to have a decent curing time leading to a crosslinked network. The optimal thermal path consisted of heating up to 330 °C with a rate of 5 °C/min, holding for 20 minutes, followed by heating at a rate of 5 °C/min to a final temperature of 370 °C and isothermal holding for 60 minutes, followed by natural cooling to room temperature at an average rate of 5 °C/min. The Time-Temperature-Viscosity curve of the 2.5N LCT precursor as measured on the Thermoscientific Mars III parallel-plate rheometer is shown in Figure 5.2 and shows that the precursor reaches a viscosity of 50 Pa·s at the start of the first holding stage and reaches a viscosity of 300 Pa·s at the end of the low temperature holding stage. At the end of the curing stage at 370 °C the viscosity had reached a value of $5 \cdot 10^5$ Pa·s.

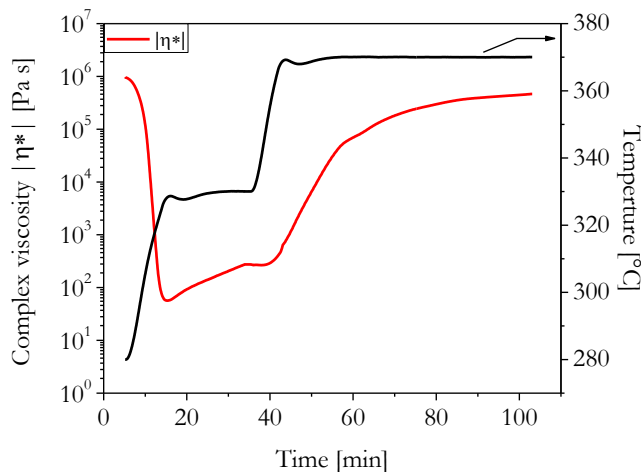


Figure 5.2 Complex melt viscosity of the 2.5N-10K oligomer as a function of time and temperature using a two-step protocol, reproducing the curing cycle used for the composite processing. Experiments were performed using a frequency 5 rad/s and a heating rate of 5 °C/min (N₂ atmosphere). The red curve shows the time dependent viscosity while the black line indicates the imposed temperature profile.

The actual composite manufacturing involved a hand lay-up process and a manual spreading of the granulated polymer powder in between the fabric layers. The fully assembled stack was placed in a custom made (KaptonTM) vacuum bag.

The thermopressing cycle used in the composite manufacturing is shown in Figure 5.3, where temperature and pressure are shown as a function of the cycle time. A low pressure of 2 bar was applied during heating to the first holding temperature of 330 °C. Upon reaching that temperature the pressure was increased to 5, 10 or 20 bar, which was held at that level during the curing and cooling down cycle. Pressure was released once the sample had reached a temperature below 50 °C.

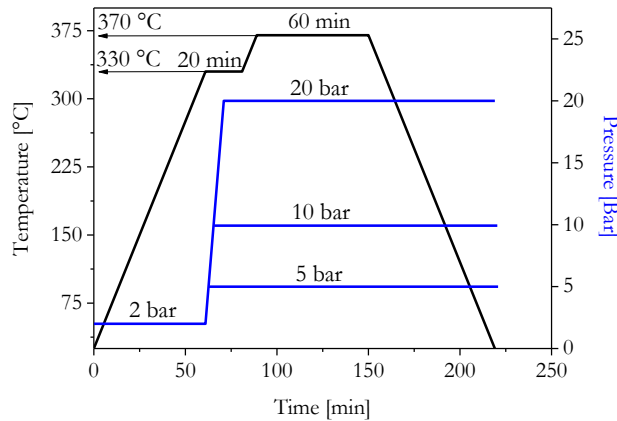


Figure 5.3 Schematic representation of the optimal curing cycle for the composites processing, here showing three different consolidation pressures. The black line shows the common temperature-time profile imposed, while the three blue lines indicate the three pressure time profiles. The pressure was removed once the sample temperature had reached room temperature.

Plaques thus produced had a typical thickness in excess of 2.30 mm for the carbon- fiber composites and 1.05 mm for the glass- fiber composites.

As stated above, PPS-reinforced composites (with the same glass and carbon fabrics) were produced for benchmarking by TenCate. However, the details of the processing conditions are company confidential information and cannot be disclosed.

Initial plaque Quality control

The plaques thus produced were analyzed using a C-scan, RapidScan 2 Automated, to determine the sample homogeneity. Typical examples are shown in Figure 5.4 and 5.5, in those figures the greyscale values represent the back-wall reflection: high values correspond to white or light color and are the areas where the laminate consolidation is optimal; low values corresponds to dark color which means poor consolidation areas. The areas with the purple color show no values of reflection. Both figures show that a pressure of > 5 bar is required to get macroscopically sufficiently homogeneous samples. A pressure of 10 bar was used for all composites tested on their mechanical properties.

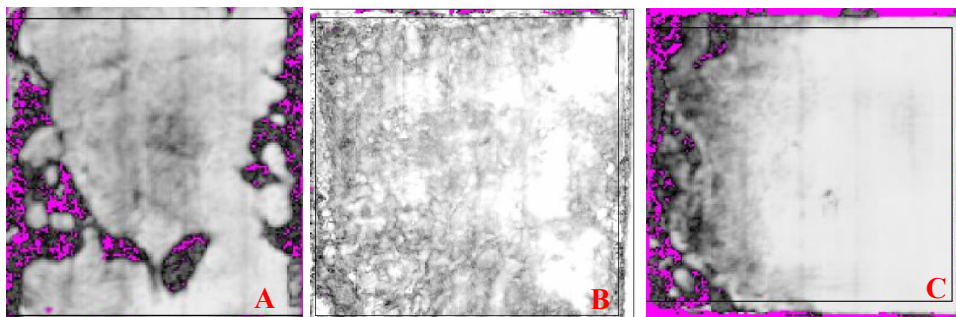


Figure 5.4 A: C-scan image of 2.5N-Carbon laminate produced with a consolidation pressure of 5 bar. B: C-scan image of 2.5N-Carbon laminate produced with a consolidation pressure of 10 bar. C: C-scan image of 2.5N-Carbon laminate produced with a consolidation pressure of 20 bar. Scale of the panel imaged is 400x400 mm

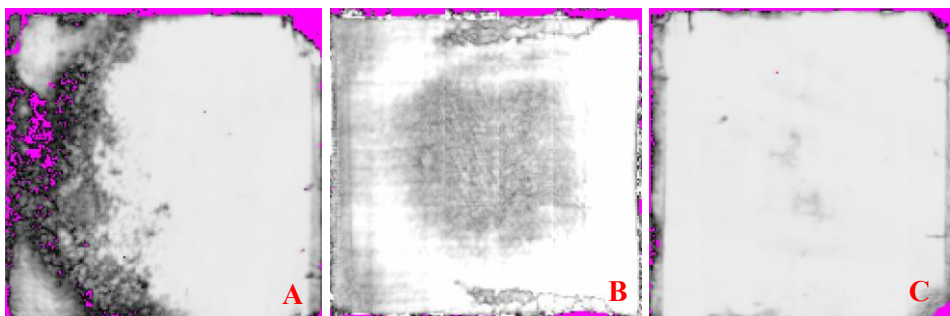


Figure 5.5 A: C-scan image of 2.5N-Glass laminate produced with a consolidation pressure of 5 bar. B: C-scan image of 2.5N-Glass laminate produced with a consolidation pressure of 10 bar. C: C-scan image of 2.5N-Glass laminate produced with a consolidation pressure of 20 bar. Scale of the panel imaged is 400x400 mm.

5.3.3 Mechanical analysis

After production the plaques were cut into samples for mechanical testing and other property evaluations. All mechanical tests were performed at TenCate (now Toray) laboratories, located in Nijverdal, NL.

Flexural properties were measured following the EN2562 standard, using a Zwick universal testing machine with a 20 kN load cell and a crosshead displacement control of 0.5 μm . A set of six specimens per sample category were tested, each specimen measuring

100 mm both in length and width.

Indications of the average density values (i.e. estimate of the porosity levels) of the composites were measured on left-over composite pieces using a micro-meter and a precision ruler to determine the sample volume and a standard lab balance was used to measure the weight. It is admitted that more accurate measurements exist to determine the porosity levels, but simple visual observation of the material available readily indicated that the local variation in porosity levels were rather high indeed. In retrospect, the sample averaged porosity levels should have been determined on the individual tensile testing samples prior to testing, but the fact that the composite samples suffered from a high degree of porosity was not known at the time of testing.

5.3.4 Microstructural analysis

Cross-sections of selected samples were made by careful diamond blade cutting followed by polishing. Optical microscopy was done using an Olympus BHM microscope equipped with a Sony CCD-IRIS black&white video camera.

X-ray tomographic measurements were done using a Phoenix Micro CT-Scanner, from the Laboratory of Geoscience and Engineering, Faculty of Civil Engineering and Geosciences, Delft University of Technology. Sample dimensions for the tomographic measurements were about 8 by 30 mm. The optical and tomographic measurements were made after the results of the mechanical tests had been obtained.

5.4 Results and discussion

5.4.1 Microstructural observations.

Optical microscopy

Following the macroanalysis of the laminate made by C-scan, the first microstructural analysis that has been carried out on the 2.5N composites, processed at 10 bar pressure, is the cross-section imaging via optical microscope.

Figure 5.6 shows cross sectional images of the 2.5N-carbon fiber laminate. High levels of porosity are present and can be seen in both laminate orientation, $\pm 45^\circ$ and $0, 90^\circ$. In the A section of Figure 5.6, a detail of the cross section of the laminate oriented at $\pm 45^\circ$ can be seen. It is evident that there are pores with dimensions between 5 and 15 μm within the fiber bundle, the so-called micro-pores,⁴⁸ however a more dramatic observation can be made: several large spherical meso-pores with a diameter of over 100 μm . The larger pores are located in the resin-rich region located at the cross-over regions of the fabric. The formation of micro-pores is mainly due to incomplete impregnation of the fiber bundles in the fabric resulting in sections of un-wetted fibers,⁴⁹ while the macro voids are mostly caused by the incomplete flow of the resin which has not covered the whole area of that laminate section. The preparation of the laminate prior to processing involved a manual distribution of the resin, as powder, over the fabric. Such action could result in non-homogeneous resin distribution.

Similar observations regarding void-rich regions can be made when analysing the 2.5N-carbon laminate $0, 90^\circ$ oriented, see Figure 5.6, B. The figure shows a meso-void area at the interphase between fibers and a resin rich region around the tow.

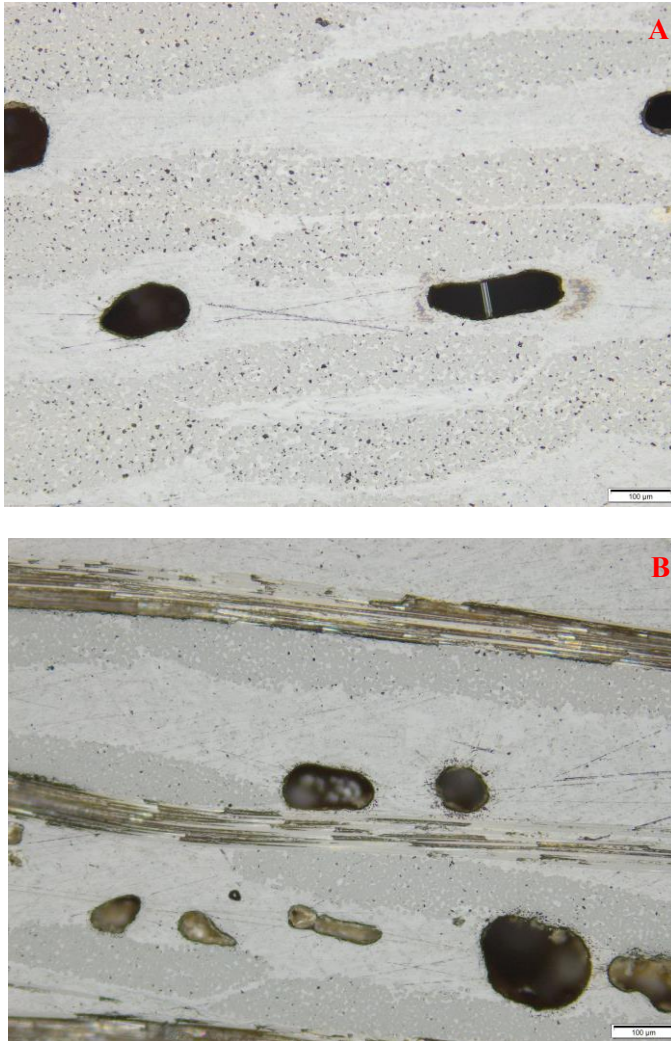


Figure 5.6 Optical microscopy image of the central part (circa 800 μm height) of the cross-section of the 2.5N-Carbon laminate, processed at 10 bar pressure. A: $\pm 45^\circ$ laminate orientation cross section image. B: 0, 90° laminate orientation.

Most large pores are located in the polymer-regions between the tows making up the fabric, but smaller pores were also encountered within the tows. Figure 5.7 shows an example of such occurrence. A macro-pore with a width of 125 μm can be seen.

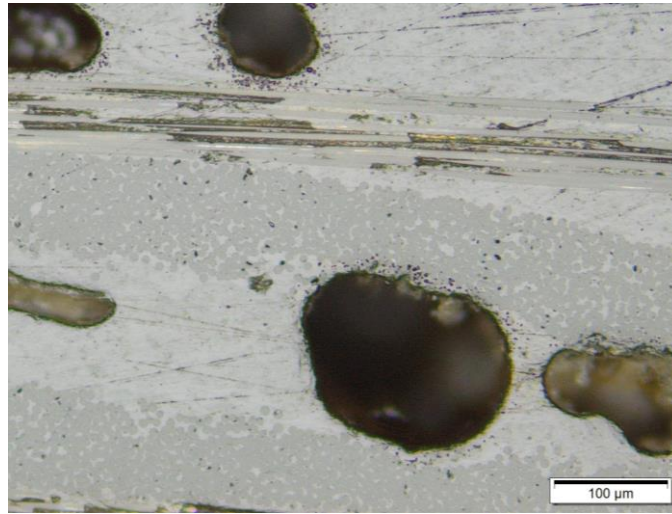
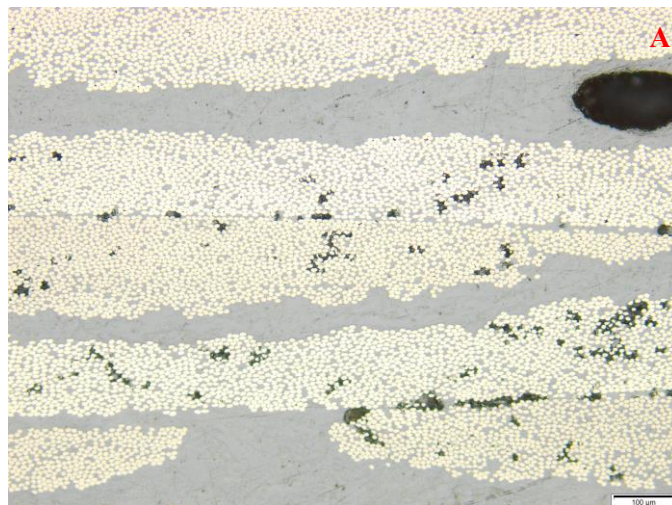


Figure 5.7 Detail of a porous section of the 2.5N-Carbon laminate processed at 10 bar pressure. Image taken at 0, 90 ° laminate orientation.

Similar observations as those on the 2.5N-Carbon composites can be made on the 2.5N-Glass composites. Figures 5.8, A and B, shows cross sectional images of such composites, respectively at $\pm 45^\circ$ and 0, 90 ° orientation, micro and meso voids can be observed, inter laminar and intra laminar as well.



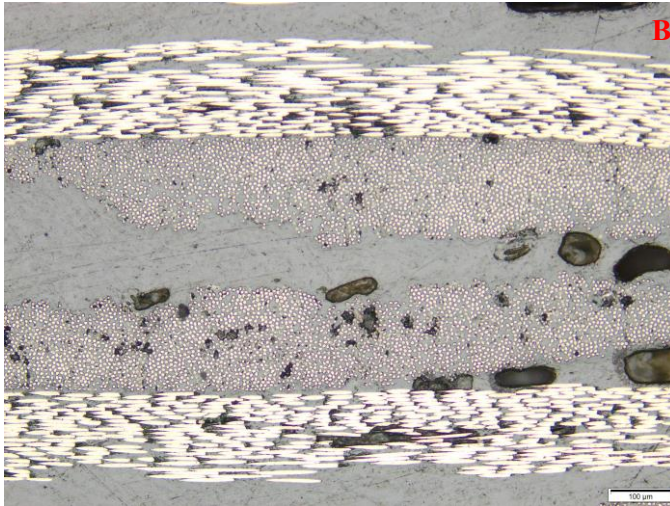


Figure 5.8 Optical microscopy image of the almost full cross-section of the 2.5N-Glass laminate, processed at 10 bar pressure. A: $\pm 45^\circ$ laminate orientation cross section image. B: $0, 90^\circ$ laminate orientation.

Tomographic observations

The tomographic images of the carbon-fiber composite are shown in Figure 5.9. As pointed out by one of the committee members, for the tomographic measurements accidentally we have used a 4-ply carbon fiber composite with a thickness of 1.7 mm rather than the 8 plies 2.3 mm sample used in the mechanical testing. Due to the sample thickness being a little too high for optimal resolution, the quality of the images is not very high, but the information they contain is informative enough. The white phase is the carbon fabric, the grey phase is the polymer and the black phase indicates the pores or delaminations. Figure 5.9.a shows a top-down view of a plane about 200 micron below the surface. It very clearly demonstrates the presence of an almost pure polymer layer, massive delamination zone near the top left-hand side of the sample, and local small delaminations within and in between the bundles. The delaminated region at a slightly lower observation plane is shown in Figure 5.9b. Figure 5.9c shows the top-down view at a non-delaminated viewing plane and reveals substantial interface cracking or non-wetting within the fabric. Finally figure 5.9d shows a side view of the sample revealing both a macro-delamination at $\frac{1}{4}$ of the sample thickness and micro porosity everywhere

in the fabric. There were no signs of a higher pore density at the mid-plane of the sample. In fact, more micro-delaminations were encountered near the sample surfaces.

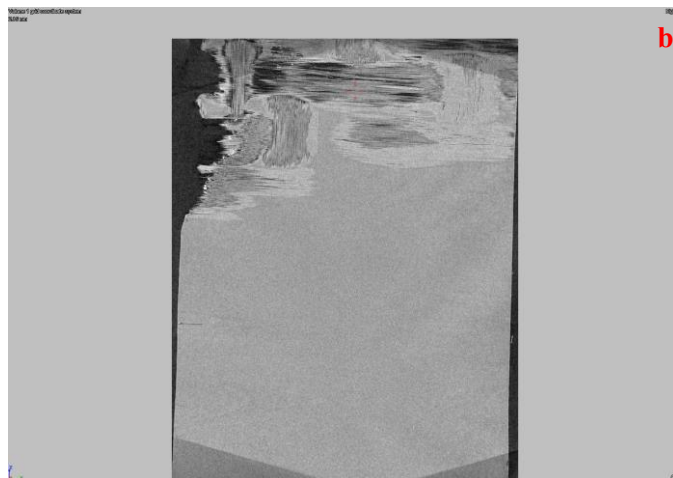
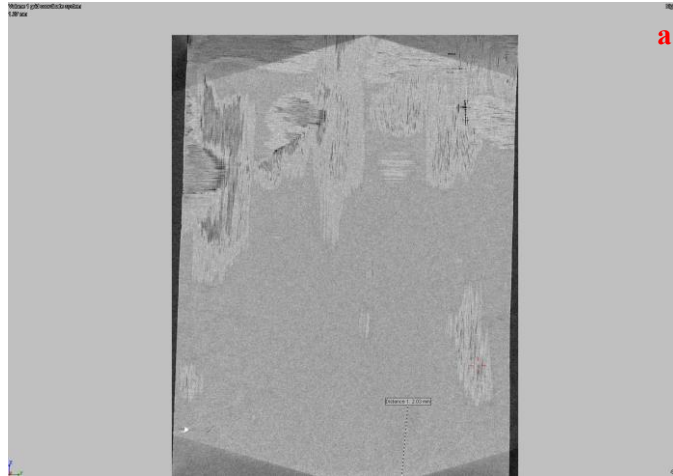


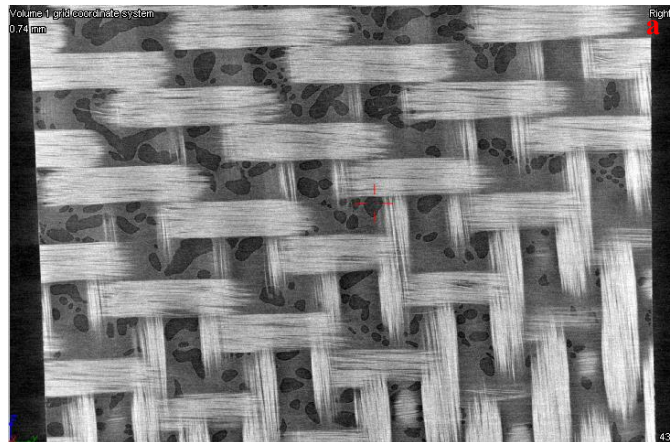


Figure 5.9 Tomographic images of the Carbon-fiber composite. a: top down view about 0.2 mm below the surface showing large scale delamination, an almost pure polymer layer and some small scale delaminations, b: 2nd view of the delaminated region at another viewing plane, c: top down view at another location and d: cross-sectional view.

The tomographic images of the glass-fiber composite are shown in figure 5.10. They clearly reflect the glass fabric (in white), the matrix (in grey) and the porosity (in dark grey). Figure 5.10a taken at the mid-thickness plane parallel to the fabric shows very clearly the presence of a multitude of (planar) pores present in almost every cross—over point in the fabric. There are also some signs that the polymer has not properly wetted

all fibers inside the tow. The cross-sectional view (Figure 5.10 b) clearly demonstrates that the big pores are located primarily at the mid-plane of the sample and that the pores easily have dimension of the width of the tow. Figure 5.10c taken at a plane about 200 microns below the top-surface of the composite, shows that, unlike at the mid-plane, here there are no macro-pores at the cross-over points of the fabric but there are clear signs of the polymer not having fully penetrated into the tows resulting in elongated intra-bundle pores.

The preferred location of the pores in the very mid-thickness plane of the panel is attributed to the fact that the heating of the panels takes place via surface contact, i.e. the surface layers heat up first, hence first melt, but also cross-link first. So, any gas released (this can be air attached to the powder surface or gasses released to some form of post-curing) cannot escape via the surface layer as this has a higher viscosity). Earlier work on LCT has shown that such polymers have a very low gas permeability. More work on linking the pore density profile to both the composite thickness and the thermal profile imposed is required.



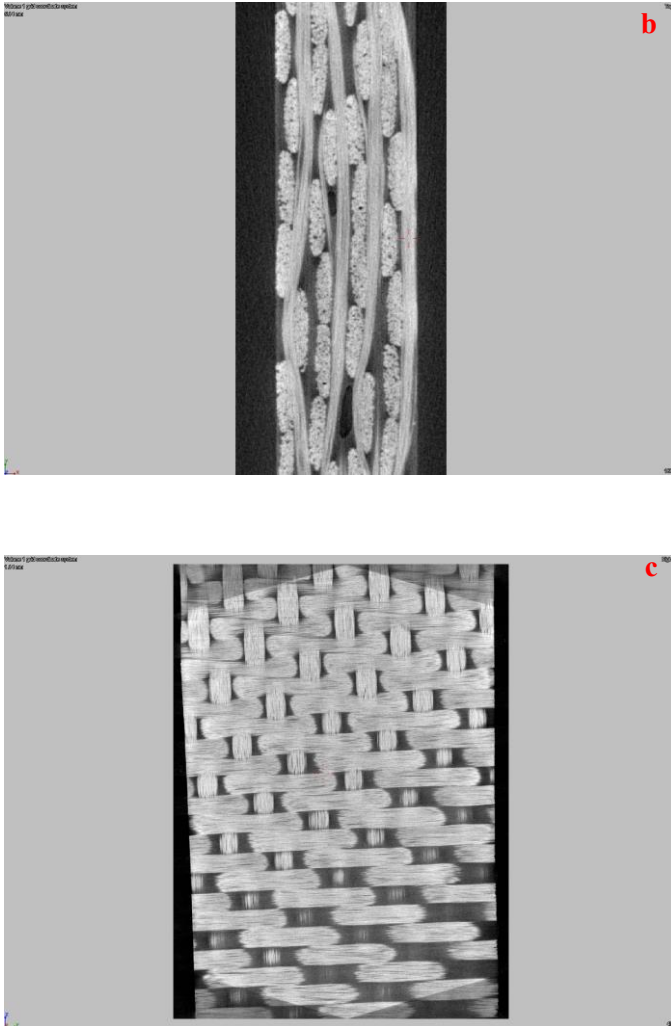


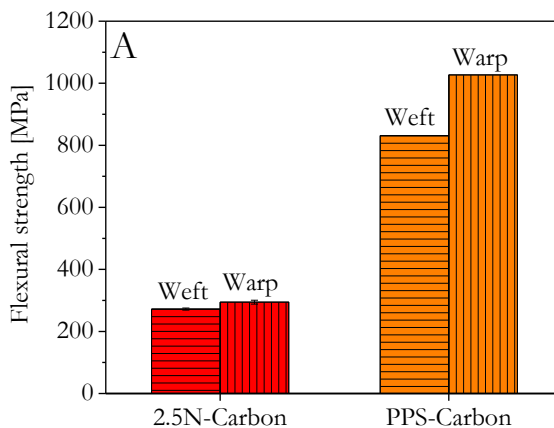
Figure 5.10 Tomographic images of the glass composite. a: top down view at mid-plane, full sample width (5 mm) b: side view, c: top down view 200 micron below the surface

5.4.2 Flexural properties

The results of the flexural tests are presented in Table 5.2 and in Figure 5.11 for the carbon fiber composites and in Figure 5.12 for the glass fiber composites.

Table 5.1 Flexural strength and modulus data of 2.5N-carbon and 2.5N-glass composites compared with PPS-Carbon and PPS-Glass composites respectively

Sample	Flexural			
	Weft Strength [MPa]	Weft Modulus [GPa]	Warp Strength [MPa]	Warp Modulus [GPa]
2.5N-Carbon	264	33	300	41
PPS-Carbon	831	45	1027	60
2.5N-Glass	187	13	222	17
PPS-Glass	390	20	512	23



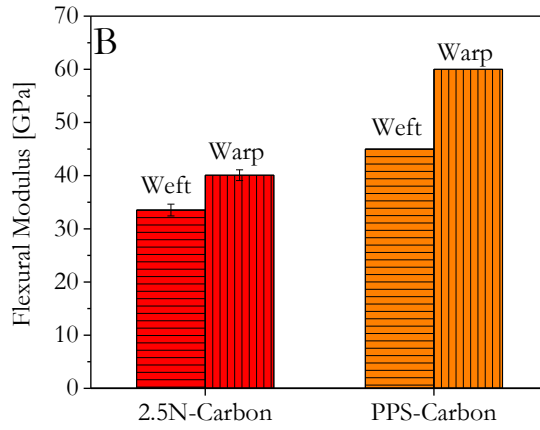
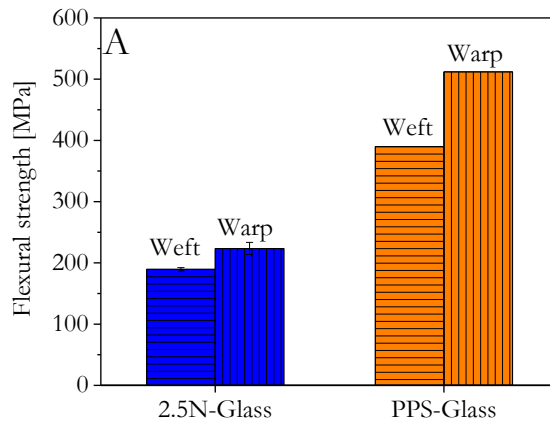


Figure 5.11 Flexural strength results of 2.5N-Carbon and PPS-Carbon. B- Flexural modulus results of 2.5N-Carbon and PPS-Carbon



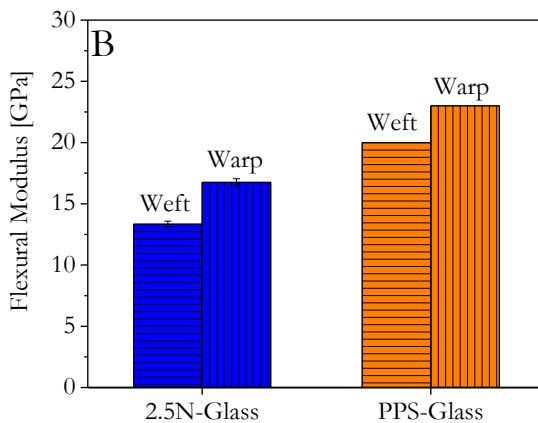


Figure 5.12 A- Flexural strength results for 2.5N-Glass and PPS-Glass composites. B- Flexural modulus results for 2.5N-Glass and PPS-Glass composites

The data clearly show that the mechanical properties (both strength and stiffness) of the composites made with the new polymer fall short of that of their reference PPS based composites. In all cases samples tested in the warp direction show a slightly higher strength.

5.5 Discussion

It is evident from the results presented in paragraph 5.4.2 that the mechanical performance of both carbon and glass fiber composites LCT does not mirror what could be expected on the basis of the mechanical properties of the neat (cured) resin and the fabric itself. It is obvious from the microstructural observations that a very high level of porosity is present in all laminates and in particular in the thicker carbon fabric composites. Most of the macro porosity was found in the mid-plane of the panels. Almost fully dense material was observed for both the glass- and the carbon fiber fabric composites when moving towards the edges of the panel. The observed macro porosity and its localisation near the mid-plane can be considered as the main cause of the low apparent mechanical properties.

The origin of the high porosity is to be found in a combination of different factors. First of all, the polymer was applied in the form of fine-grained fluffy powder. The fine powder morphology invariably leads to a lot of trapped air in the powder. Furthermore, the fusion of the powder upon heating also leads to a high likelihood of micro-gas bubbles which, if not mobile enough to diffuse to the exterior of the panel, will remain trapped in the final composite. Moreover, manual application of the powder in between the fabric layers will result in a relatively inhomogeneous polymer distribution, which in turn results in localized fluctuations in the amount of molten resin.

Next, a major problem of the current concept of reactive end-group capped oligomers is that while an attractive low viscosity level is reached indeed, this period of low viscosity can only be maintained for a relatively short period (typically 5 minutes, according to Figure 5.7) and then chain-extension and crosslinking leads to a rapid increase in viscosity making it impossible for air inclusions to effectively diffuse out of the polymer matrix. This problematic increase in viscosity is absent in the case of PPS (see also Figure 5.7) where a low viscosity condition can be maintained for at least 60 minutes. As such, the observation of many areas where excellent fiber wetting is encountered, both within the fiber bundles themselves and the between the strands, is a clear sign of the excellent wetting behaviour of the polymer-fiber surface. The short period of low viscosity also

explains why earlier research on such polymer systems but focussing on the properties of thin pre-pregs yielded such much better results. For thin samples the period of low viscosity is long enough for entrapped air to be removed using the vacuum present at the sample external surface. The time dependent viscosity also explains the enhanced presence of large pores in the thicker samples, given the fact that heating of the stack is by contact heating via the heated dies. As a result, the surface layer is the first to experience the effects of crosslinking on the viscosity. While the core of a thicker sample is yet to reach the desirable low viscosity state and the trapped air is to accumulate in microbubbles, the outer surface has already become impermeable, leading to permanent trapping of the air bubbles, likely to coalesce into larger diameter bubbles near the mid-plane of the sample.

5.6 Conclusions

It is clear that the attempts to use the new 2.5 N polymer for the construction of glass fiber fabric and carbon fiber fabric composites via a laminate thermopressing route and starting from fluffy polymer powder manually distributed between the fabric layers did not yet yield the expected performance in mechanical behaviour with respect to the reference PPS composites. The poor mechanical behaviour was shown to be due to a high volume fraction of pores (up to 10 %, but in some case locally even higher) of sizeable dimensions (in excess of 100 μm). Although many more (unsuccessful) composite manufacturing experiments were performed than reported here, the limited availability of the new polymer formed a major obstacle in finding a stable process window for the production of fully dense woven fabric composites. While the discussion of the pore formation mechanism indicated some routes to solve the problem, the release of volatiles during chain extension and crosslinking is likely to remain a real issue when processing thicker composite components using the polymer systems examined in this thesis.

5.7 References

- [1] Ratna, D. , *Handbook of Thermoset Resins*, iSmuthers ed., 2009, pp 281-290
- [2] *Encyclopaedia of Polymer Science and Technology*, John Wiley&Sons, 2005, vol. 9, pp 282-288
- [3] A. Beukers, H.E.N. Bersee, and S. Koussios. *Future Aircraft Structures: From Metal to Composite Structures*, pp 1-45. Springer London, 2011.
- [4] Offringa, A.R., *Composites Part A: Applied Science and Manufacturing*, 1996, 27-4, 329-336
- [5] Denault, J., Dumouchel, M., *Advanced Performance Materials*, 1998, 5, 83-96, 33
- [6] Kim, Y.K., Ye, L., *Composites Part A: Appl. Sci. and Manuf.*, 2004, 35, 477-487
- [7] Deporter, J., Baird, D.G., *Polymer Composites*, 1993, 14, 201
- [8] Hou, T.H., Bryant, R.G., *High Performance Polymers*, 1997, 9, 437
- [9] A. Lusliger, F. Uralil, and G. Newaz, *Polym. Comp.. 1990*, 11, 65], [Lee, Y., Porter, R.S., *Macromolecules*, 1988, 21, 2770
- [10] Lustiger, A., Uralil, F.S., Newaz, G.M., *Polymer Composites*, 1990, 11, 1
- [11] Rubin, A.M., Jerina, K.L., *Composites Engineering*, 1993, 3, 7, 601-618
- [12] Judd, N.C.W., Wright, W.W., *Voids and their effects on mechanical-properties of composites – appraisal. Sampe Journal*, 1978, 14, 10–14
- [13] Maragoni, L., Carraro, P.A., Peron, M., Quaresimin, M., *International Journal of Fatigue*, 2017, 95, 18-28
- [14] Olivier P, Cottu JP, Ferret B., *Composites*, 1995;26, 509-515
- [15] Chambers A.R., Earl J.S., Squires C.A., Suhot MA, *Int. J. Fatigue*, 2006, 28, 1389–98
- [16] Tang, J.M., Lee, W.I., Springer, G.S., *Journal of Composite Materials*, 1987, 21,5, 421–440
- [17] Scott, A.E., Sinclair, I., Spearing, S.M., Mavrogordato, M.N., Hepples, W., *Composites Science and Technology*, 2014, 90, 10, 147
- [18] Hou M., Ye L., Mai Y-W., *Journal of Reinforced Plastics and Composites*, 1996, 15, 1117

-
- [19] Mehdikhani, M., Gorbatiikh, L., Verpoest, I., Lomov, S.V., *Journal of Composite Materials*, 2019, 53,12, 1579
- [20] de Almeida, S.F.M., Neto, Z.d.S.N., *Compos. Struct.*, 1994, 28, 139
- [21] Rubin AM and Jerina KL., *Compos Eng.*, 1993; 3, 601
- [22] Yoshida H, Ogasa T and Hayashi R., *Compos Sci Technol*, 1986, 25, 3
- [23] Olivier, P.A., Mascaro, B., Margueres, P., CFRP with voids: ultrasonic characterization of localized porosity, acceptance criteria and mechanical characteristics. In: *Proceedings of 16th International Conference on Composite Materials (ICCM16)*, Kyoto, Japan, 8–13 July 2007
- [24] Naganuma T, Naito K, Kyono J, *Compos Sci Technol.*, 2009; 69, 2428
- [25] Nikishkov Y, Airoidi L., Makeev, A., *Compos. Sci. Technol.*, 2013, 89, 89
- [26] Seon, G., Makeev, A., Nikishkov, Y., *Compos. Sci. Technol.*, 2013, 89, 194
- [27] Carraro, P.A., Maragoni, L., Quaresimin, M., *Adv. Manuf. Polym. Comp. Sci.*, 2015, 1, 44
- [28] Tang, J.-M., Lee, W.I., Springer, G.S., *J. Compos. Mater.*, 1987, 21, 421
- [29] Liu, L., Zhang, B.-M., Wang, D.-F., *Compos. Struct.*, 2006, 73, 303
- [30] Hernandez, S., Sket F, Gonzalez, C., *Compos. Sci. Technol.*, 2013, 85, 73
- [31] Hernandez, S., Sket, F., Molina-Aldareguia, J.M., *Compos. Sci. Technol.*, 2011, 71, 1331
- [32] Liebig, W.V., Viets, C., Schulte, K., *Compos. Sci. Technol.*, 2015, 117, 225
- [33] Rubin, A.M., Jerina, K.L., *Compos. Eng.*, 1993, 3, 601
- [34] Gehrig F, Mannov E and Schulte K. Degradation of NCF-epoxy composites containing voids. In: *17th International Conference on Composite Materials (ICCM17)*, Edinburgh, United Kingdom, 27–31, July 2009
- [35] Hernandez, S., Sket, F., Molina-Aldareguia, J.M., Gonzalez, C., Llorca, J.-L., *Composites Science and Technology*, 2011, 71, 1331
- [36] Gurdal, Z., Tomasino, A.P., Biggers, S.B., Sampe J., 1991, 27, 39
- [37] Guo, Z.-S., Liu, L., Zhang, B.-M., *J. Compos. Mater.*, 2009, 43, 1775

- [38] Yoshida H, Ogasa T and Hayashi R. Statistical approach to the relationship between ILSS and void content of CFRP. *Compos Sci Technol* 1986, 25, 3
- [39] Cinquin, J., Triquenaux, V., Rouesne, Y., Porosity influence on organic composite material mechanical properties, ICCM 2007
- [40] Studer, J., Dransfeld, C., Cano, J.J., Keller, A., Wink, M., Masania, K., Fiedler, B., *Composites Part A*, 2019, 122, 45
- [41] Hernandez, S., Sket, F., Gonzalez, C., et al., *Composites Science and Technology*, 2013, 85, 73
- [42] Hernandez S., Sket F, et al., *Composites Science and Technology*, 2011, 71, 1331
- [43] Groupe, W.J.B., Akkerman, R., *Plastics rubber and composites*, 2010, 39, 208
- [44] M Ma, C.C., Yur, S-W., *Polymer Engineering and Science*, 1991, 31, 1, 34
- [45] Iqbal, M., Dingemans, T.J., *Composites Science and Technology*, 2011, 71, 863
- [46] Dingemans, T.J., Knijnenberg, A., Iqbal, M., Weiser, E., Stclair, T., *Liquid Crystals Today*, 2006, 15, 4, 19
- [47] Iqbal, M. (2010). *All-aromatic Liquid Crystal Thermosets and Composites Thereof*. Ph.D. Thesis. Delft University of Technology: The Netherlands
- [48] Park, C.H., Lee, W.I., *Journal of Reinforced Plastics and Composites*, 2011, 30, 957
- [49] Yamaleev, N., Mohan R., *International Journal of Multiphase Flow*, 2006; 32, 1219

CHAPTER 6

Summary, Conclusions and Recommendations

Over the past 20 years, one of the most innovative techniques to improve processing of aromatic LCPs was the use of the so-called reactive oligomer approach: synthesizing LCPs with a molecular weight in the order of 1,000–10,000 g/mol and end-capping them with reactive end-groups such as phenylethynyl. By using LCPs with reduced, oligomeric, molecular weight the melting temperature is then lowered resulting in a wider processing window. The activation of the end-groups during composite infusion leads to chain extension or crosslinking, resulting in a cured LCT with improved (thermo)mechanical properties compared to its non-cured counterpart.

The work as described in this thesis is a continuation of a longer research line in the Dingemans's group at the faculty of Aerospace Engineering aimed at exploring finding the best polymer backbone composition for optimal properties and processability. The work extends the existing knowledge database by studying the role of the phenylethynyl end group, the effect of a fourth monomer to form the backbone and finally the first attempt to use a promising polymer variant for composite panel, rather than pre-preg production.

The work in *Chapter 3* shows the thermal, rheological and (thermo)mechanical results of a LC oligomer series end-capped with reactive phenylethynyl and non-reactive end-groups. The results prove that oligomers end-capped with reactive end-groups at each chain end are essential to obtain thermosets with the optimal thermo-mechanical properties, such as T_d , T_g , mechanical properties such as stress and strain at break. As was to be expected the curing rate for dual end-capped oligomers is much higher leading

more rapidly to a higher viscosity when holding at the processing temperature leading to the lowest transient viscosity when compared to samples end-capped with one or no reactive end-groups.

The effect of the backbone modification on polymer properties and high temperature viscosity was studied for a range of LCP formulations starting with a backbone consisting of 4-hydroxybenzoic acid (HBA), terephthalic acid (TA) and 4,4'-biphenol (BP). As shown in Chapter 2, the addition of several co-monomers (making them the fourth co-monomer in the backbone) were explored: 6-hydroxy-2-naphthoic acid (HNA), 2,6-naphthalenedicarboxylic acid (NDA), 4,4'-diaminodiphenyl sulfone (DDS) and isophthalic acid (IA), always keeping their level at 5 mol%. It is evident from the thermal, rheological and (thermo)mechanical results that only the LCT modified with 2,6-naphthalene dicarboxylic acid (NDA) could drastically lower the melting temperature and the melt viscosity, yet keeping the glass transition temperature after curing at its intended high value above 250 °C.

A deeper analysis of the role of NDA was carried out in *Chapter 4*, where it was explored how different mol% of NDA affect the oligomers' thermal and processing properties before cure and (thermo)mechanical properties after cure. It was proven that by increasing the mol% of NDA in the polymer backbone the melting temperature and melt viscosity of the oligomers would be consequently lowered. Based on the results of *Chapter 4* it was decided that the LC oligomer with a composition of HBA(60%)/BP(20%)/TA(17.5%)-NDA(2.5%) was the ideal candidate matrix polymer in terms of processing and after cure properties, and to be used as the matrix polymer in the final experiments to produce and test the properties of thin composites panels using either glass fiber or carbon fiber fabric as the reinforcing phase..

In chapter 5 we describe the results of these composite manufacturing trials, using the polymer in its as-produced granular form manually sprinkled over the two fabrics and subsequently compressed according to the optimal thermomechanical profile determined for the neat polymer. The thin-ply composites thus produced were examined using C-scan, optical microscopy, X-ray tomography and mechanical testing.

The microstructural observations clearly showed a high level of porosity present in both carbon and glass fiber laminates. Pores at the intra-bundle and inter-bundle scale were observed, which measured from few microns up to hundreds of microns. The presence of such level of voids has a clear and undisputable negative influence on the mechanical properties of the laminates.

The origin of the high porosity is to be found in a combination of different factors. First of all the use of the polymer in its granular form greatly promoted the pore formation, but in addition we found that limited outgassing during curing (rapid increase in viscosity) could be held responsible for a much higher porosity level in the composites than in the reference PPS-based composites where both detrimental factors (the gas release during cross-linking in combination with the rapid increase in viscosity) were intrinsically non present. Whilst the results of the work as presented in this thesis show that the polymers produced have promising intrinsic features in term of final thermomechanical properties and low initial viscosity prior to chain-extension or crosslinking, the restricted time window for processing due to the rapid chain-extension and crosslinking reactions proves to be a major challenge when it comes to producing well consolidate composite panels. The solution to overcome these problems has to be found in both more appropriate pre-processing (starting from thin pre-infiltrated pre-pregs) and delaying the crosslinking reactions (such that any entrapped air has enough time to escape). The attractive thermo-mechanical properties measured on the neat polymer fully justify the investment in the further investment in the exploration of the concept and the oligomers presented in this thesis.

Summary

The work presented in this Thesis describes the use of reactive all-aromatic liquid crystalline thermosetting resins for fiber-reinforced composite applications. One of the challenges associated with reactive LC thermoplastic resins is that the melting temperature (T_{k-lc}) is typically close to or above the decomposition temperature. In order to improve the melt processing characteristics of reactive liquid crystal resins, but without compromising the after-cure (thermo)mechanical properties, two synthetic approaches have been explored: 1- control of the polymer molecular weight by using phenylethynyl reactive end-groups and 2- by introducing non-linear co-monomers.

In Chapter 2 we will discuss how small backbone modifications of a rigid LC oligomer based on 4-hydroxybenzoic acid (HBA), terephthalic acid (TA) and 4,4'-biphenol (BP) affect the T_{k-lc} transition and the melt viscosity. By introducing non-linear co-monomers into the oligomer backbone, we were able to substantially lower the T_{k-lc} transition of the oligomers from 325 to 280 °C, and lower the minimum complex melt viscosity from 10^5 Pa·s to 30 Pa·s. At the same time, the glass transition temperature of the resulting liquid crystal thermosets was kept well above 200 °C. Cured films exhibit a tensile strength of 85 MPa and 4% elongation at break, respectively, and Young's modulus values that were in the 2-3 GPa range.

How, and to what extent, do the phenylethynyl reactive end-groups contribute to the after-cure thermo-mechanical properties of the final LC thermosets is described in Chapter 3. We have prepared liquid crystal oligomers, end-capped with reactive (R) phenylethynyl and non-reactive (NR) phthalimide end-groups. All oligomers have been fully characterized using TGA, DSC, rheology, DMTA and tensile testing. DMTA analyses showed that having two reactive end-groups is critical for obtaining thermosets with superior high temperature stability. Fully cured films exhibit glass-transition temperatures (T_g) in the range of 120–150 °C, storage moduli (E') of ~4 GPa (25 °C), stress at break values up to 90 MPa and strain at break of 5%.

The work discussed in Chapter 4 is a continuation of the backbone modification study as described in Chapter 2, but now with a focus on how reactive LC resins can be processed into fiber-reinforced composites. A LC reactive oligomer based on 4-hydroxybenzoic acid (HBA), terephthalic acid (TA) and 4,4'-biphenol (BP) was modified with a fourth co-monomer, 2,6-naphthalene dicarboxylic acid (NDA). A series of 4 reactive oligomers with varying amounts of NDA was prepared, i.e. 0% (reference sample), 1, 2.5 and 5 mol%. The reactive oligomer with 2.5 mol% NDA gave the best combination of processability and after-cure (thermo)mechanical properties and was therefore selected as the resin of choice for our composite work, which will be described in Chapter 5.

In Chapter 5 the composite manufacturing trials and the mechanical characterization of glass- and carbon- fiber composite panels is discussed. The LC oligomer precursor, as described in Chapter 4, was used as the matrix because of its promising processing characteristics (melt viscosity of 100 Pa·s at 320 °C) and superior thermomechanical properties relative to PPS and PEKK. The resulting composites were analyzed macroscopically using the C-scan method, optical microscopy and X-ray tomography. The mechanical behaviour of the thin composites has been investigated by testing flexural, compression and in-plane shear properties, and the results were contrasted with polyphenylene sulphide (PPS) composites. Our preliminary results show that our novel LCT reinforced composites suffer from a degree of porosity, which is a result of the resin powder infusion method used. More work is needed to understand how to process thermoplastic LC oligomers that show strong shear-thinning.

In Chapter 6 we summarize the achievements of this *Thesis* and the overall conclusions of the research work. Moreover we have discussed a series of recommendations for future work.

Samenvatting

Het onderzoek zoals beschreven in dit proefschrift betreft het gebruik van reactieve, volledige aromatische, vloeibaarkristallijne thermohardende polymeren voor toepassing in vezelversterkte composieten. Een van de uitdagingen verbonden aan dit soort polymeren is het feit dat meestal de smelttemperatuur (T_{k-lc}) gelijk of zelfs hoger is dan de ontledingstemperatuur. Twee synthese-routes zijn gevolgd om het verwerkingsgedrag in de gesmolten toestand te verbeteren, zonder dat dit ten koste gaat van de thermo-mechanische eigenschappen na crosslinking: 1- sturing van het molekulgewicht van het polymeer met behulp van reactieve fenylethynyl-eindgroepen en 2- de introductie van niet-lineaire co-monomeren.

In Hoofdstuk 2 beschrijven we hoe kleine modificaties van de keten van een star vloeibaarkristallijn monomeer gebaseerd op hydroxybenzoëzuur (HBA), tereftaalzuur (TA) en 4,4'-bifenol (BP) de T_{k-lc} overgangstemperatuur sterk verlaagt van 325 tot 280 °C, terwijl de laagste waarde voor de smeltviscositeit daalt van 10^5 Pa.s tot 30 Pa.s. Desondanks blijft de glasovergangstemperatuur van het uiteindelijke polymeer ruim boven de 200 °C. Films van het uitgereageerde polymeer hadden een treksterkte en een breukrek van 85 MPa respectievelijk 4%, terwijl de E-modulus tussen de 2 en 3 GPa lag.

De manier waarop, en de mate waarin, de fenylethynyl-eindgroepen de thermo-mechanische eigenschappen van het uiteindelijke polymeer beïnvloeden is beschreven in Hoofdstuk 3. Hiertoe zijn nieuwe vloeibaar kristallijne oligomeren gesynthetiseerd met reactieve (R) fenylethynyl- dan wel niet-reactieve (NR) ftalimide-eindgroepen. Alle oligomeren zijn onderzocht met TGA, DSC, reologie, DMTA en trekproeven. De DMTA-metingen lieten zien dat de aanwezigheid van twee reactieve eindgroepen nodig is om thermohardende polymeren met goede hoge-temperatuur stabiliteit te verkrijgen. Volledig uitgeharde films vertoonden een glasovergangstemperatuur (T_g) tussen de 120 en 150 °C, een opslagmodulus (E') van ~4 GPa (bij 25 °C), een treksterkte tot 90 MPa en een breukrek van 5%.

Het onderzoek in Hoofdstuk 4 is een voortzetting van het onderzoek aan de polymeerketen zoals beschreven in Hoofdstuk 2, maar nu meer gericht op de vraag hoe de reactieve vloeibaar kristallijne polymeren verwerkt kunnen worden in vezelversterkte composieten. Hiertoe werd een vloeibaar kristallijn monomeer gebaseerd op 4-hydroxybenzoëzuur (HBA), tereftaalzuur (TA) en 4,4'-bifenol (BP) gemodificeerd door introductie van een vierde comonomeer, 2,6-naphthaleendicarbonzuur (NDA). Een viertal oligomeren met verschillende fracties NDA, 0% (*het referentiemateriaal), 1, 2,5 en 5 mol%, warden gesynthetiseerd en getest. Het reactieve oligomeer met 2.5 mol% NDA gaf de beste combinatie van verwerkbaarheid en thermo-mechanische eigenschappen na uitharden en werd daarom verkozen tot het polymeer van keuze voor het composiet onderzoek beschreven in Hoofdstuk 5.

In Hoofdstuk 5 wordt beschreven hoe de composietproductie-condities bepaald werden en worden de mechanische eigenschappen van glas- en koolstofvezel composieten gerapporteerd en besproken. Het oligomeer met 2.5 mol% NDA, beschreven in Hoofdstuk 4, werd gebruikt als matrixpolymeer vanwege zijn veelbelovende vloeigedrag (een smeltviscositeit van 100 Pa·s bij 320 °C) en zijn thermo-mechanische eigenschappen die zelfs superieur zijn aan poly-fenylensulphide (PPS) en poly-etherketonketon (PEEK). De structuur van de dunne panelen werd onderzocht met C-scan, optische microscopie en Röntgen-tomografie. De mechanische eigenschappen werden bepaald met behulp van buigproeven, compressieproeven en afschuifproeven. De resultaten werden vergeleken met die verkregen aan soortgelijke composieten op basis van PPS. De eerste resultaten lieten zien dat nieuwe LCT-composieten last hadden van porositeit als gevolg van de gebruikte poeder-infusie methode. Meer werk is nodig om te ontdekken hoe deze vloeibaarkristallijne oligomeren met hun sterke neiging tot 'shear thinning' het best verwerkt kunnen worden.

In Hoofdstuk 6 vatten we de resultaten van dit proefschrift en de algemene conclusies van het onderzoek samen. Bovendien hebben we een reeks aanbevelingen voor toekomstig werk besproken

List of Publications and Selected Presentations

Varley, R.J., Dao, B., Tucker, S., Christensen, S., Wiggins, J., Vogel, W., Marchetti, M., Madzarevic, Z., Dingemans, T.J., *Effect of aromatic substitution on the kinetics and properties of epoxy cured tri-phenylether amines*; Journal of Applied Polymer Science, 2019, 11, 47383

Marchetti, M., Dingemans, T.J., *High performance and processable liquid crystal thermosets: bridging the thermoset divide*, Oral presentation for Baeland 2016, Surrey (UK)

Luinge H., Markenstein J., Marchetti M, Dingemans T.J.; *Thermoplastic composites for aerospace applications*, Conference paper for the European Conference on Composite Materials 2016 (ECCM2016), Munich (Germany)

Marchetti, M., Dingemans, T.J., *New high temperature polymers for composite applications: bridging the thermoset divide*, Oral presentation for conference Dutch Polymer Days 2016, Lunteren (The Netherlands)

Marchetti, M., Dingemans, T.J., *High T_g liquid crystal thermosets: what is the role of the reactive end-group?*, Oral presentation for conference Thermoset 2015, Berlin (Germany)

Marchetti, M., Dingemans, T.J., *High T_g liquid crystal thermosets: what is the role of the reactive end-group?*, Poster presentation for European Polymer Federation Congress 2015, Dresden (Germany)

Marchetti, M., Dingemans, T.J., *High T_g liquid crystal thermosets: what is the role of the reactive end-group?*, Poster presentation for conference Dutch Polymer Days 2015, Lunteren (The Netherlands)

Curriculum Vitae

Martino Marchetti was born in Rome (Italy) on February 3rd, 1986. After completing classical studies in high school, he enrolled in 2007 at Rome University, *La Sapienza*, choosing Chemistry as his Bachelor. He then graduated at the end of 2009 and in 2010 he started his Master of Science in Polymer Chemistry at *La Sapienza*. In 2011 he won the Erasmus scholarship for studying one semester abroad, and during his days at the Universiteit van Amsterdam he heard the names of Prof. Theo Dingemans and Prof. Sybrand van der Zwaag and their work on high performance materials in the Novel Aerospace Materials (NovAM) Group, faculty of Aerospace Engineering at Delft University of Technology. He joined the NovAM for his Master Thesis, and after graduating in Rome, he started his Ph.D. research under the supervision of Prof. Theo Dingemans on a project funded by the Materials to innovation institute and several industrial partners: Fokker Technologies, SKF, Thermplastic Composites Research Center, TenCate and Promolding. The results of his Ph.D. work on high performance liquid crystalline thermosets for composites applications are presented in this thesis.

Since May 2017 Martino is part of the Amsterdam Innovation Center of Renolit, focusing his work on new polymer processing technologies.

Acknowledgments

The years spent at TU Delft in the NovAM group have been a crucial part of my adult life, thanks to all the people who have contributed and supported this Thesis.

First of all, I want to thank Prof. Theo Dingemans for accepting me as student and for guiding me for more than the planned 4 years of research. Thanks Theo for the support, encouragement and positive criticism when needed. I enjoyed working in the lab, going to conferences and last but not least our Italy and Star Wars themed discussions!

I want to thank Prof. Sybrand van der Zwaag as well, for helping me in becoming a better *young scientist*, for his warm welcome in the NovAM group, for the amazing Christmas dinners and the group events!

Thanks to Dr. Johan Bijleveld, for the great lab help and the countless discussions about polymers and experiments, you truly have helped me grow!

Thank you Shanta for always being of help and to organize everything that needed to be organized, NovAM would be lost without you!

Thank you to all the technicians that supported the ideas and the work over the years: Frans, Ben, Berthil, Bob, Johan, Ed, Rob, Viktor, Frank.

Thank you to Joris Markenstein from Tencate (now Toray) for the hard work on the laminates. I truly hoped we could get to better results!

I would like to thank the M2i staff as well, your support has been great over the years.

I cannot thank enough all my NovAM colleagues and friends, I had the best time with you all! Casper thank you for introducing me to the Dutch culture especially the Kapsalon, Michiel thank you for the juggling times, Wouter W. for the awesome trip to visit Michiel, Daniella for the nerdy times, Maruti to teach me everything about beers,

Arianna as my best dancing partner in the aircraft hall, Wouter P. for recoding me while singing at a conference, Zeljka for the best wedding party ever, Hari for reminding me how to swear in Italian, Michael for (but not only) the tech support on my laptop, Jimmy and Qingbao for the lab work and for teaching me the Chinese culture, Santiago for the many football discussions, and then thanks Vincenzo, Hamideh, Hussein, Mina, (ninja)Nan, Silvia, Hongli.

Then there has been the life outside NovAM an TU Delft. Thank you to Giulia for the time and adventures at Oostblok 48, thank you Alino for owning me around 250 days under his roof (pizze included), thank you Elly for taking my mattress, thank you Aris for the Greek adventures, thank you Phaidra for the running, thank you Stef and Iannis for the hundreds of movies. Thank you Brian for the mountain stories and plans and for making the most badass thesis cover. Then thank you Arman for making Rome feeling closer with your visits and our last minutes travels and adventures. Thank you Giulia, Arianna, Chiara and Valeria for the never-ending friendship.

Thank you Nonni, all of them.

Thank you Zia Chiara, perquantooo.

Thank you Zio Alftedo, Forza Roma.

Thank you Zio Andrea for the mountain days.

Thank you Megghi, Rosa and Loek for the family days in Amsterdam.

Thank you to my Parents for their love and support over the years, I couldn't have done it without you.

Thank you Monica, for fixing my arm and for a couple of other reasons more.